Formation of cranial sensory ganglia: role of neural crest–placode interactions, Slit–Robo, and Cadherins

Thesis by

Celia E. Shiau

In Partial Fulfillment of the Requirements

for the degree of

Doctor of Philosophy

CALIFORNIA INSTITUTE OF TECHNOLOGY
Pasadena, California

2009

(Defended February 11, 2009)

ACKNOWLEDGEMENTS

First and foremost, I would like to thank my advisor, Marianne Bronner-Fraser, for providing me the freedom and resources to grow and develop as an independent scientist. Through this experience, I have realized my intense and deep curiosity for developmental biology and my passion for experiments to address questions. I consider myself very fortunate to have the mentorship, guidance, and strong and constant support from my advisor who genuinely cares for the success of her students. I have also learned from her many qualities, which include effective communication of science and making our work productive.

I wish to thank my thesis committee members: Scott Fraser, Paul Sternberg, and Kai Zinn for sharing their knowledge and providing critical feedback on my work over the years during our annual meetings, and for always thinking in my best interest.

I am also indebted to all the members of the Bronner-Fraser lab with whom I have interacted. I wish to first thank Peter Lwigale, who has been very supportive and inspiring, for his collaboration and advice through my first publication from which I have truly benefited. I wish to especially thank Tatjana Sauka-Spengler who was always willing to share her deep knowledge and discuss protocols from the very beginning, from whom I have learned a great deal. I also like to thank Meyer Barembaum for being an invaluable resource on molecular biology and various scientific discussions, and also my officemate. Thanks to my peers in the lab who have shared many grad school experiences from candidacy, teaching to various on- and off- lab discussions: Meghan Adams, Jane Khudyakov, and Paola Betancur.

Many thanks to past and present members of the MBF lab: Maria Elena DeBellard for providing my first tools to explore Slits/Robos, Martin Garcia-Castro for his words of encouragement when I first started, Lisa Taneyhill for her expertise and support in my early years, Ed Coles for being a resourceful and always enjoyable lab-bench mate, Yun Kee for her heartfelt support, Dan Meulemans Medeiros for various insightful discussions, Katy McCabe and Jack Sechrist for the shared enthusiasm on the trigeminal ganglion, David McCauley, Vivian Lee, Laura Gammill, Titus Brown, Martin Basch, Sujata Bhattacharyya, and Max Ezin for sharing their technical expertise, feedback on my work, and fruitful discussions. I also extend big thanks to newer members of the lab who have made lab very enjoyable: Pablo Strobl, Tatiana Hochgreb, Natalya Nikitina, Sonja Mckeown, Ankur

Saxena, Shuyi Nie, Katherine Fishwick, Saku Jayasena, and Elly Chow. Huge thanks to Mary Flowers and also Martha Henderson who have kept lab operation at its best performance, to Gary Belford for all his help in solving my computer problems, and to all the technical staff (David, Connie, Joanne, Matt, and Sam) who have looked after the lab to ensure all the lab supplies and reagents are there: particular thanks to David Arce who made us many tasty treats and is always enjoyable, and Matt Jones who has assisted me on electrical issues. I thank my two SURF/Cambridge-Caltech exchange students, Emma Broom and Emma Hindley, for their dedication and contribution to our Cadherin-7 project. I am grateful also for the imaging support I received from the Caltech BIC center and members of the Fraser lab.

My special thoughts go to my friends who I have made over the years at Caltech. Without whom my experience would not have been filled with so many good and joyful memories— our conversations, all the dinners, theater, concerts, social outings, hiking, camping, and surfing among others. I will not list names because there have been many, but I can say that many of you have broadened my cultural experiences which I have truly loved, as many of you come from different parts of the world— you know who you are!

My deepest gratitude goes to Olivier without whom my life at Caltech would not have been complete— I have learned and experienced so much more of life than I have ever. Your love and constant support of me have made it all possible.

From the bottom of my heart, I thank my mother and my sister Carrie, who have been the rocks of my life, for their unconditional love and unwavering faith in me to pursue my dreams. I am also very grateful to my family friend and teacher Mr. Quan, my grandmother, and my family for all their constant support throughout the years.

The work presented in this thesis was funded by the National Institutes of Health.

ABSTRACT

In vertebrates, the peripheral nervous system is derived from two distinct embryonic cell populations, the neural crest and ectodermal placodes. Neural crest cells arise from the hinges of the invaginating neural plate, while ectodermal placodes form in pairs from discrete, usually thickened, head ectoderm lateral to the neural tube. While these two populations generally contribute to different structures in the nervous system, the exception is where they converge to form the cranial sensory ganglia of the trigeminal (V), facial (VII), glossopharyngeal (IX), and vagal (X) cranial nerves. The dual embryonic origin of cranial sensory ganglia has intrigued investigators for some time, but surprisingly little is known about the neural crest–placode relationship. The process of cranial gangliogenesis exemplifies a fascinating problem on how cell–cell interactions drive assembly of complex structures in the developing embryo.

To investigate this process, I have combined gene expression characterizations, embryological experiments, in vitro culture studies, and in vivo molecular perturbations (gain- and loss-of-functions by electroporation mediated DNA and oligos transfer) to uncover the cellular and molecular events underlying neural crest–placode ganglion assembly in the trigeminal region of the chick embryo. The results show that these cells are in contact and highly intermingled throughout ganglion formation. Ablation of either precursor tissue results in severe ganglion defects. Taken together, the data demonstrate the essential role of neural crest–placode interactions for proper gangliogenesis and the reciprocal nature of their relationship. Their interactions likely involve bi-directional signaling by which each population affects and coordinates with one another.

As candidate mediators, I investigated the potential role of Slits and Robos. The concurrent expression of Slit1 on migratory neural crest cells and its cognate receptor Robo2 on placodal cells raised an intriguing possibility that this ligand–receptor pair may mediate signaling from neural crest to placodal cells. This would represent one form of their cell–cell interactions. Loss of function of either the ligand Slit1 or its cognate receptor Robo2 in vivo resulted in severely disorganized placodal ganglia that were similar phenotypically to the effects of neural crest ablation. More specifically, inhibition of Robo2 resulted in aberrant placodal ingression, axonal projections, and ganglion organization and coalescence. The results suggest that neural crest cells regulate and coordinate assembly of placodal cells for proper trigeminal gangliogenesis through Slit1–Robo2 signaling in chick.

A striking defect in ganglion coalescence by blocking Slit1–Robo2 function

suggested that cell adhesion may have been affected. Thus, as a possible downstream mechanism, I next tested the function of the cell adhesion molecule N-cadherin. The results show that N-cadherin is expressed by placodal neurons, and its function is required for placodal aggregation and may be regulated by Slit1–Robo2. N-cadherin expression is modulated by Slit1–Robo2 and also can partially rescue Robo2 loss-of-function. Moreover, since neural crest and placodal neurons are highly intermixed, condensation of ganglia may require adhesion of not only placode–placode, but also crest–crest and crest–placode cells. The data suggest that another adhesion molecule Cadherin-7 may complement the role of N-cadherin in driving ganglion coalescence. Finally, the similar expression and function of these molecules in the epibranchial regions suggest that the mechanisms of Slit1–Robo2 and N-cadherin may be general for all cranial ganglia of dual origin.

In summary, the results from my thesis establish a critical role for Slit1–Robo2 signaling and cadherin-mediated cell adhesion for cranial ganglia formation. They provide the first molecular basis for neural crest–placode cell–cell signaling during cranial gangliogenesis, and highlight the critical interplay of cell–cell communication and cell adhesion in animal development.

TABLE OF CONTENTS

LIST OF FIGURES

Chapter 5 *Page*

Appendix A *Page*

Chapter 1

Introduction

1.1 Embryonic origin of the cranial sensory ganglia in vertebrates

In vertebrates, the cranial sensory ganglia have a unique, dual embryonic origin from both neural crest and ectodermal placodes. These two distinct embryonic cell types are responsible for the formation of the entire peripheral nervous system. The cranial ganglia are aggregates of neuronal and glial cells of the sensory component of the trigeminal (V), facial (VII), glossopharyngeal (IX), and vagal (X) cranial nerves. Sensory neurons in these ganglia are responsible for relaying information from external and internal stimuli back to the brain to mediate somatosensation (touch, pain, and temperature) of the head region, the special sense of taste, and autonomic visceral sensation of internal organs (such as heart and gut). Not only are these ganglia crucial for the normal function of the nervous system, but they also are an outcome of a collaborative and interactive developmental process between two cell populations.

Neural crest cells arise from the most dorsal aspect of the neural tube in a rostrocaudal progression along almost the entire extent of the body axis. They undergo an epithelial-to-mesenchymal (EMT) transition to detach from the neuroepithelium, migrate along well defined pathways, and give rise to a plethora of derivatives including the craniofacial cartilage and bone, teeth, pigment cells, endocrine cells, smooth muscle, and glia and neurons in all the peripheral ganglia (sensory, sympathetic, and parasympathetic) (Baker, 2005). Grafting experiments of the neural folds (presumptive neural crest) at cranial levels show that in general these cells are not fate restricted to the axial level of their

origin but rather that environmental cues experienced during migration and/or localization have a significant influence on their fate (reviewed in (Baker, 2005; Le Douarin and Kalcheim, 1999). Ectodermal placodes can be divided into two general classes: sense organ and neurogenic. The exception is the adenohypophyseal placode which forms the anterior pituitary gland. First, the sense organ placodes give rise to the paired sense organs (the inner ear, olfactory epithelium, the lens, and the lateral line system in anamniotes) and second, the neurogenic placodes give rise exclusively to sensory neurons in the cranial sensory ganglia (Baker, 2005); however this naming system is not to confuse the point that sense organ placodes also give rise to neurons. The neurogenic placodes are the ophthalmic (OpV) and maxillo-mandibular (MmV) placodes in the trigeminal ganglion, and the geniculate, petrosal, and nodose placodes that give rise to the distal portions of the facial (VII), glossopharyngeal (IX), and vagal (X) ganglia, respectively— generally grouped as the "epibranchial" placodes since they form around the second to the fourth branchial arches. The placodes are discrete regions of the head ectoderm, usually thickened, and found as pairs on both sides of the neural tube. For example, the surface ectoderm from which the trigeminal placodes arise is mostly uniform, except for sporadic spurs or thickenings where cells appear to be delaminating from the surface (D'Amico-Martel and Noden, 1983; Hamburger, 1961) (figures in this thesis). Unlike the neural crest, the placodes represent a diverse and rather heterogeneous population that exhibits varied fate specification processes and morphogenetic movements, which are extensively reviewed elsewhere (Baker, 2005; Baker and Bronner-Fraser, 2001; Begbie and Graham, 2001b; Schlosser, 2006).

The dual origin of the cranial ganglia was historically controversial (Hall, 1999; Hamburger, 1961; Le Douarin and Kalcheim, 1999). Although both the neural crest and placodes were independently discovered over one hundred years ago in the late 19th century— the neural crest by Wilhelm His (His, 1868) in chick embryos and placodes by

van Wijhe (van Wijhe, 1883) in shark embryos (in Greek the name “placode” means “plate” or “flat shaped” and was coined by von Kupffer (von Kupffer, 1894)), their common contribution to the cranial ganglia was not accepted until more recently. The debates largely arose from differences in direct observation of embryos from different species and the results of tissue ablation experiments (Hamburger, 1961; Le Douarin and Kalcheim, 1999; Yntema, 1944). Due to the lack of reliable cell marking techniques to follow neural crest and placodal cell lineages, the origin of cranial ganglia was argued as being from neural crest, from placodes, or from both. Direct observations and tissue ablations have several limitations. Ablation experiments cannot definitively demonstrate the fate of the cells removed, because of possible indirect effects leading to the loss of a structure and/or embryonic regulation (compensation by another tissue or regeneneration). Furthermore, it is technically impossible to make any definite conclusions about their fates without molecular or cellular labels, since neural crest and placodal cells are indistinguishable once they have migrated into the mesenchyme. These issues were resolved by the use of radioactive labels, vital dyes, and interspecific grafting techniques that allowed long-term cell marking (such as the quail-chick grafting system (Le Douarin, 1973)). The contribution of neural crest to the cranial ganglia was first clearly shown using radioautographically labeled neural folds (Johnston, 1966) and by quail neural crest grafts (Noden, 1975; Noden, 1978). Ectodermal grafts labeled by Nile blue in salamander embryos (Amblystoma) directly showed placodal contribution to the ganglia (Yntema, 1937). However, it was not until the 1980s that quail-chick chimera labeling was used to firmly establish the two components of all the cranial sensory ganglia and their patterns of distribution (Ayer-Le Lievre and Le Douarin, 1982; D'Amico-Martel and Noden, 1983). Neural crest migration and development into cranial ganglia have also been demonstrated in other vertebrate systems (zebrafish, Xenopus, mouse) reviewed in (Hall, 1999; Le Douarin and Kalcheim, 1999). However, the relationship of neurogenic placodes with

neural crest is still best characterized in chicks. Nonetheless, placodes in the ganglion region have been found across vertebrates— in mammal (Batten, 1957), amphibian (Yntema, 1937), and fish (Nechiporuk et al., 2007); reviewed in (Schlosser, 2005; Schlosser, 2006)— and thus the dual origin of cranial ganglia across vertebrates is widely accepted. Even in humans, systematic characterization of serially sectioned human embryos suggests contributions from cranial neural crest and placodes to cranial ganglia (O'Rahilly and Muller, 2007) similar to that of mouse and chick embryos.

D'Amico-Martel and Noden (1983) grafted presumptive quail neural crest or placodal tissue to replace the homologous tissues in chick embryos. The distribution of these grafted quail cells marked by their unique nuclei (condensed heterochromatin) were examined in the nearly mature ganglia at embryonic day 12 (stage 38). Their results not only confirmed the dual origin of avian cranial ganglia, but also provided a relatively complete picture of the embryonic composition of the maturing ganglion. They show the segregation of neural crest- and placode-derived neurons along the proximal-distal axis; proximal closest to the hindbrain and distal closer to their innervated targets. They further show that all the glia (Schwann and satellite cells) were derived from neural crest. This demonstration in birds provides the currently available study of the contribution of neural crest and placodal cells to the cranial sensory ganglia.

1.2 Neural crest and placode interactions

The most suggestive evidence that interactions between neural crest and placode cells are involved in formation of ganglia has come from tissue ablations in chick embryos. Experiments of ablating either the presumptive neural crest or the placodal tissue were analyzed in the nearly mature trigeminal ganglion at embryonic day 8 (stages 34–35) or

later. Absence of either neural crest or placodes resulted in either dispersed or smaller ganglion (Hamburger, 1961; Lwigale, 2001). However, the effects on cell–cell interactions and ganglion assembly were not examined. Similarly, neural crest ablation in the epibranchial region also suggest a role for neural crest in organizing placode-derived neurons (Begbie and Graham, 2001a). In contrast, neural crest was not involved in induction of the trigeminal and epibranchial placodes (Begbie et al., 1999; Stark et al., 1997). In summary, these ablation experiments suggest an important role of neural crest on integrating and organizing placodal cells in both the trigeminal and epibranchial regions. These interactions appear to occur during ganglion formation but after initial placodal induction. One point to consider, however, about neural crest ablation is that this might yield an incomplete list of neural crest effects, since complete neural crest removal is nearly impossible to achieve. Neural crest cells are highly regenerative (Saldivar et al., 1997; Sechrist et al., 1995) and can also reroute to compensate for loss of neural crest (Kulesa et al., 2005; Saldivar et al., 1997), and therefore assessing the actual extent of neural crest ablation at the time of analysis is important for accurate interpretation of data.

Taken together, results from these experiments suggest that interactions between neural crest and placodes may be involved in ganglion formation; however the underlying molecular mechanisms are still unknown. Some questions yet to be addressed include: how do neural crest and placodal cells interact on a cellular level? do they communicate with one another? do their interactions take place during ganglion assembly and are they essential for proper gangliogenesis? Understanding neural crest–placode interactions would be a key to understanding the core piece of this developmental process.

1.3 How peripheral ganglia form

In the developing vertebrate embryo, aggregates of sensory neurons and glia called "sensory ganglia" are present along almost the entire neural tube (presumptive brain and spinal cord), mirroring the earlier pattern of the migratory neural crest streams. As described above, those in the head are called the "cranial sensory ganglia", which form pairwise along the hindbrain at even numbered rhombomeres. There are also an analogous set of sensory ganglia along the trunk neural tube (presumptive spinal cord) called the "dorsal root ganglia", and also a chain of sympathetic ganglia. In contrast to the cranial sensory ganglia, these are entirely derived from the neural crest, which have made studies on trunk ganglia more tractable and easier to interpret. The parasympathetic ganglia also are derived from neural crest which form near or within their target organs throughout the body.

In the trunk, neural crest cells migrate along well defined pathways through the repeated segments of the embryonic trunk called somites. They only migrate through the anterior, not the posterior half of each somitic sclerotome (Bronner-Fraser, 1986; Rickmann et al., 1985). This migration is thought to be guided by signals emanating from the somites with permissive cues in the anterior half and repulsive signals in the posterior half reviewed in (Le Douarin and Kalcheim, 1999). Later, neural crest cells coalesce into dorsal root ganglia adjacent to the neural tube and sympathetic ganglia more ventrally around the dorsal aorta. It has been widely accepted that the discrete migratory streams were the basis for the metameric organization of trunk ganglia formation (Keynes and Stern, 1988; Lallier and Bronner-Fraser, 1988). However, recent results have provided surprising new insights into trunk gangliogenesis that uncouples trunk neural crest migration pattern and the metameric organization of ganglia formation. Genetic evidence from neuropilin 2 and semaphorin 3F mutants show that signaling between this

receptor–ligand pair is critical for normal segmental trunk migration. However, the resulting non-segmental neural crest migration through both halves of the somites did not alter the normal metameric pattern of ganglion formation (Gammill et al., 2006). In vivo time-lapse imaging of trunk neural crest cells forming the sympathetic ganglia show that they initially migrate in segmental streams, but once they have reached the ganglion assembly site, they spread rostrocaudally before later sorting into discrete, metamerically localized ganglia (Kasemeier-Kulesa et al., 2005). These results suggest that signals other than those mediating guidance of neural crest migration are critical for positioning ganglion formation. Whether these signals come from the somites, some other tissue, or within themselves (e.g. cell–cell interactions) is unknown. The aggregation of neural crest cells into sympathetic ganglia appears to involve N-cadherin mediated adhesion (Kasemeier-Kulesa et al., 2006).

In contrast to the trunk ganglia, the position and shape of the cranial sensory ganglia appear to be at least in part regulated by the migration pattern of the cranial neural crest. Loss of semaphorin and neuropilin genes, which caused abnormal migration of neural crest cells in a crest-free zone (between two streams), led to aberrantly interlinked trigeminal and facial ganglia and abnormal positioning of neurons which are presumably at least in part placode-derived (Gammill et al., 2006; Schwarz et al., 2008). These results suggest that proper neural crest migration is important for normal cranial gangliogenesis and that neural crest cells may play an important role in organizing placodal neurons. In zebrafish, it has been suggested that chemokine signaling between trigeminal neurons and the hindbrain plus nearby tissues is involved in properly positioning the trigeminal ganglion (Knaut et al., 2005), but it is unclear if neural crest, placode, or both are affected. Loss of both Msx1 and Msx2 in mouse embryos induces apoptosis in cranial neural crest and results in severely disorganized or reduced neuronal population of the cranial ganglia (presumably due to defects in the placodal component) (Ishii et al., 2005). This suggests

that loss of cranial neural crest may affect placodal ganglion organization. So far, our understanding of cranial gangliogenesis has mostly come from studies of neural crest development. These studies have suggested neural crest play an essential role in cranial gangliogenesis and its possible interactions with placodal neurons. However, the nature of this interaction is uncharacterized, the role of placodal cells is elusive and the underlying molecular mechanisms mediating neural crest–placode signaling are unknown.

From the placodal perspective, the formation of cranial ganglia is poorly understood. Studies on neurogenic placodes have focused on the specification of trigeminal and epibranchial fates, which appear to depend on neural tube–ectoderm interaction involving Wnts and PDGF signaling in the trigeminal OpV region, but may also involve other signaling molecules (Lassiter et al., 2007; McCabe and Bronner-Fraser, 2008; McCabe et al., 2007; Stark et al., 1997). Induction of epibranchial fates is thought to be mediated by pharyngeal endoderm–ectoderm interaction mediated by BMPs (Begbie et al., 1999), as well as with Fgf signaling from the cranial mesoderm (Nechiporuk et al., 2007; Nikaido et al., 2007). At an earlier time point, the different types of placodes can be traced back to the anterior cranial neural plate border in the epiblast (also known as the "preplacodal" or "panplacodal" region), prior to neurulation, and it is thought that all placodal precursors undergo a common "preplacodal" specification before they become separated and diversified (i.e. acquisition of trigeminal and epibranchial fates)(Bailey and Streit, 2006; Streit, 2007). In summary, studies from trunk and cranial regions suggest three essential steps for formation of ganglion after the specification of the precursor cell types: first, migration of precursors to the site of assembly, second, tissue or cell–cell interactions, and third, cellular aggregation into discrete structures.

1.4 Slits and Robos: structure and function

Slits and their cognate receptors Robos (short for "Roundabouts") are evolutionarily conserved signaling molecules found in animals ranging from nematodes and fruit flies to mammals (Chedotal, 2007). The Slit mutant was first described in the classic genetic screen for embryonic patterning defects in *Drosophila* (Nusslein-Volhard et al., 1984). Later Slit and Robo (initially identified in a fly screen for axon commissure defects (Seeger et al., 1993)) were both identified in another screen for mutations in *Drosophila* commissural axon guidance (Hummel et al., 1999). In vertebrates, there are three homologs of Slit (Slit1–3) and four members of the Robo family (Robo1–4), whereas in *Drosophila*, there is a single Slit as well as three Robos (dRobo and dRobo2–3), which arose from independent gene duplication; vertebrate Robo2-3 are not orthologs of dRobo2–3. Slit was shown to be the ligand for Robo receptors based on their dosage-sensitive genetic and biochemical interactions and chemorepulsive function (Brose et al., 1999; Kidd et al., 1999).

Slits are large secreted proteins (about 200 kDa) but may not diffuse far as they have been found associated with the cells that secrete them (Brose et al., 1999; Hu, 1999; Niclou et al., 2000). They share four tandem leucine rich repeats (LRRs), seven (invertebrate) or nine (vertebrate) epidermal growth factor (EGF) like domains, a laminin G domain, and a C-terminal cysteine-rich knot (Chedotal, 2007). Slit2 has been shown to be proteolytically cleaved after the fifth EGF-like domain into 140kDa N-terminal and 60kDa C-terminal fragments in vivo and in vitro, though not all Slit2 are cleaved, since full-length Slit2 was also isolated (Brose et al., 1999; Nguyen-Ba-Charvet et al., 2001; Wang et al., 1999). The N-terminal Slit2 fragment has been shown to retain axon guidance activity (Chen et al., 2001; Nguyen-Ba-Charvet et al., 2001). It is unclear if all Slits undergo proteolytic cleavage; however, this may occur broadly depending on the cellular context.

Cleavage of human Slit3 but not hSlit1 was detected in mammalian CHO cells (Patel et al., 2001), and of *Drosophila* Slit in mammalian cell lines (293T and COS) and *Drosophila* embryo extracts, but not in *Drosophila* S2 cells (Brose et al., 1999).

Robos are structurally more varied—classical vertebrate Robos (Robo1–2) have five immunoglobulin-like (Ig), three fibronectin type III (FN3), a transmembrane, and four conserved cytoplasmic (CC0–3) domains, while Robo3 (Rig-1) and Robo4 (Magic Roundabout) are divergent members. Robo3 has no cytoplasmic domain 1 (CC1) and is implicated as a negative regulator of Slit–Robo signaling, but the underlying mechanism is unclear (Sabatier et al., 2004). Robo4 has only two Ig and two cytoplasmic domains and is expressed specifically in endothelial cells with functions in angiogenesis and vasculogenesis (Bedell et al., 2005; Fujiwara et al., 2006; Huminiecki et al., 2002; Park et al., 2003; Wang et al., 2008). The intracellular tail of Robos has no apparent catalytic activity and, therefore, recruitment of cytosolic proteins is likely required for its function.

Slits can bind to any of the three Robo receptors (Robo1–3) as well as the *Drosophila* Robo with comparable affinity (Brose et al., 1999; Li et al., 1999; Sabatier et al., 2004), but it is not clear whether they bind to Robo4 (Hohenester et al., 2006; Suchting et al., 2005). Recent structure-function studies have localized the region of binding to the leucine rich repeats (LRRs) of Slit and the first two Ig domains of Robo (Chen et al., 2001; Liu et al., 2004). The minimal interaction has been mapped to the second Slit LRR and the first Robo Ig domain, which is conserved in *Drosophila* and mammal (Hohenester et al., 2006; Howitt et al., 2004; Morlot et al., 2007).

While structural studies have clearly established the binding interface of Slit and Robo, the downstream signaling upon Slit activation of Robo remains elusive. Whether this involves oligomerization of either the receptor and/or the ligand, and how and which cytosolic proteins are recruited to the intracellular Robo domains in different cellular contexts, are open questions (Hohenester, 2008). Several cytoplasmic signaling proteins

have been shown to be able to bind to the intracellular conserved Robo domains (CC0–3) such as actin binding protein Ena/VASP (Bashaw et al., 2000), adaptor protein Dock/Nck (Fan et al., 2003), Rho GTPase activating proteins (GAPS) (i.e. Vilse/CrossGAPs and Slit–Robo specific GAPs [srGAPs]) (Hu et al., 2005; Li et al., 2006; Lundstrom et al., 2004; Wong et al., 2001) and the Abelson (Abl) tyrosine kinase (Bashaw et al., 2000)— all major modulators of the actin cytoskeleton which may also have other functions.

Substantial evidence implicates direct interaction of heparan sulfate proteoglycans (HSPGs) with Slit for its function (reviewed in (Hohenester, 2008)). Structural studies show that the LRR2 that binds to Robo also binds to heparin, suggesting a Slit–Robo–HS complex (Fukuhara et al., 2008; Hussain et al., 2006). Enzymatic ablation of heparan sulfate (HS) by Heparinase III (Hu, 2001) decreases affinity of Slit–Robo binding and blocks Slit repulsive activity in vitro, which also occurs when excess HS is applied (Piper et al., 2006). In *Drosophila*, syndecan, a HSPG, has been shown to interact with Slit–Robo genetically in regulating distribution and efficiency of Slit signaling (Johnson et al., 2004; Steigemann et al., 2004). In vertebrates, the role of syndecan with Slit–Robo is not clear, but vertebrate Slit1–2 have been found to bind strongly to the HSPG Glypican-1, likely through its HS chains (Liang et al., 1999; Ronca et al., 2001). The functional relationship of HSPG and Slit–Robo in vivo is not well understood.

Functionally, Slits and Robos are best known for their conserved role in midline axon repulsion, which regulates the crossing of commissural axons and also inhibits crossing of ipsilateral axons in the *Drosophila* ventral nerve cord and the mammalian spinal cord (Dickson and Gilestro, 2006; Kidd et al., 1999; Kidd et al., 1998; Long et al., 2004). In addition to regulating the commissures, they can act as both repulsive (e.g. olfactory bulb, hippocampal, and spinal motor axons) (Bagri et al., 2002; Brose et al., 1999; Hu, 1999; Li et al., 1999; Nguyen Ba-Charvet et al., 1999; Nguyen-Ba-Charvet et al., 2002) and attractive (e.g. on DRG sensory and retinal axons) (Jin et al., 2003; Nguyen-Ba-

Charvet et al., 2001) guidance cues for various types of neurons. They can also promote axon branching and growth, as well as regulate cell migration (Kramer et al., 2001; Nguyen-Ba-Charvet et al., 2004; Wang et al., 1999), including the trunk and vagal neural crest (De Bellard et al., 2003; Jia et al., 2005). Moreover, it has become clear that Slits and Robos have broader roles than axon guidance/branching and cell migration and are not restricted to the nervous system. More recently, in *Drosophila*, novel roles for Slit and Robo have emerged in cell adhesion and morphogenesis of the forming heart tube (MacMullin and Jacobs, 2006; Qian et al., 2005; Santiago-Martinez et al., 2006; Santiago-Martinez et al., 2008). In vertebrates, they have broad expression patterns in diverse tissues including teeth (Loes et al., 2001), otic vesicle (Battisti and Fekete, 2008), lungs (Anselmo et al., 2003), limbs (Vargesson et al., 2001), and kidneys (Piper et al., 2000) and have been implicated in mammary ductal development (Strickland et al., 2006). However, the functions of Slit–Robo in these systems are not well characterized.

Aside from axon and cell migration guidance, new roles for Slit–Robo involved in cell adhesion, cell positioning, and/or other cellular functions are beginning to be realized. Further investigation of Slit–Robo function in tissue morphogenesis and organ development holds the promise of revealing their large range of biological functions and thereby elucidating general principles underlying this signaling pathway during development.

1.5 Cadherins: structure and function

Cadherins are conserved adhesion molecules found throughout the animal kingdom from nematode to mammal and are considered the main facilitators of adhesion between

cells in vertebrates through homophilic binding. For the past few decades, numerous studies have addressed the broad and important roles of cadherins in development and cancer (Gumbiner, 2005; Jeanes et al., 2008; Stemmler, 2008). In addition to adhesion, cadherins have also been implicated in cell signaling, differentiation, and survival (Radice and Takeichi, 2001). To date, over 100 members of the cadherin superfamily have been identified in the animal kingdom (Stemmler, 2008). The best known and most similar subfamilies of these are the classical type I (cadherins 1–4, also respectively named E-, N-, P-, R- cadherins) and type II (e.g. cadherins 5–12). Classical cadherins all have five extracellular cadherin domains (ECs), a single pass transmembrane protein, and two highly conserved intracellular domains—the juxtamembrane domain that binds to p120 catenin (which has been implicated in regulation of cadherin turnover at the cell surface and Rho GTPases that affect the actin cytoskeleton (Perez-Moreno and Fuchs, 2006; Reynolds and Roczniak-Ferguson, 2004)) and at the C-terminus, the binding domain for β-catenin which is indirectly linked to the actin filaments through α-catenin (Radice and Takeichi, 2001). Cadherins are defined by their tandemly arranged extracellular cadherin repeats, but the number of repeats is variable and the intracellular regions differ widely between classical cadherins and the other subfamilies (desmosomal cadherins, protocadherins, atypical cadherins, and the seven-pass transmembrane cadherin-like molecules), which do not bind to β-catenin but interact with plakoglobin and desmoplakin, kinases, and yet to be identified proteins (Gumbiner, 2005; Stemmler, 2008). Therefore, the functions of the non-classical cadherins may be distinct or may include additional roles to cell adhesion.

The expression of some classical cadherins are spatiotemporally regulated during neural crest emigration (Taneyhill, 2008). Functional experiments suggest that switching of cadherin subtypes during neural crest emigration is crucial for changes in cell adhesive properties in order to acquire the ability to migrate (Nakagawa and Takeichi, 1998).

However, the precise function of cadherins once these cells are migrating and later in development as they form the peripheral ganglia remain poorly explored. Similarly, very little is known about their potential role in development of placodal cells, with which neural crest cells interact during cranial ganglia formation.

1.6 Overview

How structures arise in the developing embryo is a fascinating process. Cell–cell interactions are the basic architectural building blocks in multicellular animals. This aspect of development is difficult to tackle because it requires grappling with a multitude of actions, reactions, and changes that are dynamically occurring in two or more different cellular components. The study of cranial gangliogenesis exemplifies such a problem. The origin of cranial sensory ganglia from a combination of two distinct cell populations, neural crest and ectodermal placodes, has intrigued the field for quite some time. Surprisingly, little is known about the nature and function of neural crest–placode interaction. How do they interact and what molecular basis may mediate their interaction? Does this have an important role for ganglion formation? With the advent of new technologies for DNA, vector, and oligos transfer using in vivo electroporation to target specific tissues (such as the presumptive neural crest or the placodal ectoderm) for both gain- and loss-of-function in combinaton with an array of molecular tools, the study of this long-time puzzle is now being elucidated. The chick is arguably the best model system to begin this investigation because of its well characterized embryology, its long history of neural crest and placode studies, and its amenability to embryological manipulation in combination with molecular

perturbation, which makes it an effective and tractable system to dissect the roles of neural crest and ectodermal placodes in vivo.

In my thesis study, the focus was the early development of the cranial sensory ganglia. This represents the time period when neural crest and placodal cells migrate to the ganglion anlage, interact, assemble, and condense into the first recognizable ganglion structure. The later processes after the first sight of a coalesced ganglion: neuronal and glial differentiation, axonal projections to the targets, and neuronal cell type specificities and functions among others, which have been more extensively studied, are reviewed elsewhere (Le Douarin and Kalcheim, 1999). The formation of the trigeminal ganglion was the prime system of study to dissect neural crest–placode interaction during ganglion assembly, due to its large size and unique semi-lunar structural shape which provided easy accessibility and structural analyses of the tissues. In addition, supporting experiments on epibranchial gangliogenesis were also conducted to evaluate the generality of the mechanisms found in our studies.

This thesis presents the results and findings from my study. The first aspect of this work, presented in Chapter 2, is the characterization of neural crest and placode cell–cell association during trigeminal gangliogenesis starting from placodal ingression. Using both cell labeling and molecular markers in successive stages of development, in combination with neural crest–placode cultures and ablation experiments, we show that these cells are in contact and closely intermingled throughout gangliogenesis. These data suggest that bi-directional signaling is likely in place to mediate their reciprocal interaction. We then present our finding that neural crest and placodal cells interact through Slit1–Robo2 signaling which is required for proper assembly of the cells into ganglion. This represents the first molecular lead into the underlying basis for neural crest–placode cell–cell interactions.

The second aspect examines possible mediators of Slit1–Robo2 signaling in driving proper ganglion formation (Chapter 3). We tested the cell–cell adhesion molecule N-cadherin as a possible candidate due to its implicated interaction with Slit–Robo in vitro and its possible role in gangliogenesis. The results show that N-cadherin is expressed by the placode-derived neurons, but not the neural crest, and its function is required for placodal condensation. We further demonstrate that N-cadherin acts downstream of Slit1–Robo2. This suggests a novel mechanism whereby neural crest–placode interaction through Slit–Robo signaling positively regulates N-cadherin mediated placodal cell adhesion.

Finally, the results above pose lingering questions on what then may be mediating adhesion of the other population, the neural crest, and also adhesion between neural crest and placodal neurons. Chapter 4 presents the results showing the role of another cell adhesion molecule Cadherin-7 in cranial neural crest migration and a potential role for Cadherin-7 in mediating neural crest cell aggregation in the trigeminal ganglion. The results raise two possible models for coalescence of trigeminal ganglion: the first is based on homotypic and novel heterotypic interactions between Cadherin-7 and N-cadherin, and the second is based entirely on homotypic cadherin mediated adhesion.

Chapter 2

Neural crest–placode interactions mediate trigeminal ganglion formation and require Slit1–Robo2 signaling

2.1 Abstract[1]

The cellular and molecular interactions allowing generation of complex cranial sensory ganglia remain unknown. Here, we show that proper formation of the trigeminal ganglion, the largest of the cranial ganglia, relies on intimate and bi-directional interactions between its two precursor cell types, placodal and neural crest cells. Removal of either population results in severe defects. We show that placodal and neural crest cells concurrently express the receptor–ligand pair, Robo2 and Slit1, respectively, during a discrete time window consistent with their potential role in initial placode–neural crest interactions and early ganglion assembly. Perturbation of this receptor–ligand interaction by blocking Robo2 function or depleting either Robo2 or Slit1 using RNA interference (RNAi) disrupts proper placodal ganglion formation which mimics the effects of ablating the neural crest. Inhibition of Robo2 in placodal cells also causes wild-type neural crest cells to aberrantly assemble with the affected placodal neurons into severely disorganized ganglia. This non-cell-autonomous effect further underscores the reciprocal neural crest–placode relationship. Our data suggest that signaling from the neural crest through Slit1–Robo2 acts as a positive regulator of placodal ingression, cell positioning, and/or axon guidance during trigeminal gangliogenesis. Thus, our data reveal for the first time, a

[1] This chapter is based on Shiau CE, Lwigale, PY, Das RM, Wilson SA, Bronner-Fraser M. Robo2–Slit1 dependent cell-cell interactions mediate assembly of the trigeminal ganglion. Nat. Neurosci. 2008 Mar; 11(3): 269-76.

putative molecular signaling event underlying neural crest–placode interactions during gangliogenesis, representing a novel and essential role for Slit–Robo in cell–cell interactions during vertebrate development.

2.2 Introduction

The origin of sensory ganglia in the developing peripheral nervous system can be traced to two transient embryonic cell populations: the neural crest and ectodermal placodes (D'Amico-Martel and Noden, 1983). Both cell types contribute to specialized structures that distinguish vertebrates from other chordates. Neural crest cells form at the dorsal-most portion of the neural tube, undergo extensive migrations and differentiate into a plethora of derivatives, including sensory and autonomic ganglia, cranial cartilage and bone, and pigment cells (Knecht and Bronner-Fraser, 2002). Placodes are transient regions of thickened head ectoderm that form on the surface epithelium lateral to the cranial neural tube. They ingress into the mesenchyme to form cranial sensory ganglia as well as essential components of the paired sense organs, contributing to lens, nose, and ears (Baker and Bronner-Fraser, 2001).

A fundamental question in gangliogenesis is how precursors interact and organize themselves to later form an anatomically correct structure with proper connections to the central nervous system and its sensory organs. The trigeminal ganglion, responsible for the senses of touch, pain, and temperature of much of the face and jaws, is the largest of the cranial ganglia and a prime example of one with dual neural crest and placode origin. Tissue ablation experiments suggest that neural crest–placode cell interactions are critical

for formation of the trigeminal ganglion (Hamburger, 1961; Lwigale, 2001), though the underlying molecular mechanism remains unknown.

The formation of ganglia from neural crest and/or placode populations involves several discrete steps. First, precursor cells delaminate by undergoing an epithelial-to-mesenchymal transition. Second, the cells migrate as individuals to the site of ganglion formation. Third, they aggregate and condense to form discrete ganglia of the sensory nervous system. For neural crest, several cell surface receptors and cell adhesion molecules have been implicated as molecular mediators of this three-step process. The epithelial-to-mesenchymal transition that results in their delamination from the neural tube involves loss of Cadherin-6b which is directly down-regulated by the transcriptional repressor and neural crest marker, Snail2 (Taneyhill et al., 2007). Several types of cell–cell and cell–matrix interactions have been implicated in guiding cranial and/or trunk neural crest migration to sites of peripheral ganglion formation, including Eph–ephrin (Kasemeier-Kulesa et al., 2006; Krull et al., 1997), neuropilin–Semaphorin (Gammill et al., 2006), laminin– (Coles et al., 2006) and integrin– (Kil et al., 1998) extracellular matrix interactions. Finally, N-cadherin has been suggested to mediate their condensation into discrete dorsal root and sympathetic ganglia (Akitaya and Bronner-Fraser, 1992; Kasemeier-Kulesa et al., 2006). In contrast to neural crest, virtually nothing is known about the molecular events involved in formation of placode-derived ganglia.

In the present study, we test the role of Robo–Slit interactions in formation of the trigeminal ganglion. Slits and their Robo receptors (Brose et al., 1999; Kidd et al., 1999) are evolutionarily conserved regulators present in the developing nervous system of diverse animals ranging from nematodes and fruit flies to vertebrates (Chedotal, 2007). Although best known for mediating repulsion, they also can promote axon branching (Zinn and Sun, 1999) and cell migration (Kramer et al., 2001) and, in *Drosophila*, have been implicated for novel roles in cell adhesion and morphogenesis of the forming heart tube (Santiago-

Martinez et al., 2006). In vertebrates, they have broad expression patterns in diverse tissues including teeth (Loes et al., 2001), lungs (Anselmo et al., 2003), limbs (Vargesson et al., 2001), and kidneys (Piper et al., 2000). Here, we show that neural crest and placode cells express Slit and Robo respectively, in a complementary manner and that the organization of the trigeminal ganglion is lost when either receptor or ligand is inhibited. Our results provide novel insights into the mechanisms underlying cranial gangliogenesis. They suggest a major role for the receptor, Robo2, in mediating this process, representing one of the first examples of Robo–Slit signaling in cell–cell interactions in vertebrate development.

2.3 Materials and methods

Embryos

Fertilized chicken (*Gallus gallus domesticus*) and quail (*Coturnix coturnix japonica*) eggs were obtained from local commercial sources and incubated at 37°C to the desired stages according to the Hamburger and Hamilton staging system.

In situ hybridization

Whole mount chick in situ hybridization was performed as previously described (Kee and Bronner-Fraser, 2001). cDNA templates used for antisense riboprobes were: chick Slits 1–3 and Robos 1–2 as described (Vargesson et al., 2001), and Sox10 (Cheng et al., 2000). Embryos were imaged and subsequently sectioned at 12–14 μm.

Immunohistochemistry

Primary antibodies used were anti-GFP (Molecular Probes), anti-HNK-1 (American Type Culture), anti-QCPN (quail specific nuclear marker) (DSHB), anti-Islet1 (DSHB), and anti-TuJ1 (Covance), as described in Appendix B. Staining was performed on whole embryos or 12 μm sections. Images were taken using the AxioVision software from a Zeiss Axioskop2 plus fluorescence microscope, and processed using Adobe Photoshop CS3.

In ovo electroporation of the trigeminal ectoderm or presumptive neural crest

Chick embryos (stages 8–10 for placode electroporation and stages 4–9 for neural crest electroporation) were injected with the DNA or miRNA vector of interest. Platinum electrodes were placed vertically or horizontally across the embryo using various electroporation conditions, as further described in Appendix B. Plasmid DNA vectors driven by a chick β-actin promoter with a CMV enhancer were used as follows: Robo2Δ-GFP (Hammond et al., 2005), and for control GFP expression, cytoplasmic pCIG (cyto-pCIG)(see Appendix B) and pCAβ-IRES-mGFP (McLarren et al., 2003).

Ecto-mesenchyme culture

Either the neural crest or the placode tissue was electroporated with cyto-pCIG as described above. The surface ectoderm and the adherent underlying mesenchyme in the presumptive trigeminal region demarcated in Fig. 3g was explanted and cultured in either 4- or 8- well chamber mounted on glass slides (Lab-TekII, NUNC) treated with 25μg/ml fibronectin in F12/N2 serum free medium in a 7% CO_2 incubator at 37˚C for ~20 hours.

Neural fold and ectoderm tissue ablations

Ablations were performed as previously described (Lwigale, 2001) with slight modifications, as described in Appendix B.

GFP labeling of the ectoderm combined with quail-chick grafts

Ectoderm electroporation with cyto-pCIG was performed on stage 9 (6–7 somites) chick embryos followed by a quail-chick neural fold graft, as described in Appendix B.

Quail-chick grafts combined with ectoderm tissue ablation

Quail-chick grafting of the neural folds in stage 9 (6–7ss) chick embryos was performed as described above. Chimeras were then re-opened at about stage 12 and the presumptive trigeminal ectoderm was ablated as aforementioned.

Analysis of Islet1+ placode cells during ingression

Percentages of Islet1+ cells associated with the ectoderm (in the ectoderm and associated with its basal margin) and in the mesenchyme were calculated from dividing the number of Islet1+ cells in the respective regions by the total number of Islet1+ cells in the entire presumptive trigeminal area (Fig. 7i, dotted box); cells were counted from frontal plane sections (12 μm). Details are described in Appendix B. Statistical significance was determined by a two-tailed student's t-test assuming equal variances.

RNAi

Electroporations were performed as described above. RNAi vectors were constructed as described previously (Das et al., 2006) with slight modification as described in Appendix B. Target sequences used were 5’ GGCACAAGCTGGAGTACAACTA (GFP) (Das et al., 2006), 5' GCTCTAATCTGTATGGATCTAA (Robo2), and 5' CTGCCAGTGCCGAG

ACCATCAA (Slit1). Rescue was performed with a full length mouse Slit1-myc fusion construct (Yuan et al., 1999).

2.4 Results

2.4.1 Cell–cell interactions during ganglion assembly

In the chick embryo, trigeminal placode cells begin to ingress at ~stage 12 (D'Amico-Martel and Noden, 1983), intermixing with a stream of migratory cranial crest cells. To better understand the behavior of neural crest and placode cells during trigeminal ganglion formation, we first carefully established the timing of their interactions at successive stages (Figs. 1 and 2) and examined their cell–cell associations using tissue-specific grafts or electroporation of GFP coupled with molecular markers (Figs. 1 and 3).

Ingression of trigeminal placode cells from the surface ectoderm peaks between stages 14–16 and ceases at ~stage 21 (D'Amico-Martel and Noden, 1983). Prior to ingression, placode cells co-express neuronal markers, Islet1 (Begbie et al., 2002) and β-neurotubulin (TuJ1) (Moody et al., 1989), as early as stages 12–13 and continue to express these markers throughout gangliogenesis (Figs. 1, 2, 3a–c). By the time placode and neural crest cells come into close contact, placode cells express neuronal markers, but are not necessarily post-mitotic as these markers also label dividing neuroblasts (Begbie et al., 2002; Moody et al., 1989). Post-mitotic placode-derived neurons are first observed at stage 16 (D'Amico-Martel and Noden, 1980). Neural crest cells, on the other hand, only begin neuronal differentiation at embryonic day 4 (D'Amico-Martel and Noden, 1980), which is equivalent to stages ~22–24. Islet1 and TuJ1 were specific for placode cells prior to this

stage, as shown by colocalization of these markers with GFP introduced in presumptive placode cells; in contrast, their expression failed to overlap with GFP-labeled neural crest cells at stages 16–18 (Fig. 2 and data not shown).

By stage 13, placode cells enter the subectodermal region and mingle with already present neural crest cells that express HNK-1 antigen (Fig. 3a,b). Placode cells ingress as individuals or in short chains and appear to maintain contact with each other in the cranial mesenchyme (Fig. 3b). At stage 13, placode-derived neuroblasts have short, randomly oriented axons (Fig. 3a,b); in the condensing ganglion at stage 17, most axons have aligned along the proximodistal axis (Fig. 3c).

To perform a detailed analysis of associations between placode and neural crest cells in the forming ganglion, we used quail/chick dorsal neural tube grafts coupled with GFP electroporation of the ectoderm in the same embryos (Fig. 3d–f). The trigeminal ganglia of these embryos are well condensed into a stereotypic bi-lobed structure comprised of ophthalmic (OpV) and maxillo-mandibular (MmV) branches. By stage 18, quail-derived trigeminal neural crest cells are intermixed with GFP-expressing placode neurons and have segregated from the rest of the midbrain crest stream that now surrounds the eye and occupies the first branchial arch (Fig. 3e). Neural crest and placode cells are observed throughout the ganglion, with the exception of the most proximal portion, which is solely neural crest-derived (Fig. 3f). This prefigures the segregation of neural crest-derived neurons in the proximal portion and placode-derived neurons in the distal part of the ganglion in the nearly mature ganglion at embryonic day 12 (stage 38) (D'Amico-Martel and Noden, 1983). These results show that throughout gangliogenesis, the trigeminal precursor cells intermingle and are in direct contact with each other. To further examine placode–neural crest interactions, we developed an ecto-mesenchyme culture system (Fig. 3g). We labeled the two cell types by in ovo electroporation with a GFP expression construct introduced into either the presumptive neural tube or ectoderm.

Trigeminal tissue was then explanted, encompassing both the placodal ectoderm and adherent underlying mesenchyme from stage 13 embryos, coinciding with the time of predicted cell–cell interactions. By visualizing the degree of contact, we found that the two cell populations remained tightly associated and intermingled. They exhibited abundant processes and regions of close cell–cell association (Fig. 3h–k). This raised the intriguing possibility that cell–cell interactions between placode and neural crest cells may mediate gangliogenesis.

2.4.2 Expression of Robo2 on placodes and Slit1 on neural crest

We next investigated whether Robo receptors and their cognate Slit ligands were good candidates for mediators of trigeminal ganglion formation by examining their gene expression patterns. Robos 1–2 receptors can bind to all three Slits with comparable affinity (Brose et al., 1999). We found that Robo2, but not Robo1, transcript is present in the trigeminal ganglion and its precursors during gangliogenesis. By stage 12, Robo2 is expressed in the ectoderm adjacent to the presumptive midbrain (Fig. 4a), in the region fated to give rise to the trigeminal placodes (D'Amico-Martel and Noden, 1983). Conversely, Slit1, but not Slit2 or Slit3, transcript is expressed by migratory midbrain and anterior hindbrain neural crest cells that contribute to the trigeminal ganglion (Fig. 4b). Trigeminal placode cells continue to express Robo2 as they ingress and intermix with migratory neural crest cells at stage 14 (Fig. 4c) and through trigeminal ganglion formation at stage 18, with the MmV lobe having an apparently weaker Robo2 signal than the OpV (Fig. 4d). In contrast, Slit1 is transiently expressed during cranial neural crest migration (Fig. 4e) and down-regulated in the ganglion by stage 18 (Fig. 4f).

Robo2 expressing GFP-labeled placode cells intermix with migratory neural crest cells (Fig. 4g,h) at times when neural crest cells are expressing Slit1 (Fig. 4i,j) during

stages 13–14. Robo2 appears to be expressed in discrete, dispersed regions in the surface ectoderm (Fig. 4g,h), characteristic of cells about to detach. All ingressed GFP positive cells are also Robo2 positive. Thus, Robo2 appears to begin marking placode cells that are either ingressing or preparing to do so. Our results show that placode and neural crest cells concurrently express the receptor–ligand pair, Robo2 and Slit1, respectively, during a discrete time window consistent with their potential role in initial placode–neural crest interactions and early ganglion assembly.

2.4.3 Placode and neural crest cells interact reciprocally

If placode–neural crest interactions are indeed important for trigeminal ganglion formation, removal of either population should result in abnormal development, including possible reduction or malformation of the ganglion. To determine the importance of heterotypic cell interactions, we first ablated the placode population and assessed its effect on the neural crest. Ablation of presumptive placodal ectoderm resulted in loss of the placodal markers, β-neurotubulin (TuJ1) and Robo2 (Fig. 5a), verifying removal of most of the tissue. After placode removal, the neural crest population did not coalesce properly into the ganglion (Fig. 5a,b). Instead, the cells appeared dispersed or shifted toward the periocular region. In fact, condensed neural crest cells were only observed in regions where some residual placode cells were present (Fig. 5b).

For the reciprocal experiment, neural folds (containing presumptive neural crest cells) were ablated and the subsequent effects on placode development examined. This resulted in the loss of most, but not all, of the neural crest marker, Sox10 (Cheng et al., 2000) (Fig. 5a). Removal of the majority of neural crest cells led to failure of trigeminal placode cells to make proper connections to the hindbrain, similar to the case previously observed for epibranchial ganglia (Begbie and Graham, 2001a). In addition, these cells

failed to integrate into a single trigeminal ganglion (Fig. 5a). This effect was most striking in the OpV region where placode cells often condense in one large and several smaller clusters of cells and exhibit disorganized axonal projections. In contrast, neural crest ablation does not appear to affect placodal ingression or differentiation since placodal cells continue to express neuronal markers (TuJ1 and Islet1) and Robo2. Taken together, these results suggest essential but distinct roles of neural crest and placodes for proper ganglion formation. Neural crest cells appear to make a scaffold that integrates placode cells into a properly shaped ganglion with appropriate connections to the hindbrain, though the latter defect may be partially due to incomplete neural tube closure following ablation. Placode cells, on the other hand, act as crucial mediators of neural crest condensation. This raises the intriguing possibility that intercellular signaling between these two cell types may coordinate gangliogenesis.

2.4.4 Robo2 function is required for proper gangliogenesis

To test a potential role for Robo signaling during ganglion formation, we sought to block the function of Robo2 in vivo. To this end, we introduced by electroporation into the trigeminal ectoderm a GFP-tagged dominant-negative version of the Robo2 receptor (Robo2Δ-GFP) (Hammond et al., 2005) that lacks the intracellular domains required for signaling. Embryos electroporated at stages 8–10 were examined either at early stages of ganglion formation (stages 15–16) or after the ganglion had condensed (stages 17–18).

The results show that in contrast to control GFP electroporated embryos (Fig. 6a–c), perturbation of Robo2 signaling inhibits proper assembly of placode cells, causing the ganglion to assume a highly dispersed morphology (78.6% in OpV and 16.7% in MmV) (Fig. 6d–f) at stages 15–16. This was shown by both displacement of placode neuronal cell bodies and misorientation of axonal projections (Fig. 6e,f). By stages 17–18,

placode-derived neurons have coalesced normally in control embryos (Fig. 6g–i) but abnormally in multiple or branch-like aggregates (57.1% in OpV; 7.7% in MmV) in Robo2Δ-GFP electroporated embryos (Fig. 6j–l). Both the OpV and MmV nerve fibers failed to properly fasciculate towards their normal targets. The effects were highly reminiscent of those following neural crest ablation, with more severe defects in the OpV than the MmV lobes. For both experimental and control cases, we scored only those embryos with broad GFP expression in most of either the OpV, MmV or both lobes. Statistical analyses of these embryos are summarized in Fig. 6m,n.

2.4.5 Perturbation of Robo2 disrupts placode ingression.

To examine whether Robo2 plays an important function in placodal ingression, we next examined the effects of blocking its signaling at stage 14, reflecting the time of maximal interactions between ingressing placode cells and migratory neural crest cells that express Slit1. Compared with stage-matched controls (Fig. 7a–c), in Robo2Δ-GFP embryos trigeminal placode cells appeared more dispersed (Fig. 7d–f). In contrast to controls where most placode cells have ingressed into the neural crest derived mesenchyme (Fig. 7g), the majority either remained in the surface ectoderm or associated with the basal margin of the ectoderm (Fig. 7h), suggesting a defect in placodal ingression and/or migration. The percentage of placode cells associated with the ectoderm in the Robo2Δ-GFP embryos (64.2 ± 8.6 %) was significantly higher than those in the control embryos (25.6 ± 4.2 %; $P<0.0001$, two-tailed t-test assuming equal variances) (Fig. 7i).

This is likely to reflect a delay rather than inhibition of cell movement since most Robo2Δ-GFP expressing placode cells migrated into the mesenchyme by stages 17–18 (data not shown). Thus, blocking Robo2 signaling appears to cause placode cells to remain

in the surface ectoderm for an abnormally long time, thereby delaying their interactions with neural crest cells until times when the latter has down-regulated the Slit1 ligand.

2.4.6 Effect of Robo2 perturbation on neural crest assembly

In contrast to its effects on placode ingression, inhibition of the Robo2 signaling in the ectoderm does not alter neural crest migration (Fig. 8e). However, unlike control embryos (Fig. 8a), during later stages as the ganglion assembles, neural crest cells, as assayed by Sox10 expression, are abnormally localized in a pattern that mirrors the abnormal organization of the placode cells with blocked Robo2 signaling (Fig. 8b,c).

Intriguingly, this phenocopies the effects of placode ablation where the neural crest cells appear to aggregate in the same places as the residual placode cells. Transverse sections through the OpV region of these embryos reveal clustering of Sox10 expressing neural crest cells with Robo2Δ-GFP expressing placode cells (Fig. 8b,c). Since Robo2Δ-GFP encodes a membrane-tethered construct, the effects are non-cell autonomous and likely mediated by interactions between aberrantly disorganized placode cells expressing Robo2Δ-GFP and the affected wild type neural crest cells.

2.4.7 RNAi knockdowns of Robo2 and Slit1 cause ganglion defects.

Use of a dominant negative construct has the caveat that it is likely to perturb all Robos rather than being specific for Robo2; in addition, it interferes with all Slits. To specifically test the role of Robo2 and Slit1 in trigeminal ganglion formation, we turned to an alternative approach using RNA interference (RNAi) mediated knockdown. To this end, we used synthetic microRNA (miRNA) vectors designed to selectively target Robo2 or Slit1, while concomitantly expressing RFP (Das et al., 2006).

Electroporation of Robo2 miRNA into the placodal ectoderm at stages 8–10, prior to ingression, caused reduction of Robo2 mRNA levels in the forming ganglia (Fig. 9) but had no effect on the placodal marker, Pax3 (data not shown). Analyzing ganglion formation by similar criteria to those employed for Robo2Δ-GFP above, Robo2 RNAi affected placode cells in a manner that phenotypically resembled that of the dominant negative construct with more severe defects in the OpV than the MmV lobe (Fig. 10). Compared to controls (Fig. 10a–c), trigeminal placode neurons transfected with Robo2 miRNA tended to form dispersed aggregates and elaborated abnormal and branched projections (Fig. 10d–f). These effects were similar but generally less severe than those noted with the dominant negative construct, likely because of incomplete knockdown since message levels were decreased but not eliminated by the miRNA. To control for non-specific effects of the backbone RNAi vector, we performed parallel experiments using the GFP miRNA which targets GFP. Although the control RNAi caused some general toxicity when introduced into the ectoderm, effects of the Robo2 miRNA were markedly more severe, specific, and distinguishable.

To examine the functional role of the Slit1 ligand, we introduced the Slit1 miRNA in the presumptive neural crest tissue by electroporation at stages 4–9. Slit1 miRNA resulted in a depletion but not absence of Slit1 on the electroporated side (Fig. 9). At stages of ganglion formation, compared to the control GFP miRNA electroporated embryos (Fig. 10g–i), Slit1 miRNA mediated depletion of Slit1 in the neural crest caused aberrant assembly of placode cells such that they aggregated abnormally in dispersed clumps and tended to form OpV and MmV lobes that were either misaligned or appeared closely apposed in the interlobic region (Fig. 10j–l). To control for possible off-target effects, we examined other neural crest markers after Slit1 miRNA as well as performed rescue experiments with a mouse Slit1 construct. Slit1 miRNA had no effect on neural crest markers, such as Slug and HNK-1; furthermore, co-electroporation with mouse Slit1

resulted in a significant rescue of the numbers of abnormal ganglia, from ~50% to 20% (n = 10, data not shown). Statistical analyses of Robo2 miRNA and Slit1 miRNA embryos are summarized in Fig. 10m,n.

Taken together, abrogating Robo2–Slit1 interaction with dominant negative Robo2, Robo2 miRNA or Slit1 miRNA mimics the effects of neural crest ablation. This suggests a mechanism whereby signaling between this receptor/ligand pair underlies interactions between neural crest and placodal cells in trigeminal ganglion formation.

2.5 Discussions

2.5.1 Tissue ablations uncover reciprocal neural crest–placode interactions

Tissue ablation experiments suggest that interactions between placode and neural crest cells are critical for formation of the trigeminal ganglion. However, the cellular and molecular nature of these interactions has been an open question. Here, we apply a combination of classical embryological and modern molecular techniques to solve this long-standing puzzle. Our data show that proper assembly of the trigeminal ganglion relies on the intimate and coordinated interactions of placode and neural crest cells, such that removal of either cell populations results in striking defects in ganglion formation. Our results are consistent with previous ablation studies, noting dispersed (Hamburger, 1961) or smaller ganglia (Lwigale, 2001) in neural crest ablated embryos and some loss of the ganglion (Lwigale, 2001) in placode ablated embryos. However, these analyses were performed at stages 34–35 or later, by which time a considerable amount of tissue regeneration may have occurred. To minimize such regulation, we removed broader tissue

regions encompassing the entire presumptive trigeminal placode or neural crest domains and analyzed the effects at times of cell ingression and ganglion formation. Our ablation experiments show that neural crest–placode interactions are prevalent and interdependent at early stages. Removal of neural crest results in dispersed placodal aggregates, and a lack of proper axonal trajectories to the brain and sensory organs. This suggests that neural crest cells make a scaffold on which placode cells organize. In the absence of this scaffold, placode cells appear to be able to aggregate, but do so with abnormal morphology. Additionally, neural crest cells may play a critical role in guiding placodal axons. Previous attempts of ablating the trigeminal placodes have so far been marked by incomplete placodal removal and regeneration and thus results were inconclusive (Hamburger, 1961; Stark et al., 1997). In our study, to minimize possible regeneration, we have conducted our ablations at later stages— at about 16 somite stage (late stage 11 to stage 12)— and also subsequently verified the extent of the placodal ablation by staining for placodal neurons. In many cases, we were successful in removing nearly all the placodal ganglion and in others most was removed except for a small placodal component. Both extents of ablation provided insightful information about the role of placodal cells on neural crest. From these data, we clearly demonstrate for the first time the dependence of neural crest on placodal cells in condensation into ganglion. We show that neural crest cells, by a mechanism that is currently unknown, appear to only assemble and coalesce in the same places as the placodal cells.

Similar coordination between neural crest and placode cells may be a general feature of all developing cranial ganglia of dual origin. For example, there is evidence that neural crest ablation disrupts central axon targeting of the epibranchial ganglia, suggesting that the neuroglial hindbrain crest cells may guide epibranchial placode cells into the mesenchyme and towards the central nervous system to establish their central projections (Begbie and Graham, 2001a). However, the underlying mechanisms were not clear.

2.5.2 Mechanism of Slit1–Robo2 on organizing trigeminal placodal cells and its indirect effect on neural crest

The complementary expression patterns of the Robo2 receptor in placode cells and its cognate ligand, Slit1, in the cranial neural crest raised the intriguing possibility that Slit–Robo signaling may be responsible for coordinating cell–cell interactions during trigeminal ganglion formation. To test this idea, we functionally perturbed Robo2 signaling in vivo and found that this results in delayed placodal ingression and migration to the trigeminal anlage. This in turn causes a dramatic disorganization of the forming placodal ganglion and secondarily, leads to abnormalities in the assembly of neural crest cells. The non-cell autonomous effect on neural crest cells is not surprising considering the high degree of interactions between neural crest and placodal cells during ganglion assembly that we found from our cell–cell interactions and ablation studies. Since Slit1 is a large, secreted molecule, it is unlikely that this is caused by reverse signaling in which Robo2 on placode cells activates Slit1 in neural crest cells. Rather it is likely to be mediated by other, as yet unknown, secondary factors. Effects of Robo2 inhibition on placode cells were similar to those of neural crest ablation that effectively removes the source of the ligand Slit1. This is supported by our RNAi data, showing that depleting either receptor or ligand causes malformation of the ganglion. The data support a mechanism whereby the Robo2 receptor on placode cells binds to the Slit1 ligand on neural crest cells to mediate proper ganglion assembly. This is the first demonstration of involvement of signaling molecules in trigeminal cell–cell interactions. In addition, Slit-independent functions of Robo2 may also occur, since Robo–Robo2 interactions have been implicated in other systems (Hivert et al., 2002; Parsons et al., 2003).

Our results reveal a novel role for Robo2 signaling as a mediator of cell–cell interactions during gangliogenesis. Ligand–receptor interactions between Slits and Robos

have been widely implicated in repulsive axon guidance in various aspects of nervous system development, such as commissural axon crossing in the central nervous system (Kidd et al., 1999) and formation of the lateral olfactory tract (Fouquet et al., 2007). The function of Slit as a repulsive cue at the midline is conserved across invertebrates (Kidd et al., 1999; Kidd et al., 1998) and vertebrates (Long et al., 2004). However, Slit1 does not seem to act as a repulsive signal between placode and neural crest, as we noted no evidence of avoidance or inhibitory behavior. In fact, both in vivo and in vitro analyses suggest that the neural crest and placode cells extensively intermix and contact one another throughout phases of migration and ganglion formation. Rather, the results suggest that these cell types intimately interact to reciprocally organize one another into the proper anatomical structure of the trigeminal ganglion. Consistent with our results, novel roles for Slit–Robo signaling have emerged more recently in the fly heart (Santiago-Martinez et al., 2006) and mammary duct (Strickland et al., 2006) where they function as cell adhesion and alignment cues. Our data suggest that Slit–Robo signaling acts as a positive regulator of placode ingression, cell positioning, and/or placode axon guidance during trigeminal gangliogenesis, consistent with a novel role in cell–cell interactions during morphogenesis. Intriguingly, Slit1 is down-regulated while Robo2 receptor expression persists, suggesting that interactions are time-limited. At later stages, it is possible that Robo2 might interact with itself or Slits in other tissues. Finally, we cannot rule out a possible function for Robo3 (Rig-1) and Robo4 in ganglion formation, since these are yet to be isolated in aves. However, based on their expression and function in other systems, this possibility seems unlikely since Robo4 is only expressed in endothelial cells with a function in angiogenesis (Park et al., 2003; Suchting et al., 2005), and its ability to bind to Slits is controversial (Suchting et al., 2005). Robo3 expression is known to be mainly restricted to the mammalian central nervous system where it acts as a negative regulator of Slit responsiveness (Sabatier et al., 2004).

2.5.3 Implications on the differences between OpV and MmV placodes

Although defects were observed in both trigeminal lobes, we observed more severe anomalies in the OpV than MmV lobes for both Robo2 perturbation (either using Robo2Δ-GFP or Robo2 miRNA) and neural crest ablation. This may reflect inherent differences between the OpV and MmV placodes which arise from distinct regions to give rise to the respective OpV and MmV lobes of the trigeminal ganglion (Baker and Bronner-Fraser, 2001; D'Amico-Martel and Noden, 1983; Schlosser, 2005). This is consistent with the fact that these populations may be in part molecularly distinct in aves (Baker and Bronner-Fraser, 2001; Begbie et al., 2002), having mutually exclusive expression of Pax3 and neurogenin-2 (at least transiently) in the OpV and neurogenin-1 in the MmV placode. Furthermore, OpV and MmV placode cells are thought to be ancestrally separate. In amphibians, two separate ganglia form and later fuse (Northcutt and Brandle, 1995; Schlosser and Roth, 1997). Some gnathostomes, including basal ray-finned fishes and small-spotted dogfish sharks, have two distinct ganglia (O'Neill et al., 2007; Piotrowski and Northcutt, 1996; Schlosser, 2005), namely the profundal and trigeminal ganglia which are considered analogous to the OpV and MmV lobes in amniotes, respectively. Thus, although the Robo2 receptor is expressed by both OpV and MmV placode cells (albeit weaker expression in the MmV lobe), its role in cell–cell interactions may be more prominent in the OpV placode cells. Accordingly, a selective defect in arborization of the OpV branch was found in Slits and Robos mutant mice (Ma and Tessier-Lavigne, 2007), though gangliogenesis was not studied. Regardless of differences in severity of the defect, our data suggest that the Robo2 receptor plays a crucial role in mediating proper integration of the placode neurons in both lobes.

2.5.4 Possible downstream mechanism of Slit1–Robo2 in gangliogenesis

As a possible downstream mechanism, Slit activation of Robo has been shown to inhibit the cell adhesion molecule N-cadherin (Rhee et al., 2002) that has been implicated in formation of other peripheral ganglia (Kasemeier-Kulesa et al., 2006) and various morphogenetic events (Hatta and Takeichi, 1986). This raises the intriguing possibility that Slit–Robo interactions may regulate N-cadherin function in trigeminal precursors. In this scenario, the expression of Slit1 during early neural crest–placode interactions may be responsible for maintaining Robo2 expressing placode neurons in a less aggregated state, thus allowing intermixing of the two precursor cell types prior to their condensation. At later times when Slit1 is downregulated, N-cadherin may be upregulated and thus promote ganglionic condensation.

2.5.5 Conclusions

In summary, we demonstrate an essential function for the Robo2 receptor expressed by the trigeminal placodes in organizing both placodal neurons and Slit1-expressing neural crest cells into the proper anatomical structure of the trigeminal ganglion. This represents a previously unknown role for vertebrate Robo–Slit signaling in cell assembly and gangliogenesis. The results provide novel insights into cranial ganglion formation and, for the first time, a putative molecular signaling event underlying placode–neural crest interactions during aggregation of the largest of the cranial ganglia. Understanding the mechanisms that drive integration of the two embryonic structures that give rise to nearly all cranial ganglia sheds important light on the mechanisms mediating organization of the vertebrate sensory nervous system.

2.6 Acknowledgements

I thank Raman Das and Stuart Wilson for the design and construction of the RNAi vectors, Sarah Guthrie for the Robo2Δ-GFP plasmid, Peter Lwigale for our work on the ablation and grafting experiments and many insightful discussions, and members of the MBF lab for technical support. This work was supported by NIH NRSA 5T32 GM07616 to C.E.S., NIH Minority Supplement grant DE016459-07S1 to P.Y.L., Biotechnology and Biological Sciences Research Council (U.K.) to R.D., and NIH grant DE16459 to M.B.F.

Figure 1.

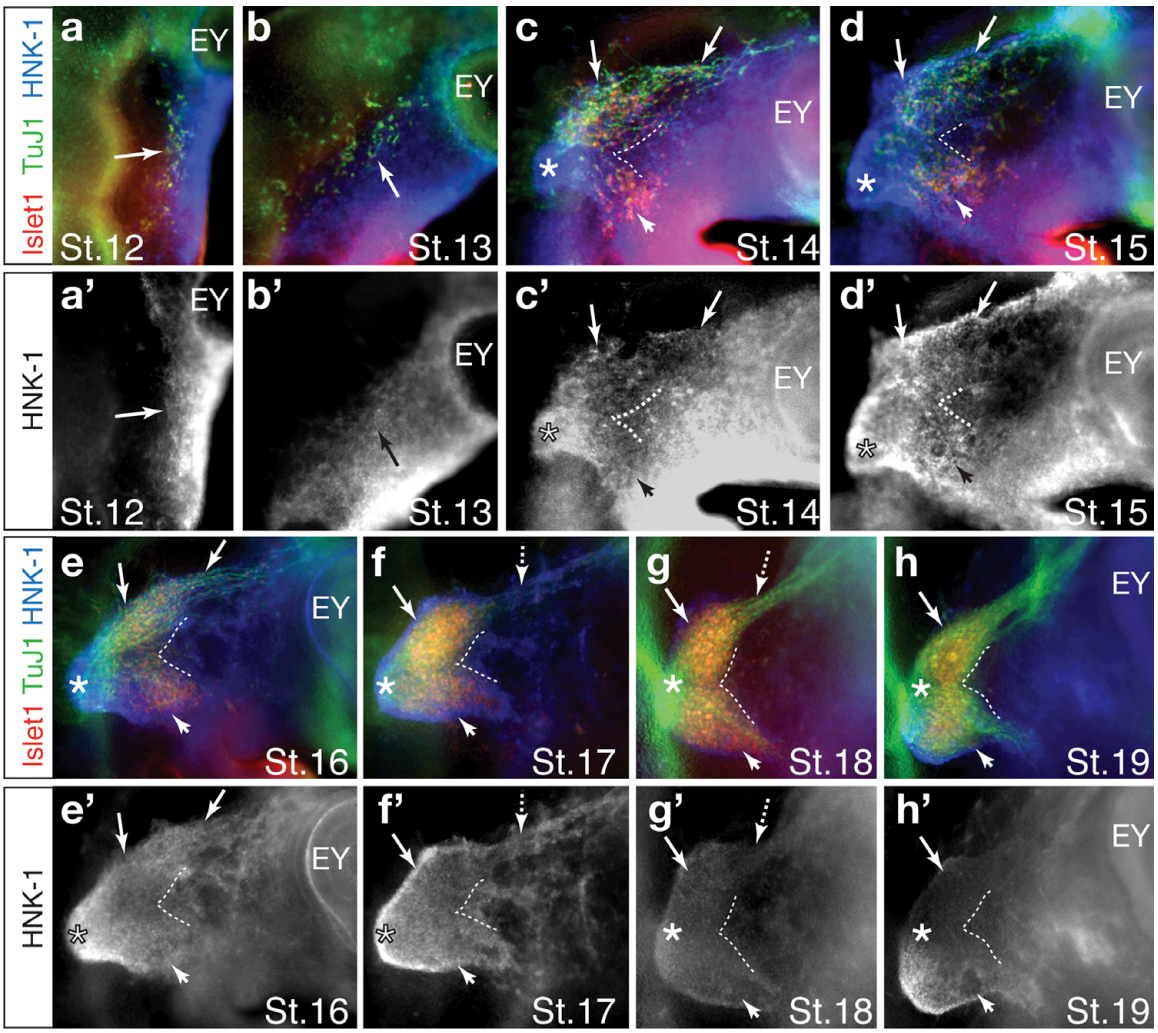
Islet1 TuJ1 HNK-1
a
EY
St.12
b
EY
St.13
c
EY
St.14
d
EY
St.15
HNK-1
a'
EY
St.12
b'
EY
St.13
c'
EY
St.14
d'
EY
St.15
Islet1 TuJ1 HNK-1
e
EY
St.16
f
St.17
g
St.18
h
EY
St.19
HNK-1
e'
EY
St.16
f'
St.17
g'
St.18
h'
EY
St.19

Figure 1. Chick embryos at successive stages between 12 and 19 show progressive development of the trigeminal ganglion. (**a**–**h**) During these stages, there is extensive overlap and intermingling of placodal and neural crest cell populations, as visualized using antibodies against Islet1 and TuJ1 for placodal cells and HNK-1 for neural crest cells (also shown in **a'**–**h'**). By stage 12, (**a**) several placodal cells can be detected diffusely distributed along the dorsal edge of the (**a'**) neural crest stream (arrow) between the levels of the developing eye and anterior hindbrain. (**a**–**d**) From stages 12–15, the OpV placodal neurons (arrows) appear first and are already located more dorsally than the MmV placodal cells (arrowheads). Though diffuse, placodal cells already prefigure the morphology of the future bi-lobed ganglion. (**a'**–**h'**) Assembly of trigeminal placodal cells takes place within the domain of the trigeminal neural crest stream throughout development; (**c**) by stage 14 the most proximal region (asterisk) already appears to be occupied by only neural crest cells. (**e**) By stage 16, the interlobic region (demarcated by the white dotted lines) that lies between the OpV and MmV lobes is mostly devoid of placodal neurons, and the trigeminal neural crest has begun to segregate from the periocular neural crest. This results in an increasingly more defined trigeminal morphology. (**f**–**g**) By stages 17–18, placodal and neural crest cells are well condensed into the ganglion and few placodal cell bodies are found along the OpV projection (dotted arrow). EY, eye; *, most proximal region to hindbrain.

Figure 2.

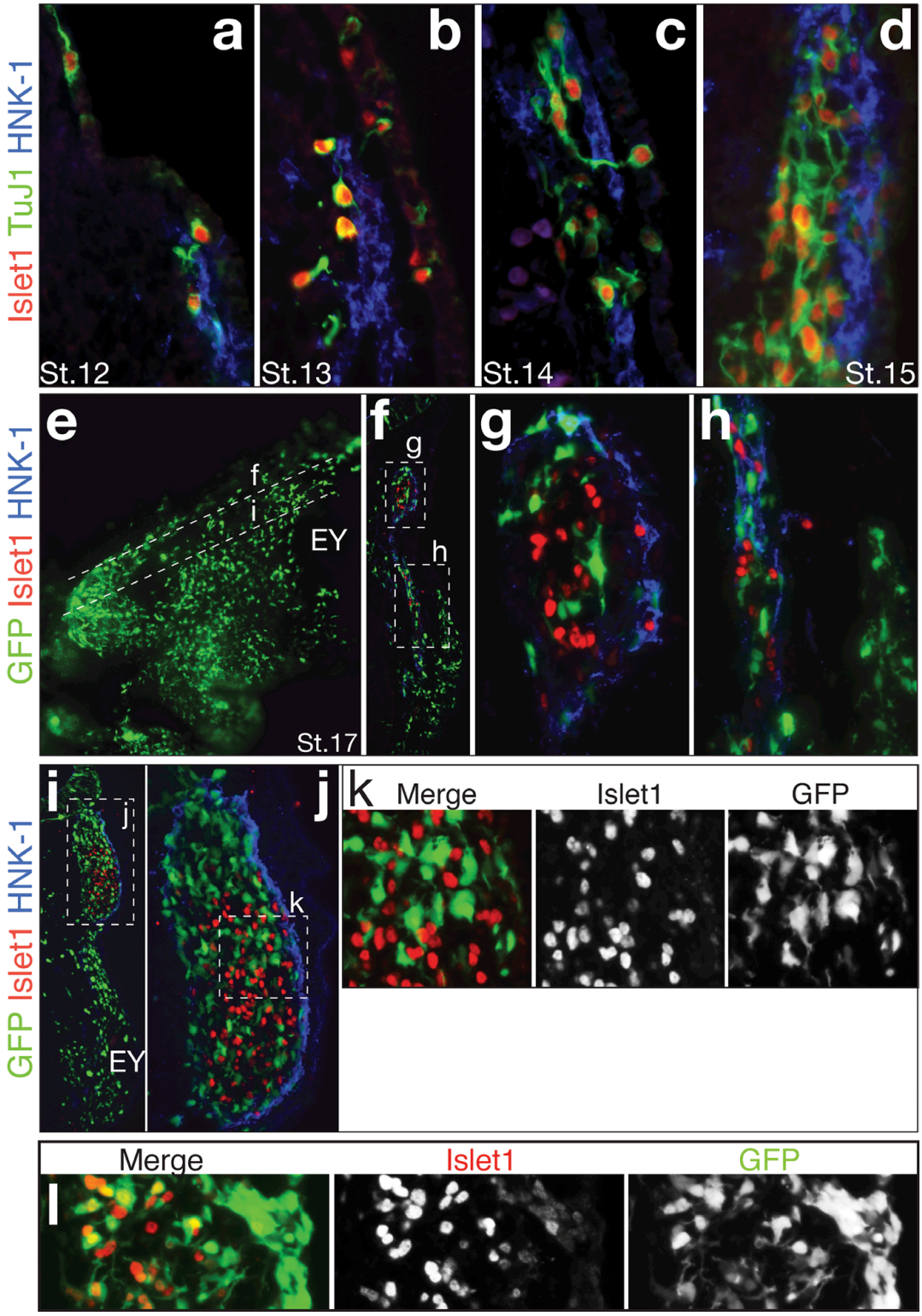
a
b
c
d
Islet1 TuJ1 HNK-1
St.12
St.13
St.14
St.15
e
f
g
h
GFP Islet1 HNK-1
EY
St.17
i
j
k
Merge
Islet1
GFP
l

Figure 2. Placodal neurons and neural crest cells intermingle intimately to form the ganglion in vivo. (**a**–**d**) Transverse sections of chick embryos showing neural crest and placodal cells at stages 12 –15. Placodal neurons (Islet1+ and TuJ1+) begin to ingress from the ectoderm by stage 12 and continue to be generated in the ectoderm prior to undergoing an epithelial-to-mesenchymal transition to migrate into the same region as the HNK-1+ neural crest cells. Placodal cells make abundant cell contacts among themselves as well as with the neural crest cells. (**e**–**k**) Placodal and neural crest cells continue to exhibit intimate contacts throughout gangliogenesis, as visualized by GFP-labeled neural crest cells closely intermixing with Islet1+ placodal cells in the condensed ganglion at stage 17. (**e**) At stages of placodal condensation into the ganglion, the trigeminal neural crest cells also condense into the ganglion and have separated from the other neural crest populations which are surrounding the eye and migrating into the first branchial arch. (**f**–**k**) Neural crest cells labeled by GFP condense wherever the Islet1+ placodal cells are present, intermixing with placodal cells (**g**, **i**–**k**) in the ganglion lobe and (**h**) along the OpV projection. (**l**) A section through the trigeminal ganglion of an embryo that was electroporated with a GFP construct in the ectoderm; coexpression of neuronal marker Islet1 with GFP expression in the placode-derived cells at stage 17 affirms the placodal origin of the neurons. EY, eye.

Figure 3.

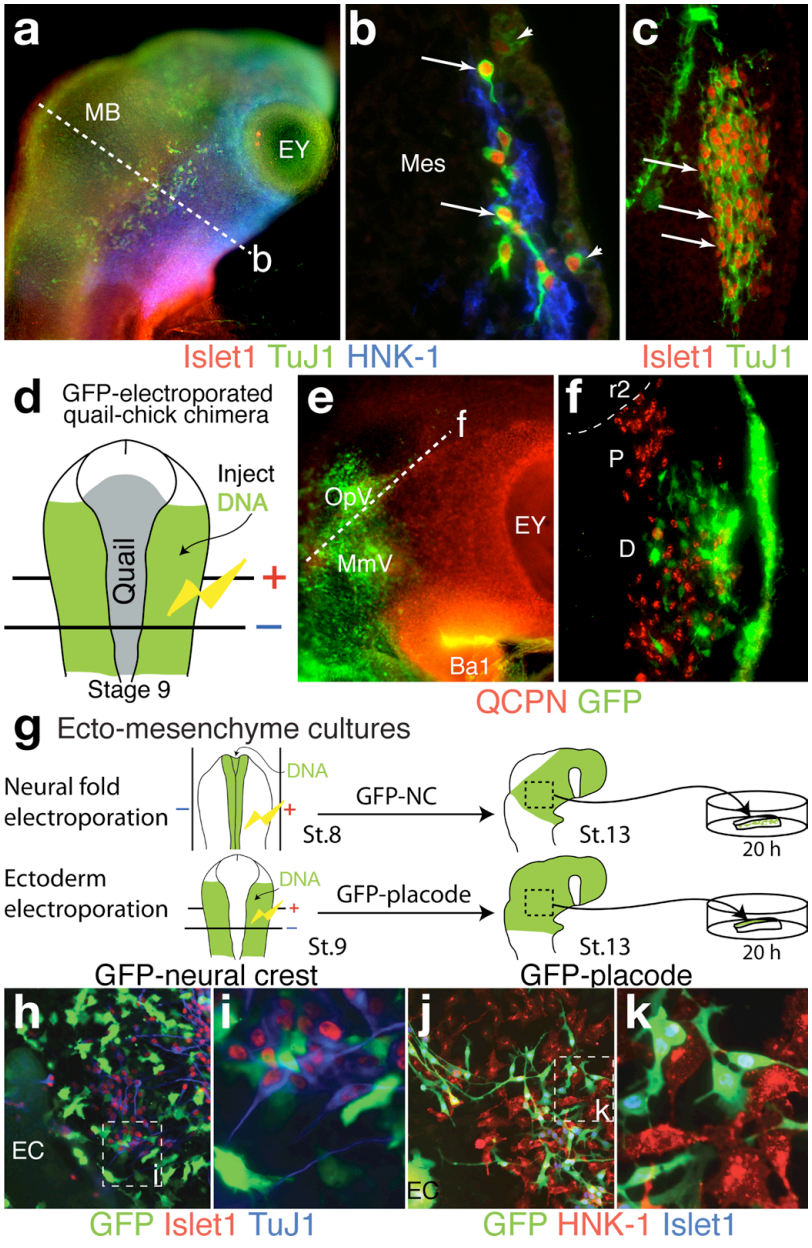
a
MB
EY
b
b
Mes
c
Islet1 TuJ1 HNK-1
Islet1 TuJ1
d
GFP-electroporated
quail-chick chimera
Inject
DNA
Quail
+
−
Stage 9
e
f
OpV
EY
MmV
Ba1
f
r2
P
D
QCPN GFP
g
Ecto-mesenchyme cultures
Neural fold
electroporation
DNA
GFP-NC
St.8
St.13
20 h
Ectoderm
electroporation
DNA
GFP-placode
St.9
St.13
20 h
GFP-neural crest
GFP-placode
h
i
j
k
EC
i
k
EC
GFP Islet1 TuJ1
GFP HNK-1 Islet1

Figure 3. Placode and neural crest cells are in contact during trigeminal gangliogenesis. (**a**) Stage 13 chick and (**b**) cross section at the dotted line in **a** showing TuJ1+ and Islet1+ placodal cells (arrowheads) in the surface ectoderm and (arrows) in close contact with HNK-1+ neural crest cells. (**c**) Cross section through the OpV region of the condensed trigeminal ganglion at stage 17. (**d**) Schematic of chick embryo with ectoderm electroporated with a GFP construct and a quail neural fold graft. (**e**) Resulting chimera showing contribution of quail-derived neural crest cells (positive for the quail nuclear marker QCPN) and placodal cells (GFP+) in the stage 18 ganglion. (**f**) Transverse section through the OpV region at the dotted line in **e** showing distribution of QCPN+ neural crest cells and GFP+ placodal cells. (**g**–**k**) Using a tissue culture system to examine trigeminal placode–neural crest interactions. GFP labeling either the neural crest cells or the placodal cells show direct contacts between cytoplasmic protrusions of neural crest cells and the neuronal processes of placodal cells. MB, midbrain; EY, eye; Mes, mesenchyme; OpV, ophthalmic; MmV, maxillo-mandibular; Ba1, first branchial arch; r2, hindbrain rhombomere 2; P, proximal; D, distal; NC, neural crest; EC, ectoderm explant.

Figure 4.

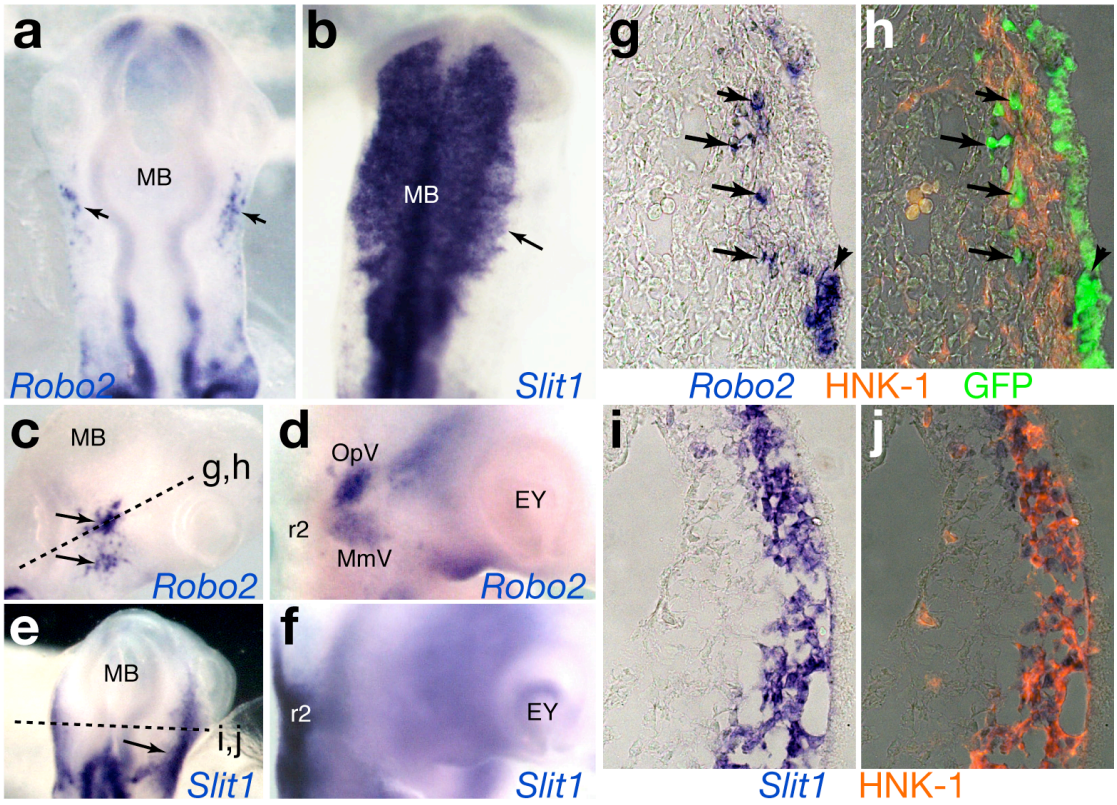

Figure 4. Expression of *Robo2* mRNA in placode and *Slit1* mRNA in neural crest cells during early development of the trigeminal ganglion. (**a**) Presumptive trigeminal placodal cells express *Robo2* (arrows) as they begin to ingress from the ectoderm. (**b**) Migratory cranial neural crest cells express *Slit1* (arrow) as early as stage 10. (**c**) *Robo2* is expressed in the OpV and MmV placodal cells at stage 14 (arrows) and (**d**) persists in the placodal component of the condensed ganglion at stage 18. (**e**) Trigeminal neural crest cells express *Slit1* at stage 13 (arrow) but (**f**) down-regulate *Slit1* in the ganglion by stage 18. (**g**) Transverse section through the OpV region at the dotted line in **c** shows *Robo2* expression both in the ectoderm (arrowhead) and ingressing placodal cells (arrows). (**h**) Overlay image of **g**, showing that *Robo2* expressing cells are GFP+, indicating their ectodermal origin, and intermingle with HNK-1+ neural crest cells. (**i**,**j**) Transverse section through the midbrain-hindbrain region of **e** shows (**i**) *Slit1* expression by (**j**) HNK-1+ migratory neural crest cells. MB, midbrain; EY, eye; r2, hindbrain rhombomere 2; OpV, ophthalmic; MmV, maxillo-mandibular.

Figure 5.

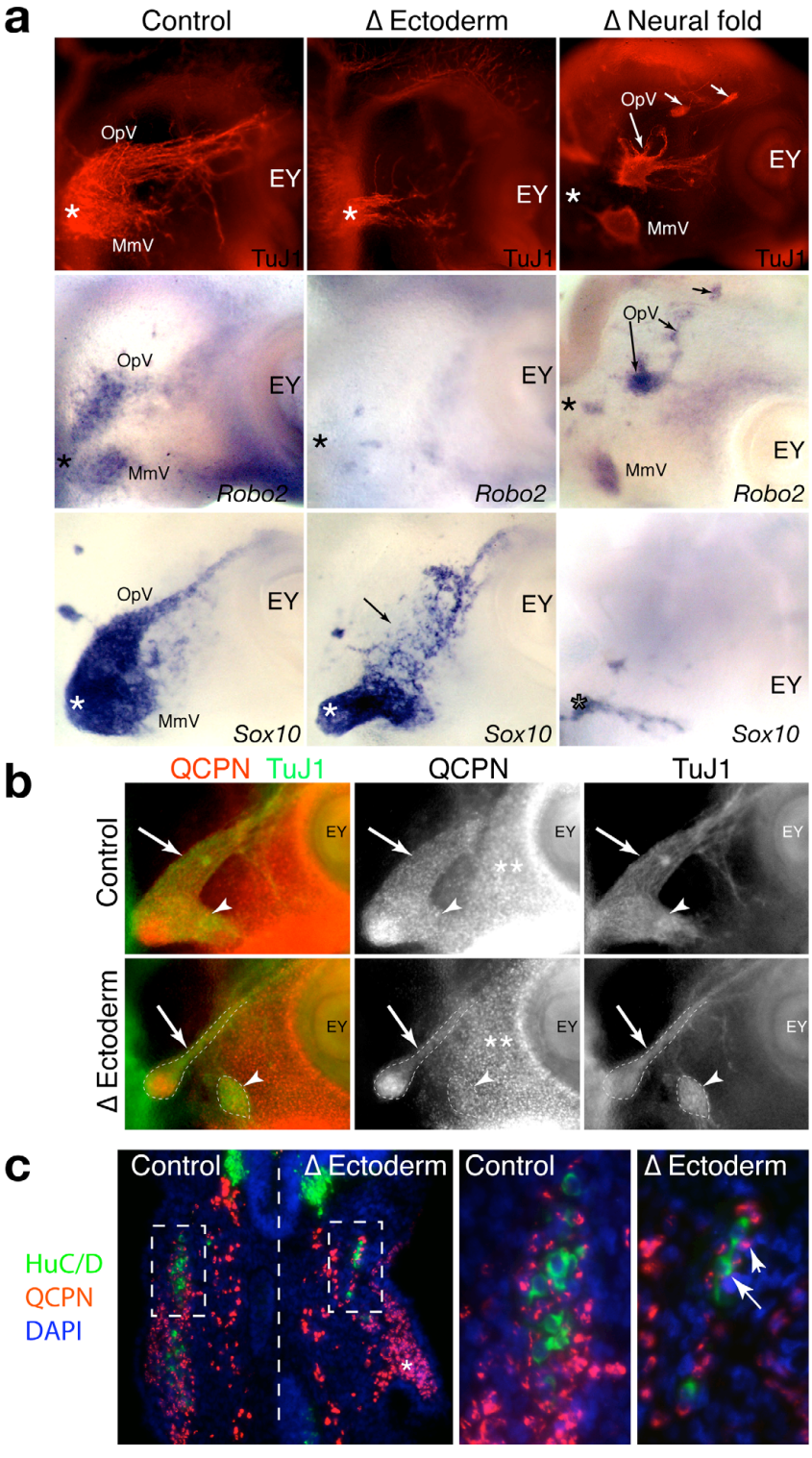
a
Control
Δ Ectoderm
Δ Neural fold
OpV
EY
MmV
TuJ1
Robo2
Sox10
b
QCPN TuJ1
QCPN
TuJ1
Control
Δ Ectoderm
c
Control
Δ Ectoderm
HuC/D
QCPN
DAPI

Figure 5. Proper formation of the trigeminal ganglion relies on reciprocal interactions between placodal and neural crest cells. (**a**) Unablated control sides show normal ganglion formation as revealed by placodal markers, TuJ1 protein and *Robo2* mRNA, and a neural crest marker, *Sox10* mRNA. Trigeminal ectoderm ablation (Δ) results in apparent removal of placode cells as shown by loss of TuJ1 and *Robo2*, and leads to aberrant neural crest condensation (*Sox10*, arrow), albeit aggregation in the most proximal region (*). Neural fold ablation leads to neural crest depletion as shown by loss of *Sox10* and results in unintegrated placodal aggregates (TuJ1+ or *Robo2*+, arrows), including disconnected OpV and MmV lobes. (**b**) Loss of neural crest condensation in placodal ectoderm ablated quail-chick chimeras. Unablated control side shows normal incorporation of QCPN+ neural crest and TuJ1+ placodes. In contrast, on ablated side of the same embryo, QCPN+ neural crest cells only condense in the region of placodal aggregation (dotted lines) formed by residual placodal cells, derived from regeneration or incomplete ablation; neural crest cells that do not condense in the ganglion appear dispersed in the periocular region (**). (**c**) Frontal plane section through an ectoderm ablated chimeric quail-chick embryo as that shown in **b** shows aggregation of quail derived neural crest cells (QCPN+) and placodal neurons (HuC/D+), and confirms that the neurons were not of neural crest origin. DAPI was used to stain all nuclei. On both the control and ablated sides, neural crest and placodal cells were found to intermix and form ganglion aggregates, albeit far fewer of them on the ablated side. On the ablated side, closely associating QCPN+ neural crest cells can be found only near the first branchial arch region (*) and not in the ganglion anlage. Each subpanel in **a** shows a different ablated embryo, except that the controls correspond to the same embryo as the adjacent ectoderm-ablated embryo. EY, eye; OpV or arrow, ophthalmic; MmV or arrowhead, maxillo-mandibular; *, in **a**, trigeminal region most proximal to the hindbrain.

Figure 6.

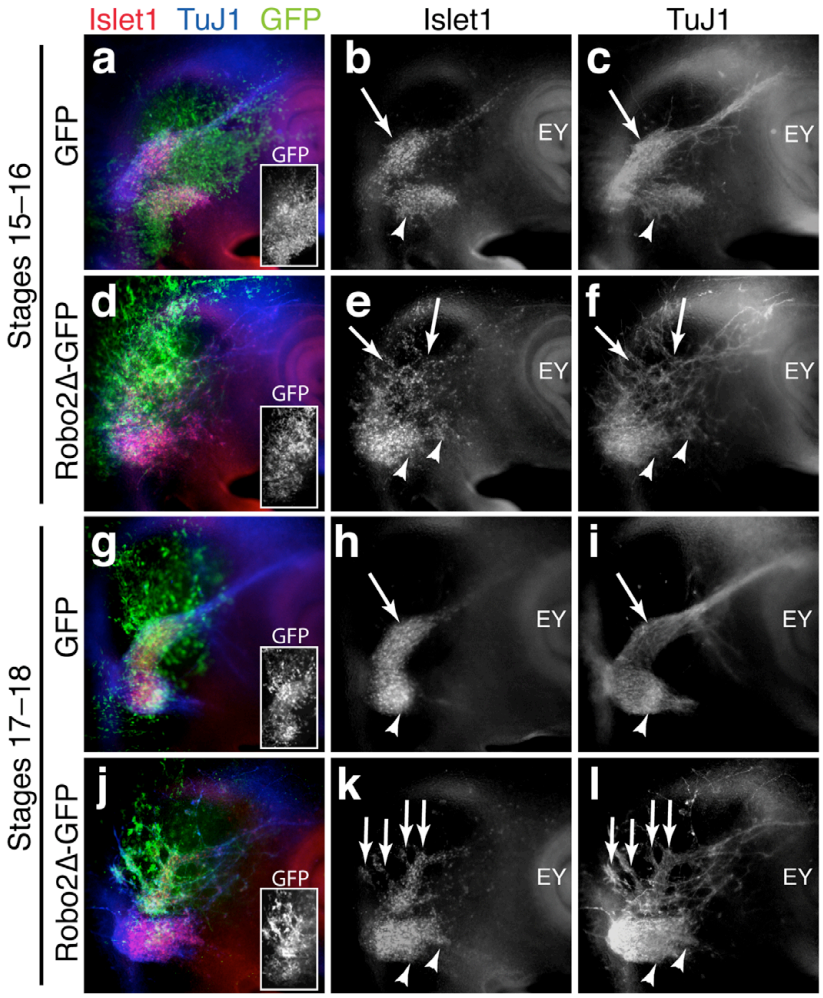

m

	Stages		*n*	Phenotype Mild	Severe
OpV	15–16	*Robo2Δ-GFP*	28	10.7% (3)	78.6% (22)
	17–18	*Robo2Δ-GFP*	21	4.8% (1)	61.9% (13)*
MmV	15–16	*Robo2Δ-GFP*	24	58.3% (14)	16.7% (4)
	17–18	*Robo2Δ-GFP*	13	53.8% (7)	7.7% (1)

n

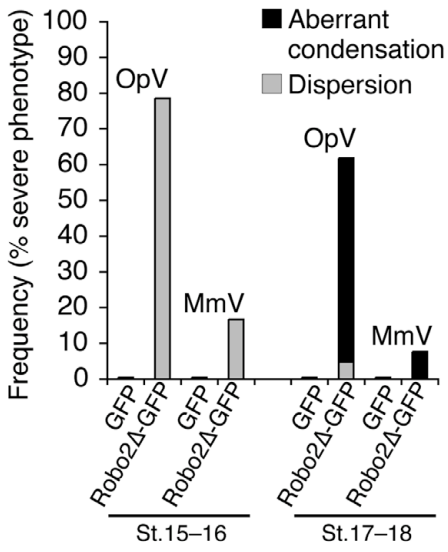

Figure 6. Inhibition of Robo2 signaling disrupts trigeminal ganglion formation. (**a**–**c**) Control GFP embryo and (**d**–**f**) Robo2Δ-GFP embryo at stages 15–16. (**g**–**i**) Control GFP embryo and (**j**–**l**) Robo2Δ-GFP embryo at stages 17–18. Placodal cell bodies (Islet1+) and neuronal processes (TuJ1+) are shown. GFP (green in color overlay panels; also shown in insets) reveals region of DNA transfection. (**m**) Effect of Robo2Δ-GFP is reported in two levels of severity: "mild" means intact but misshapen ganglia and "severe" means dispersion or aberrant condensation (branch-like or multiple aggregations) of the ganglia. Only one case (*) at stages 17–18 exhibited dispersion, and no aberrant condensation was observed at stages 15–16. Control GFP embryos showed no apparent phenotype at stages 15–16 in OpV (n = 13) and MmV (n = 12), and at stages 17–18 in OpV (n = 22) and MmV (n = 21). Numbers in parentheses represent the number of transfected ganglia showing the phenotype. (**n**) Histogram of data presented in **m** showing more severe effects in the OpV region. EY, eye; OpV or arrow, ophthalmic; MmV or arrowhead, maxillo-mandibular.

Figure 7.

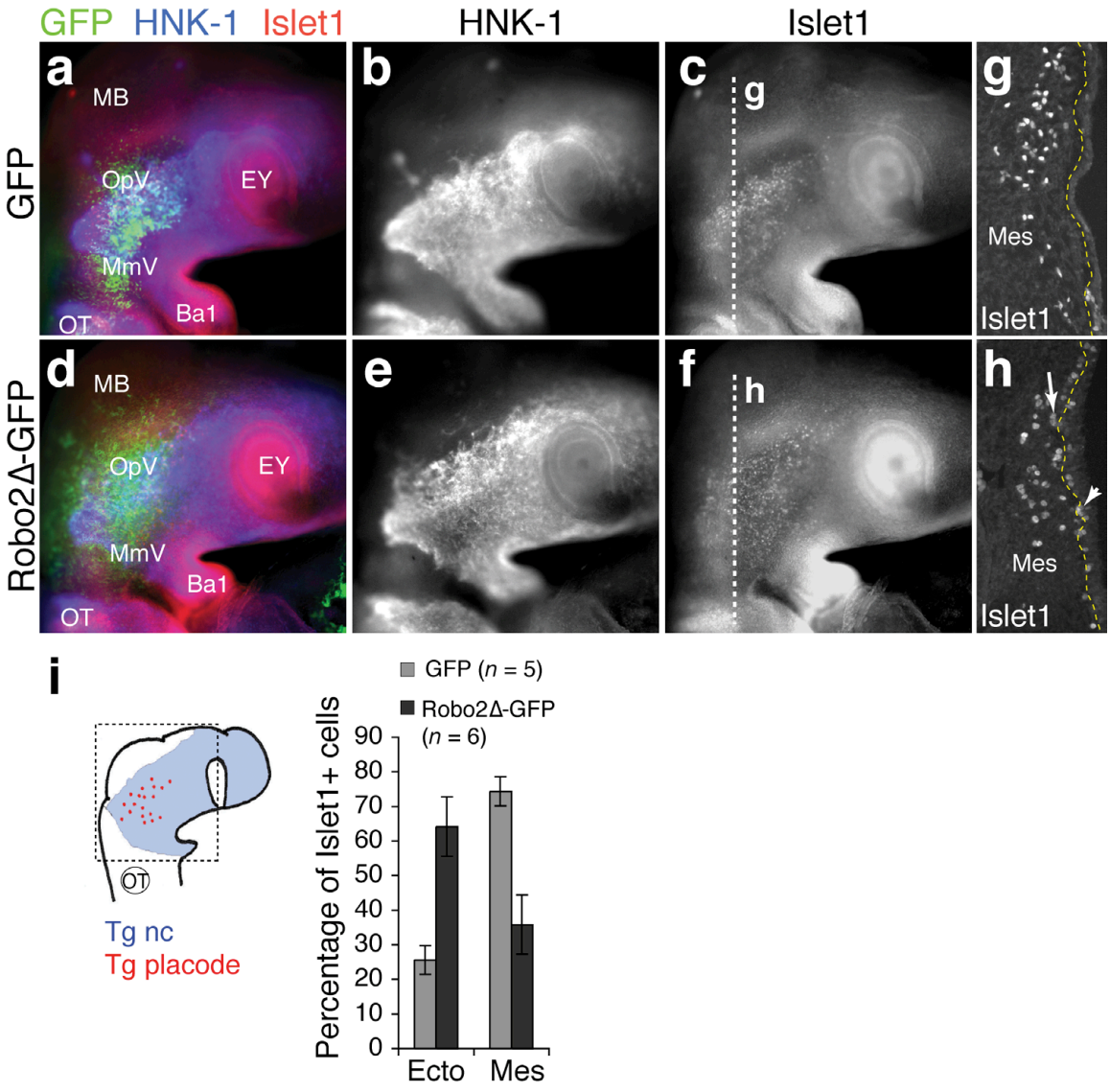
GFP HNK-1 Islet1
HNK-1
Islet1
GFP
Robo2Δ-GFP
a
b
c
g
d
e
f
h
MB
OpV
EY
MmV
Ba1
OT
Mes
Islet1
i
Tg nc
Tg placode
GFP (n = 5)
Robo2Δ-GFP (n = 6)
Percentage of Islet1+ cells
0
10
20
30
40
50
60
70
80
90
Ecto
Mes

Figure 7. Inhibition of Robo2 signaling disrupts the ingression of trigeminal placodal cells. (**a**–**c**) Control GFP electroporated embryo analyzed at stage 14 showing (**a**) transfected GFP+ cells and (**b**) HNK-1+ neural crest cells and (**c**) Islet1+ placodal cells. (**d**–**f**) Robo2Δ-GFP electroporated embryo analyzed at stage 14 showing that placodal cells (Islet1+, **f**) are more dispersed than in controls, but (**e**) HNK-1+ neural crest cell migration does not appear perturbed at this stage. (**g**) Frontal plane section through the control embryo at the dotted line in **c**, showing placodal cells (Islet1+). (**h**) Frontal section through the Robo2Δ-GFP embryo in **f** reveals numerous placodal cells (Islet1+) remaining in the ectoderm (arrowhead) and adjacent to the basal margin (dotted line) of the ectoderm (arrow). (**i**) Left, schematic of a stage 14 chick embryo head showing the region of analysis (dotted box), encompassing the entire presumptive trigeminal area. Right, percentage of the total number of Islet1+ placodal cells associated with the ectoderm was significantly higher in Robo2Δ-GFP than in control GFP embryos. Bars indicate s.d.; $P < 0.0001$, two-tailed Student's t-test. EY, eye; OpV, ophthalmic; MmV, maxillo-mandibular, Ba1, first branchial arch; Mes, mesenchyme; Ecto, ectoderm; Tg, trigeminal; nc, neural crest.

Figure 8.

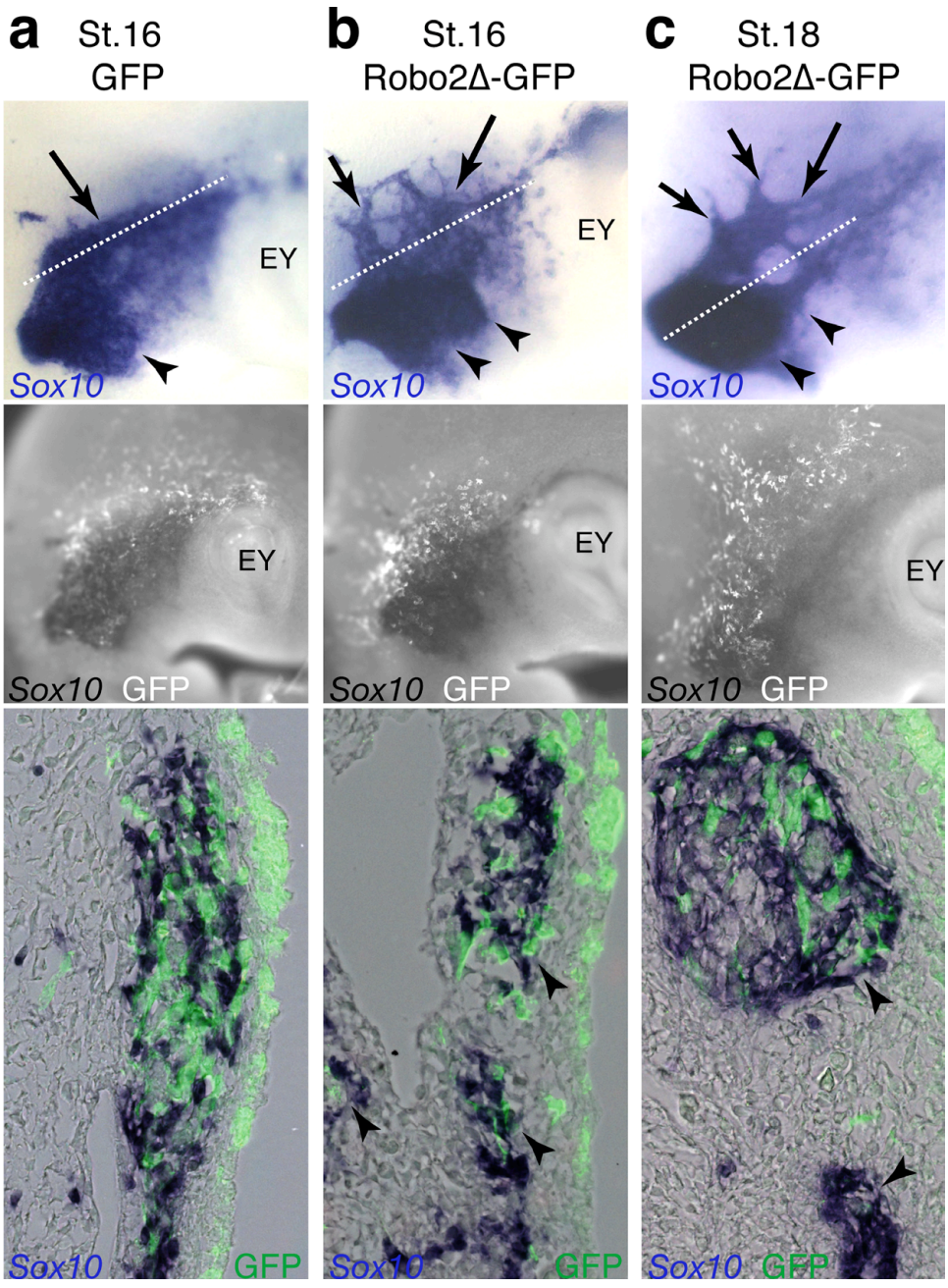
a St.16 GFP
b St.16 Robo2Δ-GFP
c St.18 Robo2Δ-GFP
EY
Sox10
Sox10 GFP
GFP

Figure 8. Inhibition of Robo2 signaling disrupts neural crest aggregation into the trigeminal ganglion. In situ hybridization with *Sox10* to label neural crest cells after electroporating ectoderm with the control GFP or Robo2Δ-GFP construct. (**a**) Stage 16 control embryo showing *Sox10* expression in the trigeminal region overlapping with GFP expression (middle panel). Cross section (bottom panel) through the OpV lobe at dotted line in the top panel shows that *Sox10* expressing neural crest cells assemble together with GFP expressing placodal cells in one cluster. (**b**) Stage 16 embryo electroporated with Robo2Δ-GFP showing dispersion of *Sox10* expressing neural crest cells in the OpV lobe (arrows) and formation of a misshapen MmV lobe (arrowheads, top panel) which correlates with the dispersion of Robo2Δ-GFP expressing placodal cells. Cross section through the OpV lobe shows that *Sox10* expressing neural crest cells assemble wherever the Robo2Δ-GFP expressing placodal cells are clustered (arrowheads, bottom panel). (**c**) The effect of inhibiting Robo2 signaling in placodal cells on neural crest persists even later at stage 18 after the ganglion is well condensed. Cross section through the dispersed region of the ganglion shows that *Sox10* expressing neural crest cells form branch-like aggregates corresponding to where the Robo2Δ-GFP expressing placodal cells are clustered (arrowheads, bottom panel). EY, eye.

Figure 9.

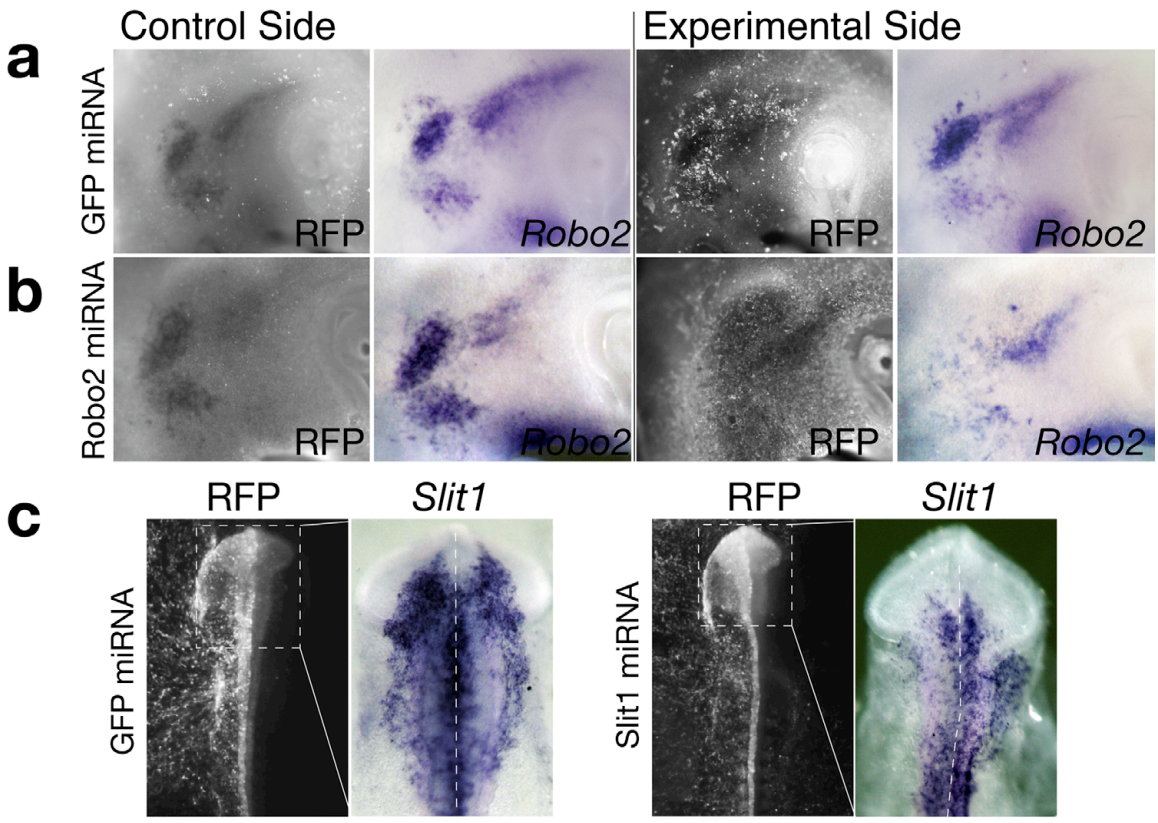

Figure 9. Robo2 and Slit1 RNAi constructs deplete *Robo2* and *Slit1* transcripts. (**a, b**) Embryos were electroporated with the RNAi vectors in the trigeminal ectoderm at stages 8–10 and then assessed for *Robo2* depletion by in situ hybridization in the trigeminal ganglion at stages 15–18. Control (which lacks RNAi) and experimental sides (with RNAi and RFP marker expression) were compared in each embryo. In contrast to the control GFP miRNA embryo in **a**, a marked depletion of *Robo2* is detected in the Robo2 miRNA embryo in **b**. (**c**) Embryos were electroporated with the RNAi vectors on the left side at stages 4–6 and then assessed for *Slit1* knockdown in the premigratory and migratory neural crest cells at stages 8–10. Control GFP miRNA electroporated embryo displays normal *Slit1* expression whereas the Slit1 miRNA electroporated embryo shows reduction of *Slit1* expression on the side with the RNAi vector expression (RFP+).

Figure 10.

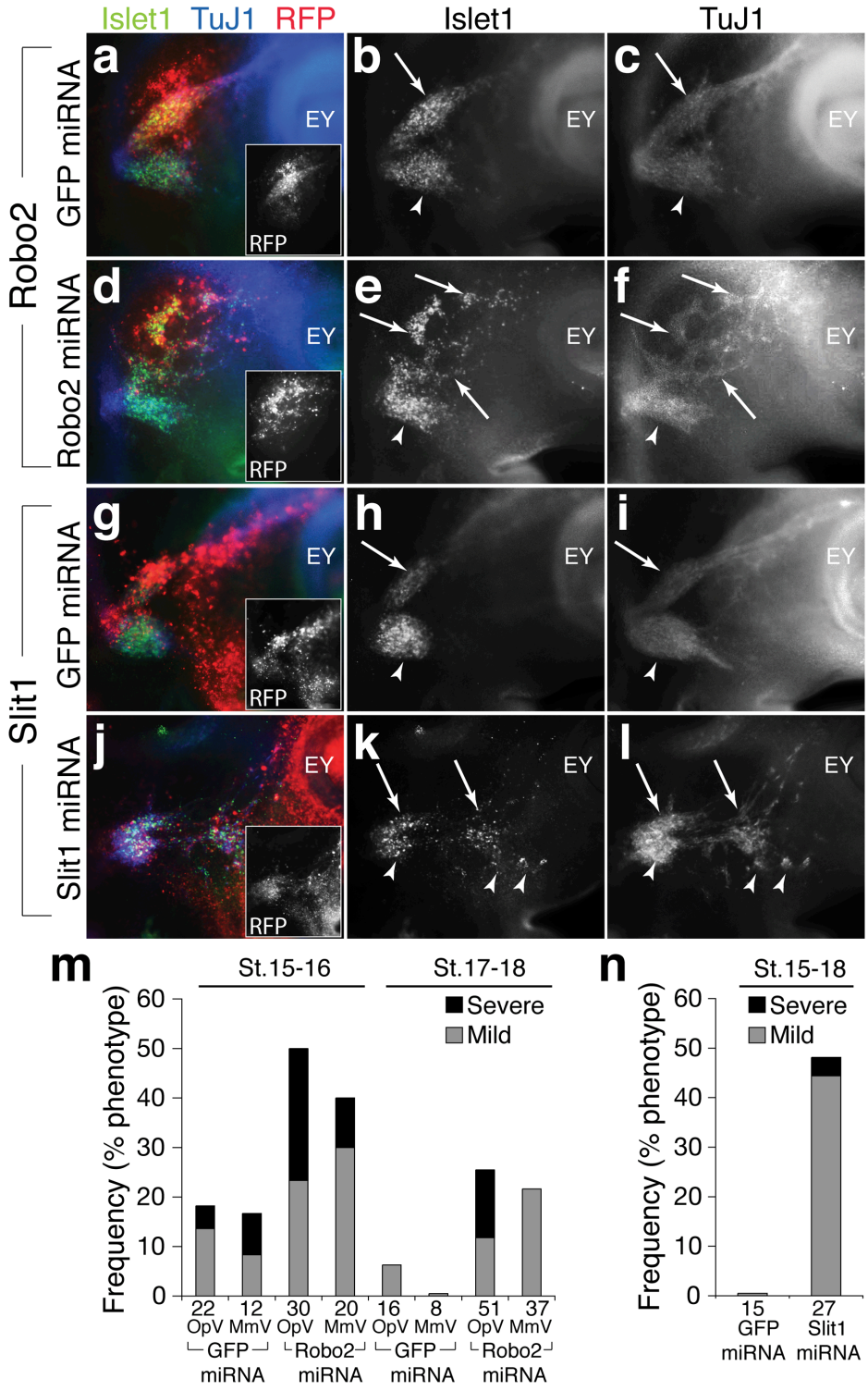
Islet1 TuJ1 RFP
Islet1
TuJ1
Robo2
GFP miRNA
Robo2 miRNA
Slit1
GFP miRNA
Slit1 miRNA
a
b
c
d
e
f
g
h
i
j
k
l
EY
RFP
m
St.15-16
St.17-18
Severe
Mild
Frequency (% phenotype)
0
10
20
30
40
50
60
22 OpV
12 MmV
30 OpV
20 MmV
16 OpV
8 MmV
51 OpV
37 MmV
GFP miRNA
Robo2 miRNA
GFP miRNA
Robo2 miRNA
n
St.15-18
Severe
Mild
Frequency (% phenotype)
15 GFP miRNA
27 Slit1 miRNA

Figure 10. RNAi-mediated knockdown of Robo2 or its ligand Slit1 causes abnormal trigeminal ganglion assembly. (**a**–**c**) Control embryo electroporated with GFP miRNA in the trigeminal ectoderm at stage 16. (**d**–**f**) Robo2 miRNA embryo at stage 16. Both placodal cell bodies (Islet1+) and neuronal processes (TuJ1+) form abnormal clusters and branch-like aggregates in the OpV and interlobic regions (arrows); the MmV which lacks RNAi is relatively normal. (**g**–**i**) Control embryo electroporated with GFP miRNA in the neural crest at stage 17. (**j**–**l**) Slit1 miRNA embryo at stage 17. Placodal neurons are disorganized and form aberrant aggregates, and are often found dispersed and/or occupying the interlobic region. Histograms show that (**m**) Robo2 RNAi and (**n**) Slit1 RNAi embryos showed markedly higher percentages of trigeminal ganglion defects than the controls. Phenotypes considered as severe include aberrant condensation into dispersed or branch-like clumps or widespread cell dispersions, and as mild were regional cell dispersion or misshapen lobe, including displacement or misalignment of OpV and MmV lobes. Numbers below the bars are numbers of transfected ganglia analyzed. EY, eye; OpV or arrow, ophthalmic; MmV or arrowhead, maxillo-mandibular.

Chapter 3

N-cadherin mediates aggregation of placodal neurons and may be regulated by Slit1–Robo2 signaling during formation of the cranial ganglia

3.1 Abstract[1]

We have shown in Chapter 2 that in the largest of the cranial ganglia, the trigeminal ganglion, Slit1–Robo2 signaling mediates neural crest–placode interactions and their function is required for proper ganglion assembly. However, the effector molecules that coordinate proper ganglion formation are not known. Furthermore, whether Slit1–Robo2 may also coordinate assembly of the other cranial sensory ganglia has not been examined. Here, we demonstrate a critical role for the cell adhesion molecule N-cadherin downstream of Slit1–Robo2 during gangliogenesis. In the chick embryo, we found that N-cadherin is expressed by placodal neurons in the surface ectoderm and ganglionic anlage of all cranial sensory ganglia, but not by migrating cranial neural crest. Like the trigeminal, epibranchial placodes express the receptor Robo2, whereas the hindbrain neural crest expresses its ligand Slit1, and blocking Robo2 function leads to disorganized epibranchial ganglia. Loss of N-cadherin function in placodal cells results in formation of dispersed ganglia, similar to that observed after loss of Robo2. Perturbing Slit1–Robo2 signaling (increasing Slit1 or reducing Robo2 function) alters N-cadherin expression, suggesting that N-cadherin functions downstream or at least is regulated by Robo2 signaling. Consistent with this, coexpression of full-length N-cadherin partially rescues the Robo2 loss-of-function phenotype. Together, the data suggest a novel and general mechanism whereby Slit–Robo

[1] This chapter is based on the submitted manuscript Shiau CE and Bronner-Fraser M: N-cadherin is linked with Slit1–Robo2 signaling in regulating aggregation of placode-derived cranial sensory neurons.

signaling between neural crest and placodal cells may positively regulate N-cadherin mediated placodal cell adhesion, required for proper ganglion formation in all cranial sensory ganglia of dual origin.

3.2 Introduction

During development, proper formation of various organs and structures requires coordinated interactions between different cell types. In vertebrates, a prime example is the interaction between neural crest and ectodermal placodes, two cell types of distinct embryonic origin, both of which contribute to the ganglia of the head (D'Amico-Martel and Noden, 1983). The cranial sensory ganglia— trigeminal, facial, glossopharyngeal, and vagal— are essential components of the peripheral nervous system that relay sensory information— such as pain, touch, and temperature, from the head and various organs to the brain (Baker, 2005). These ganglia form adjacent and external to the forming midbrain and hindbrain and make central connections to even-numbered rhombomeres (Noden, 1993). Formation of the cranial sensory ganglia requires cell–cell communication that facilitates intermixing, proper positioning, and aggregation of placode and neural crest cells into discrete ganglion structures. However, the signals and the effector molecules that coordinate their proper condensation into the cranial ganglia are largely uncharacterized.

The position and shape of the cranial ganglia largely mirror the migration patterns of the cranial neural crest. Neural crest ablation at the time of trigeminal ganglion assembly demonstrates that this cell type is required for proper organization and integration of

placodal neurons into ganglia (Shiau et al., 2008). Loss of the receptor Neuropilin-2, expressed by neural crest cells, and/or Semaphorin ligands, expressed in the adjacent mesenchyme, cause defects in neural crest migration that lead to malpositioning of neuronal cell bodies and axons. This results in aberrantly interlinked trigeminal and facial ganglia (Gammill et al., 2006; Schwarz et al., 2008). Thus, neural crest cells play a critical role in regulating aggregation of placodal neurons during early ganglion assembly. Cell–cell signaling between neural crest and placodes likely mediates their coordinated and cooperative interactions in forming the cranial ganglia. For example, trigeminal placode cells express Robo2, while neural crest cells express its cognate ligand Slit1. Blocking either receptor or ligand function causes severe malformations such as aberrantly or diffusely condensed ganglia (Shiau et al., 2008).

Slit signaling through Robo receptors plays a broadly conserved role in axon repulsion from the central nervous system midline in both invertebrates and vertebrates (Brose and Tessier-Lavigne, 2000; Dickson and Gilestro, 2006). In addition, Slits and Robos have been implicated in heart tube morphogenesis in the fruit fly, where they appear to regulate cell adhesion and cell polarity genes (MacMullin and Jacobs, 2006; Qian et al., 2005; Santiago-Martinez et al., 2006), including E-cadherin (Santiago-Martinez et al., 2008). In chick neural retinal cultures, as well as mouse fibroblast L-cells that express N-cadherin, Slit activation of Robo appears to inhibit N-cadherin function (Rhee et al., 2002). The cell biological effects downstream of Slit–Robo signaling during vertebrate development are not yet known.

Because cell–cell interactions appear critical for trigeminal ganglion formation, we examined the possible role of the cell–cell adhesion molecule N-cadherin in ganglion assembly and tested for possible links between N-cadherin-mediated adhesion and Robo–Slit signaling. N-cadherin is a member of the type I classical cadherins (as are E-

and R-cadherins). These are transmembrane, Ca^{2+} dependent adhesion molecules that preferentially bind homophilically through the extracellular domains (Gumbiner, 2005). In vertebrates, N-cadherin is expressed in neural crest-derived spinal ganglia (Akitaya and Bronner-Fraser, 1992; Inuzuka et al., 1991; Packer et al., 1997; Redies et al., 1992) and has been implicated in shaping the sympathetic chain ganglia (Kasemeier-Kulesa et al., 2006). N-cadherin is also expressed in sensory fibers at chick stages 29–37 (E6–E11) (Redies et al., 1992) and mouse E12.5 cranial nerves (Packer et al., 1997). However, little is known about its early expression or function during cranial ganglia assembly in amniotes. In zebrafish, N-cadherin appears to be important for cranial ganglia formation (Kerstetter et al., 2004; Liu et al., 2003), though it is not yet clear if it functions in neural crest cells, placodes, or both.

Here, we show that N-cadherin on placode-derived sensory neurons is required for cranial ganglion condensation. Furthermore, knockdown of Robo2 or ectopic expression of Slit1 alters N-cadherin levels and N-cadherin can partially rescue the Robo2 loss-of-function phenotype. Taken together, these data suggest a novel and synergistic relationship between N-cadherin-mediated cell adhesion and Slit1–Robo2 signaling in driving aggregation of placodal neurons into cranial ganglia.

3.3 Materials and methods

Embryos

Fertilized chicken *(Gallus gallus domesticus)* eggs were obtained from local commercial sources and incubated at 37°C to the desired stages according to the criteria of Hamburger and Hamilton (Hamburger and Hamilton, 1992).

In situ hybridization

Whole mount chick in situ hybridization was performed as described (Shiau et al., 2008). cDNA templates used for antisense riboprobes were: chick Slit1 and Robo2 as described (Vargesson et al., 2001). Embryos were imaged and subsequently sectioned at 12 μm.

Immunohistochemistry

Whole chick embryos were fixed in 4% paraformaldehyde overnight at 4ºC, washed in PBT (PBS + 0.2% tween) and either immunostained as whole embryos and/or processed for 10 μm cryostat sections. Primary antibodies used were anti-N-cadherin (DSHB, MNCD2 clone; 1:1), anti-N-cadherin (Abcam; 1:250), anti-GFP (Molecular Probes; 1:1000 to 1:2500), anti-HNK-1 (American Type Culture; 1:3 or 1:5), anti-Islet1 (DSHB, clone 40.2D6; 1:250), and anti-TuJ1 (Covance; 1:250). Secondary antibodies: cyanine 2 or rhodamine red-x conjugated donkey anti-rat IgG (Jackson ImmunoResearch) used at 1:1000 and all others were obtained from Molecular Probes and used at 1:1000 or 1:2000 dilutions (except 1:250 dilution for Alexa Flour 350 conjugated antibodies). Images were taken using the AxioVision software from a Zeiss Axioskop2 plus fluorescence microscope, and processed using Adobe Photoshop CS3.

In ovo electroporation of the trigeminal ectoderm

DNA or morpholino oligomers were injected overlying the presumptive trigeminal placodal ectoderm at stages 8–10 by air pressure using a glass micropipette. Platinum electrodes were placed vertically across the chick embryo delivering 5 × 8 V in 50 ms at 100 ms intervals current pulses. Electroporated eggs were re-sealed and re-incubated at 37˚C to reach the desired stages.

Plasmid constructs and morpholinos

DNA plasmids previously described were used as follows: Robo2Δ-GFP (Hammond et al., 2005), pCMV-cN/CBR(-)/FLAG-pA (pCMV-dn-Ncad) and pCMV-cN/FLAG-pA (pCMV-Ncad) (Nakagawa and Takeichi, 1998), and for control GFP expression, cytoplasmic pCIG (cyto-pCIG) (Shiau et al., 2008) and pCAβ-IRES-mGFP (McLarren et al., 2003). Full-length chick Slit1 cDNA was isolated from a 4– to 12– somite chick macroarray library as described (Gammill and Bronner-Fraser, 2002) for creating the cytopcig-Slit1-LRR construct, which contains the coding sequence for the first 863 amino acids of chick Slit1 with a 3x FLAG tag. The Slit1-LRR-3xFLAG fragment (~2.7 kb) was inserted into cyto-pCIG at XhoI and EcoRI sites. Morpholino oligomer (Gene Tools, LLC) against the start site of chick N-cadherin (Ncad MO) has a 5' –> 3' sequence of: GCGGCGTTCCCGCTATCCGGCACAT. Standard control oligomer from Gene Tools, LLC (control MO) and NCad MO were both 3' lissamine tagged, diluted with water, and used at 1 μM.

3.4 Results

3.4.1 N-cadherin is expressed by trigeminal and epibranchial placodal neurons but not cranial neural crest during gangliogenesis

To determine if N-cadherin is expressed at the right time and place to play a role in cranial gangliogenesis, we examined its expression pattern in the cranial regions of the developing chick embryo from stages 13–17, as the trigeminal and epibranchial ganglia

assemble and aggregate (Fig. 1). Placodal neurons differentiate early, prior to or at the time of ingression (Baker and Bronner-Fraser, 2001; D'Amico-Martel, 1982; D'Amico-Martel and Noden, 1980; Shiau et al., 2008). Neural crest cells migrate to the site of ganglion assembly first but remain undifferentiated as they intermingle with ingressing placodal neurons (Shiau et al., 2008). Neural crest cells begin to differentiate into neurons late in development after the ganglia are well condensed at ~stages 22–24 (D'Amico-Martel and Noden, 1980; D'Amico-Martel and Noden, 1983). Therefore, broad neuronal markers, such as Islet1 and/or β-neurotubulin (TuJ1), uniquely label placodal cells during early ganglion assembly.

During initial ganglion formation, N-cadherin expression is restricted to placode but not neural crest cells. Using immunohistochemistry with antibodies to N-cadherin coupled with HNK-1 to label neural crest cells, and TuJ1 or Islet1 to identify placodal neurons, we observed overlapping expression of N-cadherin with TuJ1 and Islet1 but not with HNK-1 at all stages leading to well-condensed cranial sensory ganglia (Fig. 1), with the exception of a few Islet1 negative cells in the condensed ganglia at stage 17 which express N-cadherin (as an example see Fig. 1I, asterisk). These cells may be non-Islet1 expressing placodes or mesenchymal cells of mesoderm or neural crest origin. N-cadherin staining was apparent both in the placodal ectoderm as well as in those placode cells that have ingressed; expression continued through the time of cranial ganglia assembly (Fig. 1). Consistent with previous reports, we also found high levels of N-cadherin expression in the neural tube, notochord, and the lens (Hatta et al., 1987; Hatta and Takeichi, 1986), and slightly lower levels in the mesoderm-derived mesenchyme. The intensity of immunostaining in placodal cells is generally lower than in the neural tube, and is more similar to that in the mesenchyme cells.

Interestingly, N-cadherin levels fluctuate dynamically in placodal tissue as a function of time. In the trigeminal region, at times of early ingression at stage 13, N-

cadherin is expressed in most of the surface ectoderm around the head, with the exception of the region overlying the dorsal hindbrain (Fig. 1A,B). Later by stages 15–17, expression is mostly down-regulated in the ectoderm overlying the site of ganglion assembly (Fig. 1C-E), though the ectoderm that overlies the frontonasal region (including the lens) still expresses N-cadherin (data not shown). The discrete spots of low-level expression in the surface ectoderm later in development may correlate with sites of placode ingression, which continues through stage 21 (D'Amico-Martel and Noden, 1983), well after the ganglion is condensed. The expression of N-cadherin in the ingressed placodal neurons appears to increase with time and change from a punctated to a more continuous cell surface expression from stage 13 (Fig. 1A,B) to 17 (Fig. 1C-G) as the trigeminal ganglion is condensing. Similar to the trigeminal placode, we observed N-cadherin expression in the epibranchial ectoderm and ingressing epibranchial placodes (Fig. 1H-P). The expression of N-cadherin by placodal neurons in all cranial ganglia raises the possibility that N-cadherin may play a general role in placodal ingression and/or aggregation.

3.4.2 Loss of N-cadherin phenocopies Robo2 loss-of-function

To test the possible function of N-cadherin in placode cells during gangliogenesis, we focused on the forming trigeminal ganglion because of its large size and characteristic semilunar shape, which aids in systematic scoring of ganglionic phenotypes. To deplete N-cadherin in the placodal cells, we used both a translation blocking antisense morpholino oligomer (MO) against chick N-cadherin (Ncad MO) and a dominant-negative N-cadherin construct (pCMV-dn-Ncad) (Nakagawa and Takichi, 1998) which encodes chick N-cadherin lacking the intracellular β-catenin binding domain. Such mutations to cadherins lacking binding site to β-catenin have been shown to block cadherin function (Nakagawa and Takeichi, 1998; Shoval et al., 2007).

The effects of both knockdowns were similar but Ncad MO gave a more pronounced phenotype, giving rise to highly dispersed placodal neurons in the forming ganglia at stages 15–16 (29% severe and 42% mild defects, n=24) and in largely misshapen ganglia at later stages 17–18 (8% severe and 23% mild, n=13) after the ganglion is well condensed (Fig. 2B,E). In contrast, control MO embryos showed little or no effect (Fig. 2A,E). The effects of dispersed and disorganized placodal neurons (both cell bodies and axon projections) in the forming trigeminal ganglion observed with Ncad MO were reminiscent of the defects caused by Robo2 loss-of-function using the Robo2Δ-GFP construct (Shiau et al., 2008) which encodes a dominant-negative Robo2 that lacks its intracellular tail, replaced by the GFP. However, defects in axon guidance were more pronounced in Robo2 deficient embryos.

The effectiveness of Ncad MO in depleting N-cadherin protein was confirmed using immunohistochemistry in the neural tube and lens, where N-cadherin expression is persistent and strong. Chick embryos electroporated with Ncad MO in these tissues showed a marked reduction of N-cadherin protein as compared with control MO embryos (Fig. 3). Similar reductions were observed in the trigeminal region (Fig. 5). Ncad and control MOs were tagged with 3' lissamine for detection.

Similar to but less severe than the Ncad MO, pCMV-dn-Ncad electroporated embryos resulted in dispersed trigeminal ganglion at early ganglion assembly (stages 15–16) (7% severe and 40% mild phenotypes, n=19) (Fig. 2C-E). In contrast to the MO, dn-Ncad protein expression driven by pCMV-dn-Ncad appeared to incorporate rather mosaically. Expression levels were checked by co-electroporating pCMV-dn-Ncad with a control GFP vector. In these embryos, we detected dn-Ncad-FLAG expression in only a sub-population of transfected GFP expressing cells (Fig. 4), perhaps accounting for the milder defects observed with this construct as compared to the Ncad MO. These results

show that placodal neurons require N-cadherin function for proper ganglion condensation in common with Robo2 function.

3.4.3 N-cadherin is essential for ganglion condensation, but not placodal ingression

Since N-cadherin is expressed dynamically in both the surface ectoderm from which placodal cells arise and in the ingressing placodal cells after detaching from the ectoderm, we asked whether N-cadherin is critical for placodal ingression. To this end, we counted the total number of placodal cells (Islet1+) in 10 μm frontal sections collected from the entire presumptive trigeminal region at times of early and abundant ingression at stage 14 (boxed region in Fig. 5) and analyzed the number associated with the surface ectoderm (either in ectoderm or adjacent to its basal margin) versus the mesenchyme as previously described (Shiau et al., 2008). These two categories represent the population of placodal neurons that are undergoing ingression or preparing to do so, and those that have already ingressed, respectively. In contrast to the effect of Robo2 inhibition that caused more than a two-fold increase in percentage of placodal cells remaining associated with the ectoderm than those in controls (Shiau et al., 2008), we found no significant difference between the numbers of ingressing cells in Ncad loss-of-function (36.3 ± 3.9%, n=3) versus control (32.2 ± 7.6%, n=4) embryos (Fig. 5A-C). Furthermore, the total number of Islet1+ placodal cells was not significantly different between Ncad MO and control MO embryos, suggesting no effect on placodal cell number when N-cadherin is reduced. This suggests that Robo2 dependent ingression process does not rely on N-cadherin. On the other hand, the placodal cells appear more dissociated in Ncad MO embryos (Fig. 5B,C). Thus, N-cadherin appears to be one of several downstream mediators and interacting partners of Slit1–Robo2 signaling. However, we cannot rule out that the efficiency of Ncad MO

mediated knockdown is not sufficient to reveal an early role for N-cadherin during ingression.

In contrast to these early stages, significant alterations were noted in Ncad MO mediated ganglion compared with controls during ganglion assembly (stage 16). The results suggest that loss of N-cadherin in placodal cells reduces cell–cell contact and abrogates clustering of placodal neurons (Fig. 5D,E). Ncad MO placodal neurons appear dissociated and have reduced levels of N-cadherin expression (Fig. 5E). These results are consistent with the dispersed ganglia observed in whole-mount. Though N-cadherin deficient placodal cells are more dispersed, they generally occupy the same approximate area within the head mesenchyme where the trigeminal ganglion forms, in close proximity to the surface ectoderm (Fig. 5E). Thus, knockdown of N-cadherin appears to compromise placode–placode cell association and aggregation, but not ingression or ganglion position.

3.4.4 Perturbation of Slit1–Robo2 signaling can alter N-cadherin expression

The similar loss-of-function phenotypes of both N-cadherin and Robo2 raise the intriguing possibility that they may function in the same pathway to mediate interactions between placodal neurons in the forming ganglion. To test this, we first examined the effects of Slit1–Robo2 signaling on N-cadherin in placodal cells and asked whether blocking or activating Slit1–Robo2 signaling would alter N-cadherin expression. The results show that inhibiting Robo2 signaling by Robo2Δ-GFP causes down-regulation of N-cadherin expression in the placodal ectoderm at stages 13–14 at times of early ingression (Fig. 6A). Later, at stage 17, there was a reduction of N-cadherin expression in aberrantly dispersed individual placodal neurons in the forming ganglion (Fig. 6E-G). However, many of the Robo2Δ-GFP placodal neurons still express some levels of N-cadherin, particularly

ones that appear more closely associated with each other. Thus, Robo2 may modulate N-cadherin expression but is unlikely to be the sole regulator of N-cadherin in placodal cells.

Conversely, to test the effects of Slit activation of Robo on N-cadherin, we designed a construct encoding the N-terminal portion of chick Slit1, that encompasses the four leucine rich repeats (cytopcig-Slit1-LRR), which has been shown to be sufficient for binding and activating Robo (Morlot et al., 2007, Howitt et al., 2004, Chen et al., 2001, Battye et al., 2001), and more potent than full length Slit to rescue midline axon defect in fly slit mutants (Battye et al., 2001). cytopcig-Slit1-LRR was introduced into the placodal ectoderm by in ovo electroporation to test the effect of Slit1 expression in placodal cells on N-cadherin expression. Strikingly, ectopic expression of Slit1 in the placodal ectoderm causes aberrant placodal aggregates in the forming trigeminal ganglion (44% at stages 15–16 with n=9 and 31% at stages 17–18 with n=13 showing severe defects in condensation, including ectopic aggregates and/or axonal disorganizations) (Fig. 7F-L). Furthermore, in these ganglia, we found that N-cadherin expression was up-regulated in discrete regions of the surface ectoderm corresponding to locations near aberrant placodal clusters (Fig. 7J) at times when N-cadherin is normally down-regulated in the surface ectoderm, as seen in stage 16 GFP control embryos (Fig. 7E). This defect was more severe in the ophthalmic (OpV) than in the maxillomandibular (MmV) region of the forming ganglion, consistent with our previous finding that Robo2 inhibition has more severe effects on the OpV (Shiau et al., 2008). Thus, the effect of ectopic Slit1 expression on N-cadherin is reciprocal to that of blocking Robo2, consistent with the idea that N-cadherin is positively regulated by Slit1–Robo2. Taken together, inhibition of Robo2 or its activation by Slit1 can either decrease or increase N-cadherin expression respectively, suggesting that Slit1–Robo2 interaction can modulate N-cadherin expression.

3.4.5 Overexpression of N-cadherin partially rescues Robo2 perturbation

The observation that Robo2 loss-of-function leads to reduction of N-cadherin suggest that N-cadherin is downstream of and may be epistatic to Robo2. To test whether N-cadherin can rescue the effects of Robo2 inhibition in the placodal cells, we co-electroporated full length N-cadherin (pCMV-Ncad) and Robo2Δ-GFP into the placodal ectoderm. Despite its mosaic expression (similar to pCMV-dn-Ncad described above), the results show that N-cadherin partially rescues the severely dispersed ganglion phenotype of Robo2 inhibition at stages 15–16 by about 18% (n=8, Fig. 8A-C). Embryos co-electroporated with pCMV-Ncad and Robo2Δ-GFP had ganglia that were markedly less dispersed and more coalesced than those with Robo2Δ-GFP alone. In contrast, N-cadherin gain-of-function alone, achieved by electroporating pCMV-Ncad with a control GFP vector to visualize DNA incorporation into the placodal ectoderm, had no obvious effects on ganglion organization, yielding rather normal (87%, n=15) or slightly smaller (13%, n=15) ganglia (data not shown). All together, results show that N-cadherin can act downstream of Robo2 signaling as its gain-of-function compensates for the effects of blocking Robo2 and Slit1–Robo2 signaling modulates N-cadherin expression.

3.4.6 Robo2–Slit1 and N-cadherin expression and function are common to trigeminal and epibranchial regions

Since Slit1–Robo2 interactions have been implicated in assembly of the trigeminal ganglion (Shiau et al., 2008), we asked whether this receptor/ligand pair may generally function in neural crest–placode assembly of all cranial sensory ganglia. To this end, we further characterized the expression patterns of Robo2 and Slit1 in the hindbrain regions of the chick embryo during epibranchial gangliogenesis at stages 16–18. The results show that

the complementary expression pattern of Robo2 in the placodes and its ligand Slit1 in the neural crest is common to all forming epibranchial ganglia. By in situ hybridization coupled with immunohistochemistry with the neural crest marker HNK-1, we find that all epibranchial placodes (geniculate, petrosal, and nodose corresponding to the facial, glossopharyngeal and vagal ganglia respectively) express Robo2 mRNA during early assembly at stage 16 (Fig. 9A) and continue expression up to ganglion condensation at stage 18 (Fig. 9B), while the migratory hindbrain neural crest at rhombomeres 4 and 6 expresses Slit1 mRNA at stage 16 (Fig. 9C) and begins to down-regulate Slit1 expression at stage 18 (Fig. 9D) after the ganglia have condensed. Robo2 also is expressed in the otic placode as previously reported (Battisti and Fekete, 2008) and in parts of the ectoderm surrounding the branchial arches.

Transverse sections reveal that Robo2 expressing cells in the ectodermal and ingressing placodes intermingle with HNK-1 positive migratory neural crest cells that coexpress Slit1 at stage 16 in the forming facial ganglion (Fig. 9E-H) and glossopharyngeal ganglion (Fig. 9I-L). Furthermore, blocking Slit–Robo signaling by introducing Robo2Δ-GFP into the epibranchial placodal cells led to disorganization of the epibranchial placodal ganglia similar to the effects in the trigeminal ganglion (Fig. 9M). Similar to Robo2 inhibition, N-cadherin depletion by Ncad MO in the epibranchial placodes caused a more pronounced effect on the central axonal projections to the hindbrain than in the trigeminal region (Fig. 9N). The central projections in the forming trigeminal ganglion are generally not affected upon Robo2 or N-cadherin perturbation. This could reflect the difference in the cell movements and integration of trigeminal versus epibranchial placodal neurons into ganglia, as the latter forms more distal to the hindbrain. Nevertheless, these results highlight the intriguing possibility that Slit1–Robo2 signaling and N-cadherin function may be a general mechanism for neural crest–placode interaction during cranial gangliogenesis.

3.5 Discussions

3.5.1 Cross-talk between Slit–Robo and cadherins

Our results suggest a novel mechanism in chick cranial gangliogenesis whereby Slit1–Robo2 signaling between neural crest and placodal cells regulates adhesion of placodal neurons via modulation of N-cadherin levels. Recent in vitro studies (Rhee et al., 2007; Rhee et al., 2002) show that Slit activation of Robo causes phosphorylation of β-catenin by Robo-bound Abelson (Abl) tyrosine kinase, thus inhibiting N-cadherin's link to the actin cytoskeleton. In vivo studies in *Drosophila* demonstrate that Slit–Robo signaling inhibits E-cadherin to allow cell shape changes for lumen formation in the developing heart tube (Santiago-Martinez et al, 2008). Contrasting with this negative regulation of cadherins, our data in vertebrates suggests that Slit–Robo signaling can also positively regulate cadherin mediated cell adhesion during chick cranial gangliogenesis. Since this receptor–ligand pair can mediate both repulsive and attractive functions in cell migration and axon patterning (Chedotal, 2007), it may not be too surprising that Slit–Robo may both positively and negatively regulate cadherin mediated adhesion, in a context dependent manner. This may depend on the target tissue, the presence or absence of interacting molecules, and the levels of Slit signaling. The mechanism by which Slit binding to Robo transduces downstream signaling remains an unresolved question, but has been proposed to involve the state of oligomerization of Robo and recruitment of cytosolic adaptor proteins (Hohenester, 2008).

3.5.2 Role of N-cadherin in cellular condensation and its link with Slit1–Robo2

The dynamic expression pattern of N-cadherin in various developing tissues (nervous system, connective tissues, somite, limb, lung, kidney, and heart) undergoing morphogenesis suggests a potentially general role for this cell adhesion molecule in cellular condensation and/or organ formation (Duband et al., 1987; El Sayegh et al., 2007; Hatta et al., 1987). N-cadherin has been found to promote coalescence in the forming heart, somite and limb mesenchyme (Linask et al., 1998; Oberlender and Tuan, 1994; Radice et al., 1997). Accordingly, we find that N-cadherin function is essential for condensation of placodal neurons into cranial ganglia. Our data further suggest a role for Slit1–Robo2 in regulating N-cadherin expression in placodal neurons. However, there are likely to be many other regulators of N-cadherin as its expression is broad in the surface ectoderm and other tissues. Consistent with this, blocking Slit–Robo signaling by Robo2Δ-GFP does not completely eliminate N-cadherin expression in the placodal cells. Interestingly, the more severe defects in trigeminal placodal ingression and axonal projections observed in Robo2 deficient embryos cannot be completely explained by N-cadherin loss-of-function, which affects ganglion condensation but seemingly not ingression or axonal pathfinding. Thus, other yet unknown effector molecules may mediate Slit1–Robo2 signaling in conjunction with N-cadherin, and N-cadherin likely also has independent functions in the placodal ectoderm. Nonetheless, the similarity of the ganglionic loss-of-function phenotype of both N-cadherin and Robo2, together with the partial rescue of Robo2 inhibition by full-length N-cadherin and the changes in N-cadherin expression caused by altering Slit1–Robo2 signaling, combine to provide strong evidence for modulation of N-cadherin by Robo2 dependent signaling in trigeminal placodal aggregation.

3.5.3 Possible mechanisms on how Slit1–Robo2 regulate N-cadherin

How does Slit1–Robo2 regulate N-cadherin expression and/or function in the placodal cells? One possibility is that this is mediated by convergence of common or interacting intracellular molecules involved with both Robo2 and N-cadherin functions, such as the small Rho GTPases (Rho, Rac, Cdc42) that regulate the actin cytoskeleton. Cadherins have been known to not only act as cell adhesion proteins but also as signaling molecules that can elicit changes to intracellular signals (Yap and Kovacs, 2003). Both Robo (Chedotal, 2007; Ghose and Van Vactor, 2002; Guan and Rao, 2003) and cadherin (Charrasse et al., 2002; Noren et al., 2001; Yap and Kovacs, 2003) signaling have been shown to regulate Rho GTPases, which conversely can feedback on cadherin (Braga, 1999; Fukata and Kaibuchi, 2001). Slit signaling can upregulate a Rho family member, Rac1, in the *Drosophila* CNS midline (Fan et al., 2003), and increased Rac1 expression upregulates N-cadherin expression during chondrogenesis (Woods et al., 2007). Therefore, an intriguing possibility is that activation of Rac1 by Slit–Robo may promote N-cadherin expression. The relationship between cadherins and Rho GTPases is likely complex and bi-directional. The effects of Rho and Rac signaling on cadherins have been found to vary for different cadherin subtypes and cellular contexts (Braga et al., 1999). Conversely, cadherins can affect Rho GTPases. For example, a recombinant Fc fused cadherin ectodomain that activates cadherin adhesion causes a rapid increase of Rac activity (Kovacs et al., 2002; Noren et al., 2001). Thus, like Robo signaling, cadherins can regulate Rac, suggesting a point of cross-talk between Robo and cadherin signaling. Independently, Robo2 may regulate other intracellular associations of N-cadherin, such as the catenins, by phosphorylation to promote and/or inhibit cadherin function. Consistent with this possibility, p120-catenin has been shown to stabilize cadherins and regulate their turnover at the cell surface (Kowalczyk and Reynolds, 2004; Perez-Moreno and Fuchs, 2006).

3.5.4 General mechanism involving Slit1–Robo2 and N-cadherin in cranial sensory gangliogenesis in chick

The common expression of Robo2 and N-cadherin in the trigeminal and epibranchial placodes and Slit1 in all migratory cranial neural crest streams underscores a possible general mechanism in mediating neural crest–placode interactions in all cranial sensory ganglia. During development, the trigeminal ganglion forms adjacent to the midbrain while the epibranchial (facial, glossopharyngeal and vagal) ganglia form around the second to the fourth branchial arches, respectively. Epibranchial ganglia have a long tubular-like morphology distinct from the bi-lobed shape of the trigeminal ganglion. However, at times of early cell assembly, the two regions have many similarities. The distribution of neural crest- and placode- derived cells in the trigeminal and epibranchial ganglia is very similar in that neural crest cells intermix with placodal neurons and the most proximal regions of the ganglia are solely neural crest-derived (Begbie and Graham, 2001a; Shiau et al., 2008). Neural crest ablations in both regions cause aberrant projection patterns of placode-derived neurons (Begbie and Graham, 2001a; Shiau et al., 2008). In addition, Slit1 is expressed by neural crest cells in the epibranchial region in a discrete time window correlating with ganglion assembly as is the case in the trigeminal region (Shiau et al., 2008). Slit1 is down-regulated in the hindbrain neural crest after stage 16, slightly later than in the midbrain, likely reflecting the rostral to caudal order of ganglion development from trigeminal to epibranchial gangliogenesis. Functional perturbations of Robo2 and N-cadherin in the epibranchial placodes led to ganglion disorganization, which further lend support for the common mechanism of Slit1–Robo2 mediated neural crest–placode assembly of ganglion.

3.5.5 Expression of N-cadherin may not be placode-specific but rather neuronal cell type-specific in the forming ganglia

The expression and function of N-cadherin in placodal cells but not in cranial neural crest cells probably relates to the state of neuronal differentiation rather than the precursor cell type within the ganglia. Since cranial neural crest cells differentiate into neurons (D'Amico-Martel, 1982; D'Amico-Martel and Noden, 1980) much later in development than placode cells, well after the cranial ganglia have formed, they may not begin to express N-cadherin until past gangliogenesis. In support of this, at trunk levels, which lack placodal cells, N-cadherin is expressed in all neural crest-derived peripheral ganglia- dorsal root and sympathetics (Akitaya and Bronner-Fraser, 1992; Kasemeier-Kulesa et al., 2006). As at cranial levels, migrating trunk neural crest cells do not express N-cadherin until after they have begun to coalesce and differentiate into neurons (Akitaya and Bronner-Fraser, 1992).

3.5.6 Conclusions

In summary, the present results show that N-cadherin plays a crucial role in driving aggregation of placodal neurons and may be regulated by Slit1–Robo2 interactions between neural crest and placodal cells during trigeminal gangliogenesis. This represents the first in vivo evidence of a functional link between cadherin and Slit–Robo signaling in vertebrate development. The similar expression patterns of these molecules in all cranial ganglia suggest a possible general mechanism whereby Slit–Robo signaling controls morphogenesis associated with cadherin function in forming cranial sensory ganglia. Beyond the nervous system, Slits and Robos are emerging as important players in development of the lung, mammary gland, and kidney, as well as pathological conditions

such as cancer and inflammation (Hinck, 2004; Legg et al., 2008; Piper and Little, 2003), where cadherins are also expressed (Hatta et al., 1987; Jeanes et al., 2008; Knudsen and Wheelock, 2005; Stemmler, 2008). The results demonstrate the importance of heterotypic cell interactions during condensation of the cranial sensory ganglia, and implicate a possibility for cross-talk between Slit–Robo signaling and cadherin function in other systems.

3.6 Acknowledgements

I thank Masatoshi Takeichi for the pCMV-dn-Ncad and pCMV-Ncad plasmids and Meyer Barembaum for critical reading and comments. This work was supported by US National Institutes of Health (NIH) National Research Service Award 5T32 GM07616 to C. E. S. and NIH grant DE16459 to M.B.-F.

Figure 1.

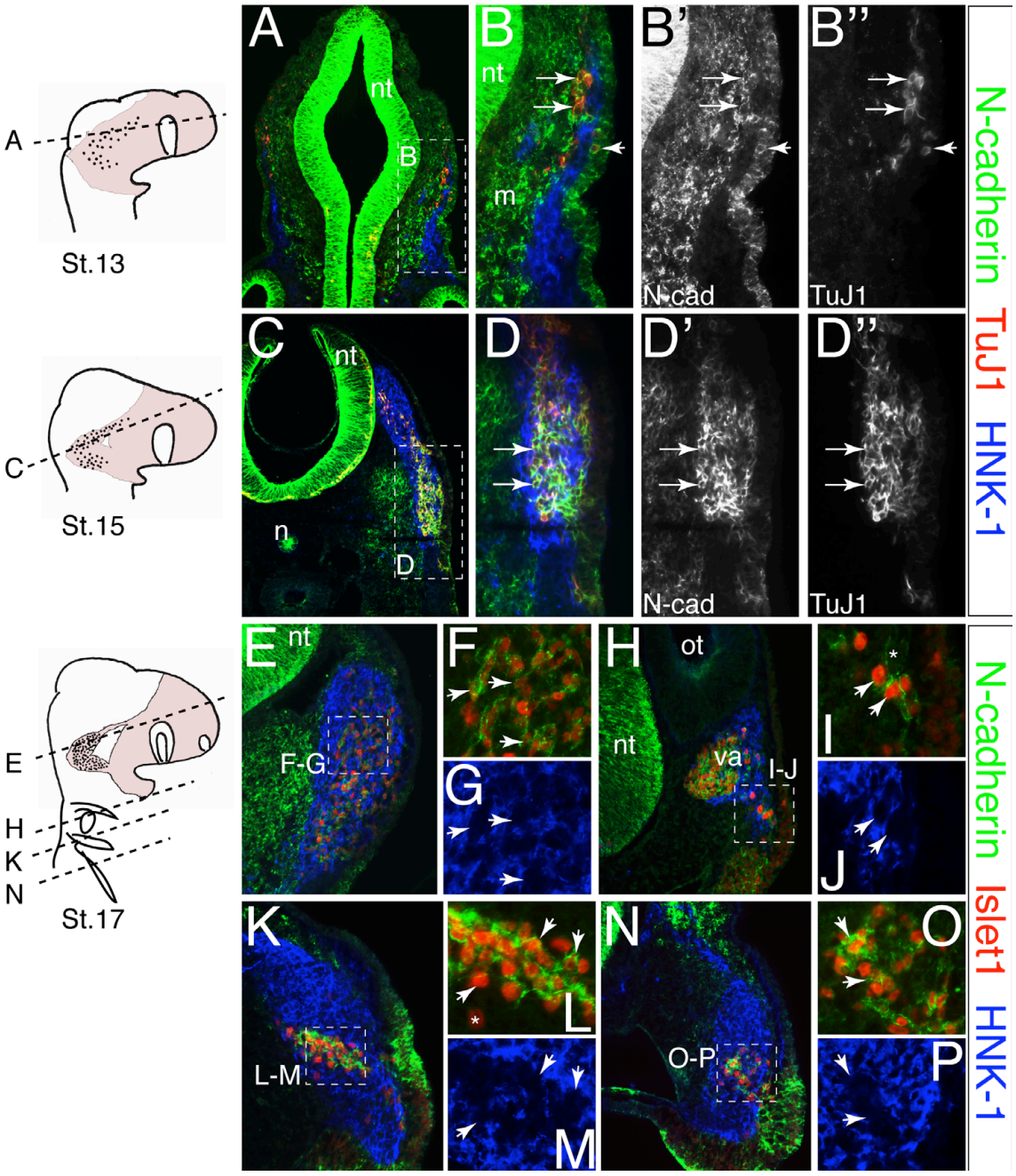
A
St.13
C
St.15
E
H
K
N
St.17
A
nt
B
B
nt
m
B'
N-cad
B''
TuJ1
C
nt
n
D
D
D'
N-cad
D''
TuJ1
N-cadherin TuJ1 HNK-1
E
nt
F-G
F
G
H
ot
nt
va
I-J
I
*
J
K
L-M
L
*
M
N
O-P
O
P
N-cadherin Islet1 HNK-1

Figure 1. Expression of N-cadherin in trigeminal and epibranchial placodal cells but not cranial neural crest during gangliogenesis. Through stages of gangliogenesis, N-cadherin protein is expressed by placodal neurons (labeled by TuJ1 or Islet1) but not by neural crest cells (labeled by HNK-1) in the forming trigeminal ganglion at (**A**) stage 13 with higher magnification of boxed area in **B**, **B**' and **B''** showing coexpression of N-cadherin and TuJ1 (arrows), (**C–D''**) stage 15 in early forming ganglion showing overlap of N-cadherin and TuJ1 (arrows) and (**E–G**) stage 17 in the well condensed ganglion (arrows). Expression of N-cadherin in epibranchial neurons (Islet1+) but not the neural crest cells (HNK-1+) is shown in the (**H–J, arrows**) facial (or geniculate), (**K–M, arrows**) glossopharyngeal (or petrosal), and (**N–P, arrows**) vagal (or nodose) ganglionic regions. By stage 17, a few cells Islet1 negative cells were found to express N-cadherin in the condensing ganglia at stage 17 (**I**, asterisk). The vast majority of Islet1 positive placodal cells express N-cadherin with a few exceptions (**L**, asterisk). All images are derived from 10 μm cryostat sections which generally encompass about one to two cell layer thickness. Schematics of the stage 13, 15, and 17 chick embryos show the levels of the sections with pink area representing the neural crest cells and black dots the placodes. N-cad, N-cadherin; nt, neural tube; m, mesoderm; n, notochord; ot, otic vesicle; va, vestibuloacoustic ganglion.

Figure 2.

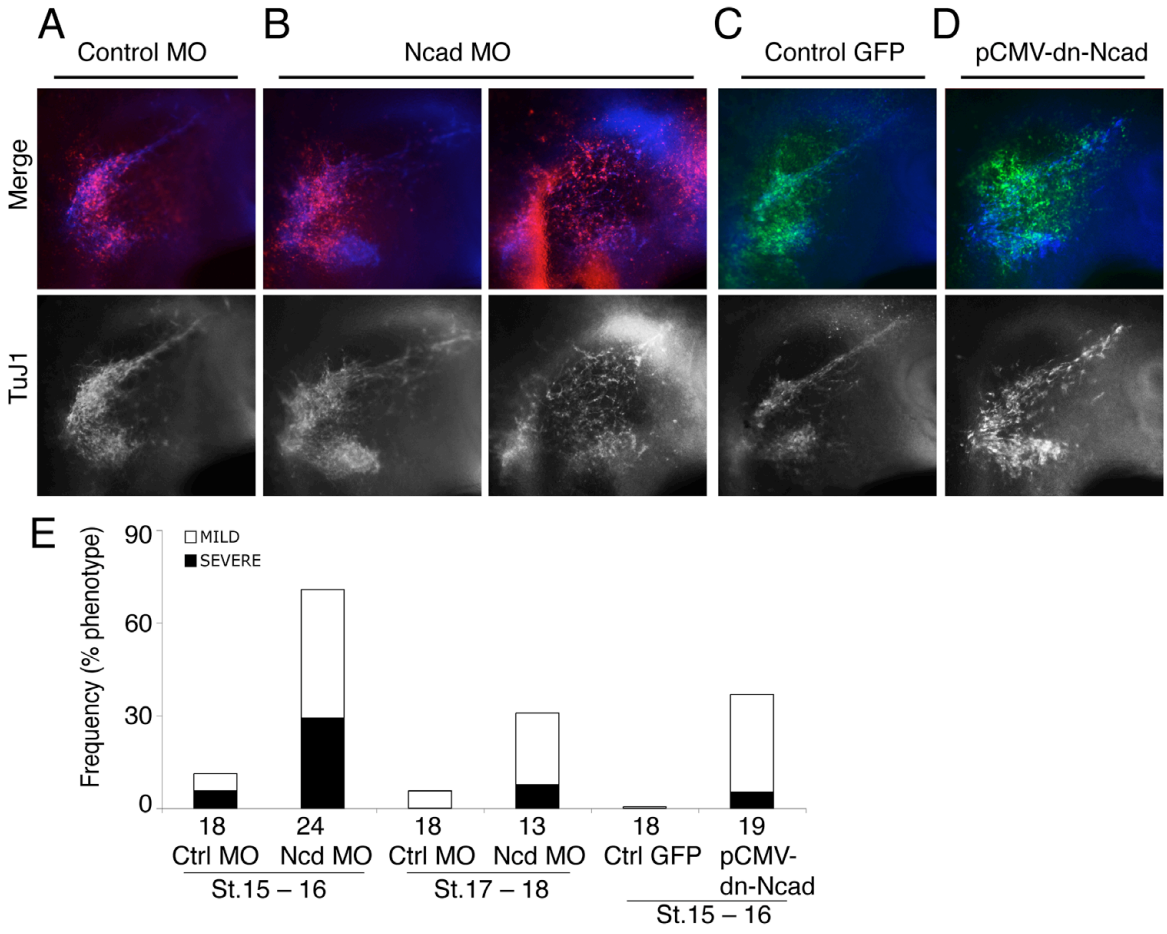
A
Control MO
B
Ncad MO
C
Control GFP
D
pCMV-dn-Ncad
Merge
TuJ1
E
MILD
SEVERE
Frequency (% phenotype)
90
60
30
0
18
Ctrl MO
24
Ncd MO
18
Ctrl MO
13
Ncd MO
18
Ctrl GFP
19
pCMV-dn-Ncad
St.15 – 16
St.17 – 18
St.15 – 16

Figure 2. N-cadherin loss-of-function phenocopies Robo2 loss-of-function. (**A**) Control morpholino electroporated chick embryos in the trigeminal placodal ectoderm analyzed at stage 16 have normal morphology. (**B**) In contrast, stage 16 Ncad MO embryos showed either mildly dispersed and/or misshapen (left) or severely dispersed and disorganized (right) ganglia (TuJ1+). Control and Ncad morpholinos are labeled by 3' lissamine (red in color overlay panels). Compared to (**C**) GFP controls, (**D**) pCMV-dn-Ncad embryos also resulted in aberrantly dispersed placodal ganglia, though less severe than the Ncad MO effects. (**E**) Histogram of data shows the high percentage of dispersed ganglia defects in Ncad MO and dn-Ncad embryos above controls. The more severe effects of Ncad MO at stages 15–16 than at later stages 17–18 likely is due to dilution of morpholino in the placodes over time. Numbers below bar graphs represent the number of transfected ganglia analyzed. Ganglia phenotypes scored as "mild" means misshapen, slight cell dispersion, and/or regional severe defects (in only part of the transfected area), and "severe" means widespread dispersion in most transfected area, including the interlobic region, and/or strikingly aberrant placodal condensation. Ctrl, control; Ncd, N-cadherin.

Figure 3.

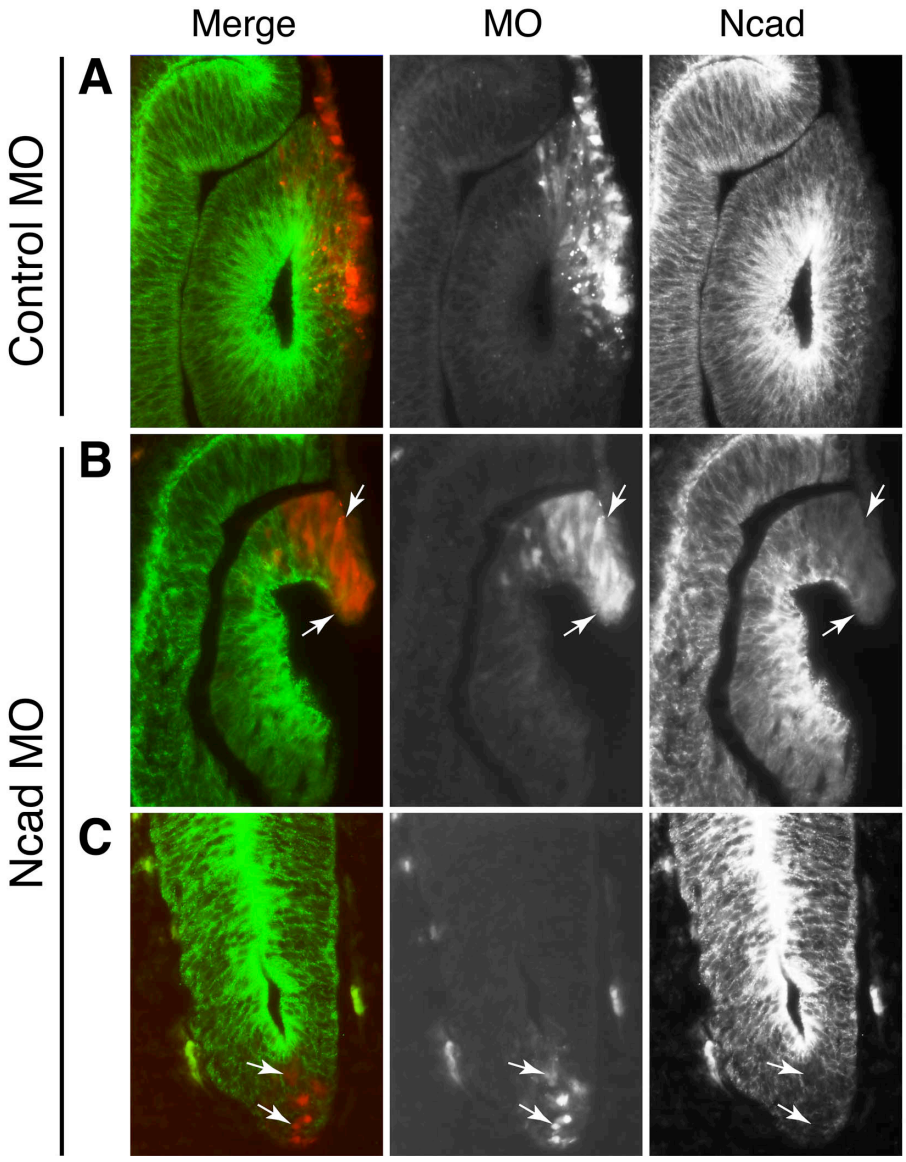

Figure 3. Ncad morpholino is effective in depleting the N-cadherin protein. In contrast to (**A**) the control MO, Ncad MO is effective in blocking translation of N-cadherin protein in the (**B**) lens and (**C**) neural tube where N-cadherin expression is high and persistent, as shown by loss of N-cadherin expression (green; also shown in right panel) in Ncad MO cells (red; also shown in middle panel).

Figure 4.

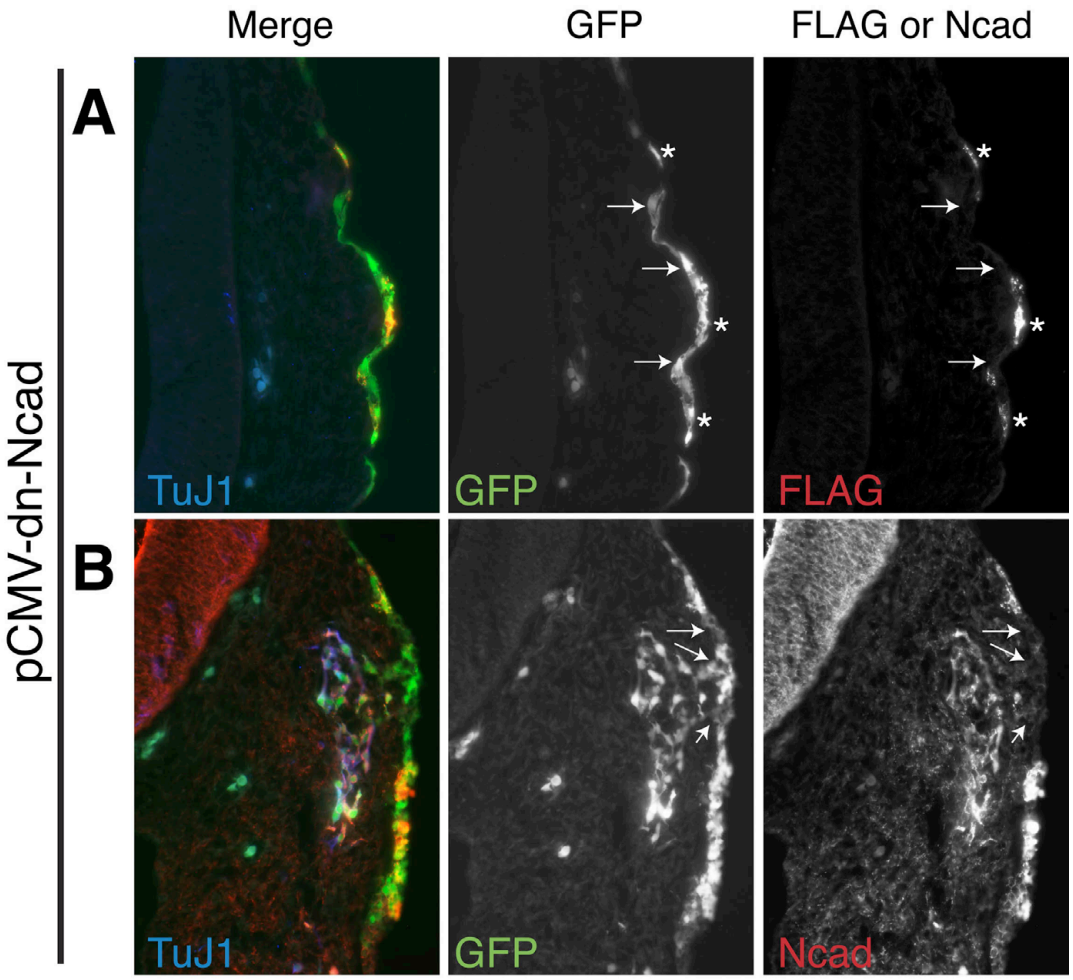

Figure 4. pCMV-dn-Ncad expression leads to mosaic dn-Ncad protein expression. Placodal cells co-electroporated with a control GFP vector and pCMV-dn-Ncad do not all express the dn-Ncad protein. Not all GFP expressing cells express the dn-Ncad protein as visualized by (**A**) the FLAG epitope which is fused to the dn-Ncad (arrows), instead only a subpopulation does (asterisk). (**B**) Similar results were observed using the MNCD2 antibody which recognizes the extracellular domain of N-cadherin and can also detect dn-Ncad; arrows show cells that express GFP but not dn-Ncad. Nonetheless, a large population of the electroporated cells do express the dn-Ncad protein.

Figure 5.

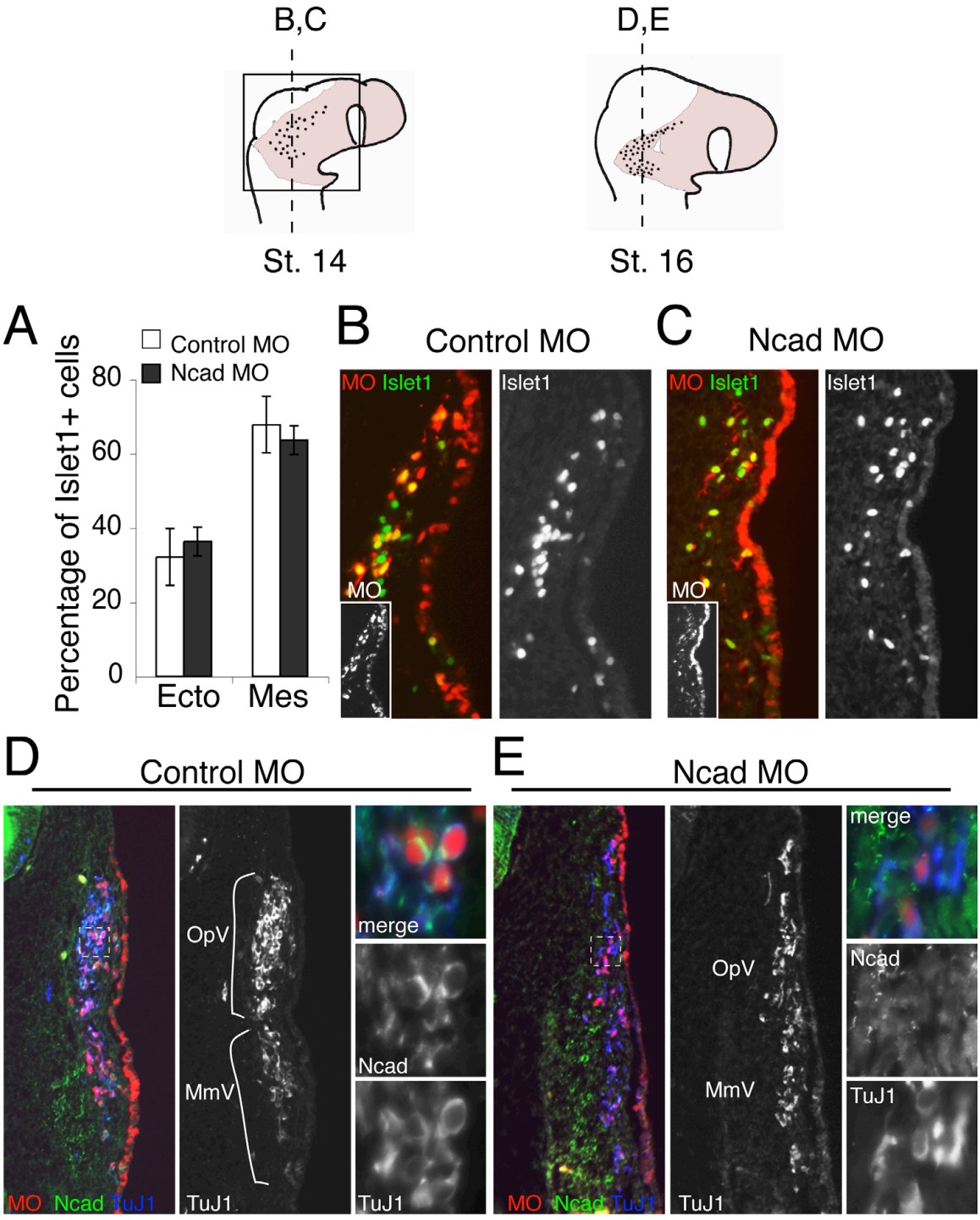
B,C
D,E
St. 14
St. 16
A
Control MO
Ncad MO
Percentage of Islet1+ cells
80
60
40
20
0
Ecto
Mes
B
Control MO
C
Ncad MO
MO Islet1
Islet1
MO
D
Control MO
E
Ncad MO
OpV
MmV
merge
Ncad
TuJ1
MO Ncad TuJ1

Figure 5. N-cadherin is required for placodal condensation, but not ingression. (**A**) Histogram shows that the percentages of Islet1+ placodal cells associated with ectoderm or in the mesenchyme between control MO (n=4) and Ncad MO (n=3) embryos were not significantly different, suggesting that N-cadherin may not be required for ingression. (**B**, **C**) Left, color overlay of MO transfection (red and inset) and Islet1 (green) expression on placodal cells, and right, single channel image of Islet1 of the same section. Compared to (**B**) control MO embryos, placodal cells in the (**C**) Ncad MO embryos appear more scattered early on during ingression at stage 14. (**D**, **E**) Left, color overlay of MO (red), N-cadherin (green), and TuJ1 (blue) on placodal cells; middle, single channel of TuJ1 of the same section; right column of panels, high magnification images of the dotted boxed region in color overlay panels (left). (**D**) Frontal plane section through a stage 16 control MO embryo shows beginning of coalescence of placodes into distinct OpV and MmV lobes (demarcated by white brackets). High magnification of the boxed region shows that these control MO placodal cells retain N-cadherin expression and appear clustered as revealed by TuJ1. (**E**) By contrast, Ncad MO placodal cells appear abnormally dispersed and the OpV and MmV lobes are not easily distinguishable. High magnification of the boxed region shows that these cells have reduced or no N-cadherin expression and have less cell contacts with one another. Schematic of stage 14 chick embryo shows the boxed region of analysis for placodal ingression and the level of sections in **B** and **C** and stage 16 chick embryo schematic shows the level of sections in **D** and **E**. Ecto, ectoderm associated; Mes, mesenchyme; OpV, ophthalmic; MmV, maxillo-mandibular.

Figure 6.

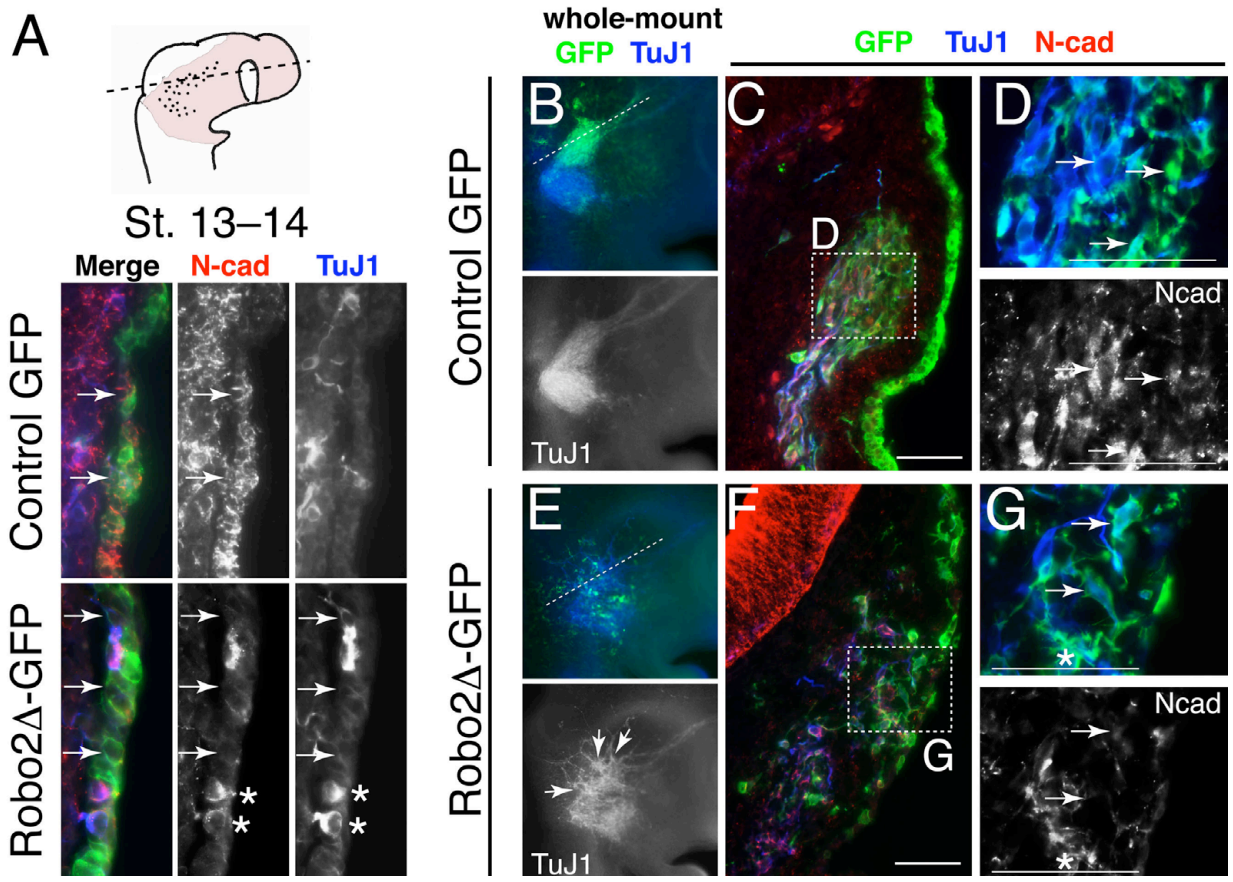
A
St. 13–14
Merge
N-cad
TuJ1
Control GFP
Robo2Δ-GFP
whole-mount
GFP TuJ1
GFP TuJ1 N-cad
B
C
D
E
F
G
TuJ1
Ncad
Control GFP
Robo2Δ-GFP

Figure 6. Blocking Robo2 function can downregulate N-cadherin expression in placodes. (**A**) Cross section through the OpV in stages 13–14 control GFP embryos shows N-cadherin expression in the placodal ectoderm and ingressing placodal cells labeled by TuJ1 (arrows). However, Robo2Δ-GFP placodal cells at the same stages and region have lower intensity of N-cadherin immunostaining in the placodal ectoderm (arrows), though some TuJ1 expressing placodal cells in the ectoderm still retain some levels of N-cadherin (asterisks). Later in the forming ganglion at stage 16, (**B**) control GFP placodal cells coalesce normally into ganglion. (**C**) In a section through the OpV indicated in **B**, these GFP expressing placodal neurons express N-cadherin (**D,** arrows). However, (**E**) Robo2Δ-GFP placodal neurons do not assemble properly. (**F**) In a section at the level shown in **E**, they appear abnormally disorganized with aberrant axonal projections and these individual cells that appear more dispersed have markedly reduced N-cadherin expression (**G,** arrows). Some Robo2Δ-GFP cell clusters still express N-cadherin (**G,** asterisk). Scale bars, 100 μm in C and F, and 50 μm in D and G. OpV, ophthalmic.

Figure 7.

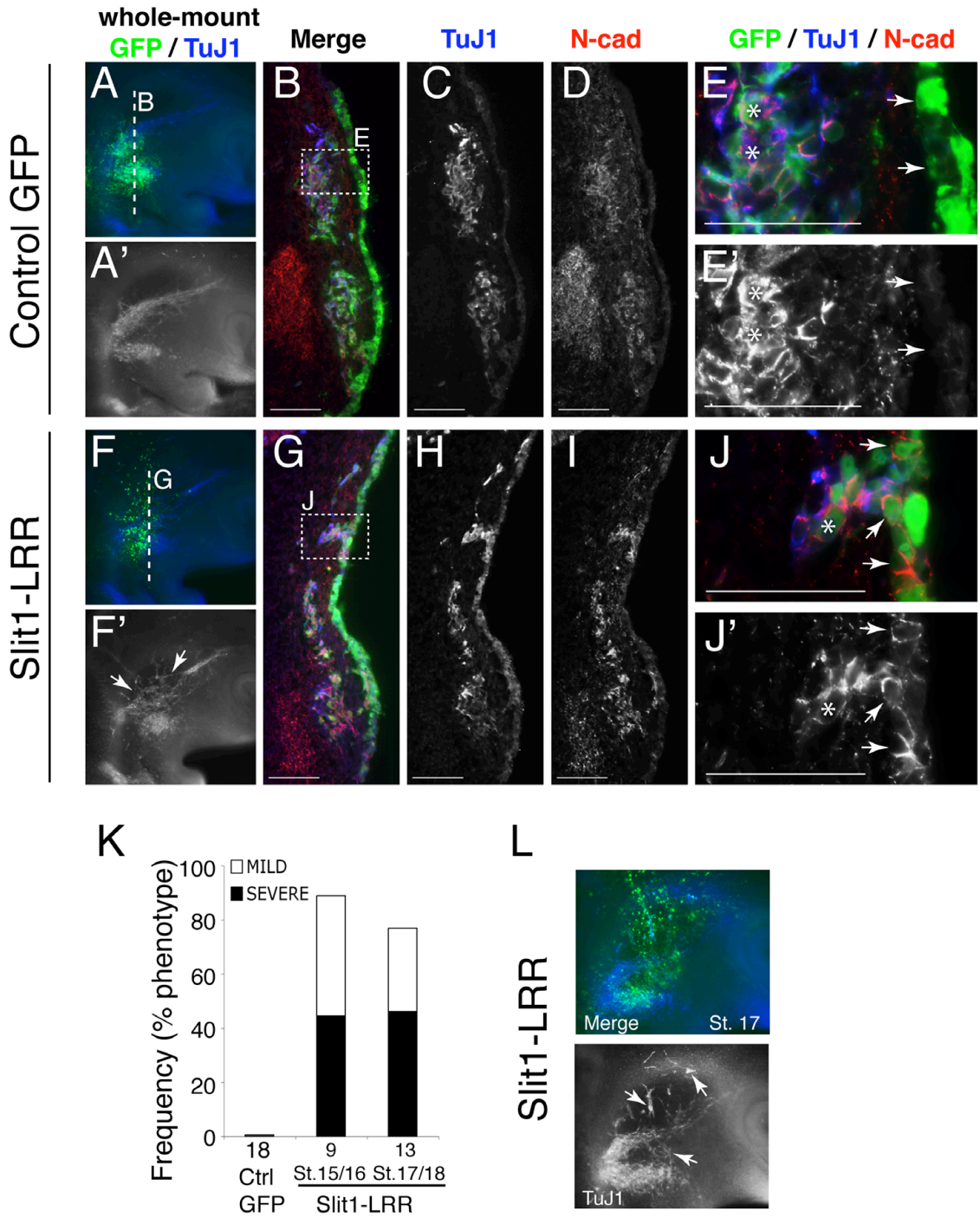
whole-mount
GFP / TuJ1
Merge
TuJ1
N-cad
GFP / TuJ1 / N-cad
Control GFP
Slit1-LRR
A
B
C
D
E
A'
E'
F
G
H
I
J
F'
J'
K
Frequency (% phenotype)
100
80
60
40
20
0
MILD
SEVERE
18
9
13
Ctrl
GFP
St.15/16 St.17/18
Slit1-LRR
L
Slit1-LRR
Merge
St. 17
TuJ1

Figure 7. Slit1 overexpression causes upregulation of N-cadherin expression in the placodal ectoderm. In stage 16 control GFP embryos shown in (**A**) color overlay of GFP (green) and TuJ1 (blue) and (**A'**) TuJ1 single channel. (**B–D**) Section at the level indicated by the dotted line in **A** shows proper coalescence of placodal cells in both OpV and MmV regions. (**E**,**E'**) High magnification of boxed region in **B** showing that N-cadherin is highly expressed by ingressed and condensing placodes (asterisks), but down-regulated in the placodal ectoderm which has no or little N-cadherin expression (arrows). By contrast, (**F**, **F'**) Slit1-LRR expressing placodal cells do not assemble properly into ganglion and appear to aberrantly aggregate at stage 16. (**G–I**) Section at the level indicated by the dotted line in **F** shows that these placodal neurons aberrantly cluster and sometimes remain in contact with the surface ectoderm. (**J**,**J'**) High magnification image of boxed region in **G** shows that in these abnormal placodal clusters, placodal cells (TuJ1+) have markedly increased N-cadherin expression in the surface ectoderm (arrows), where N-cadherin is normally down-regulated, and ingressed placodes also express N-cadherin (asterisks). (**K**) Histogram of data shows that the frequency of aberrant ganglionic aggregations is significant in Slit1-LRR embryos though the stages of gangliogenesis (stages 15–18). (**L**) At later stages 17–18, ectopic placodal neuronal clusters and abnormal placodal coalescence were found in Slit1-LRR embryos (arrows). Scale bars, 100 μm in B–D and G–I, and 50 μm in E, E', J, and J'.

Figure 8.

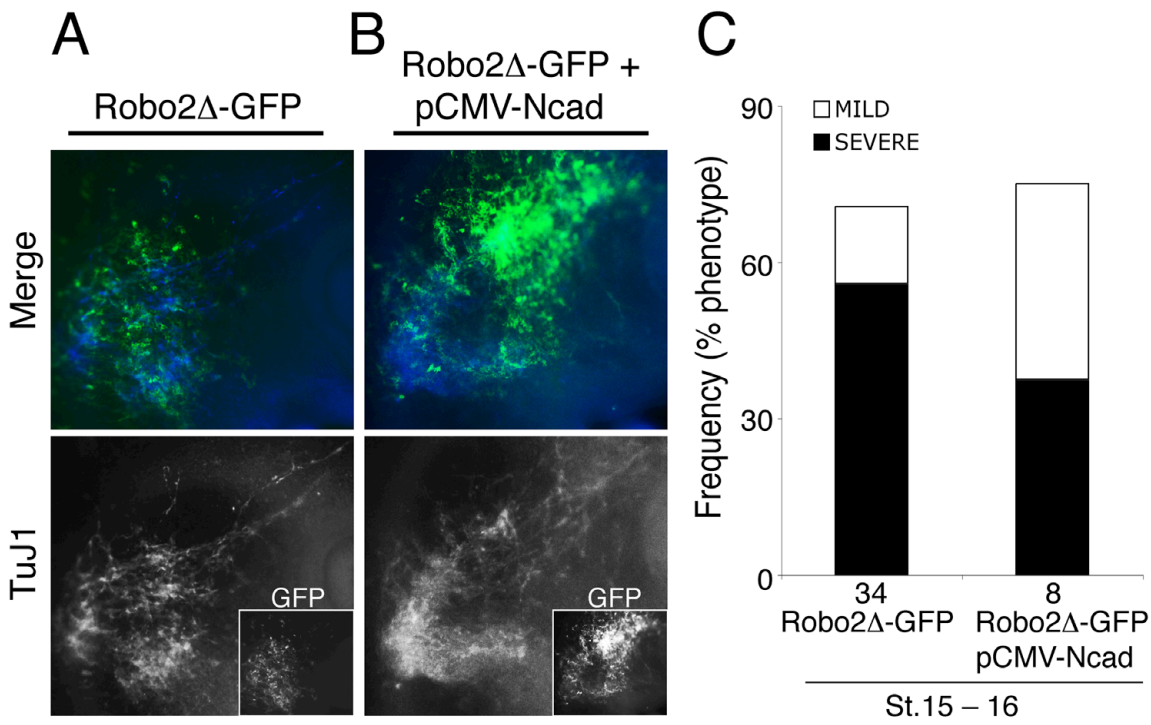

Figure 8. Full-length N-cadherin partially rescues effects of Robo2 inhibition. (**A**) The severe effects of Robo2Δ-GFP causing severely disorganized and dispersed placodal ganglia can be suppressed by (**B**) coexpression of full-length N-cadherin, which leads to more coalesced ganglia. Insets, GFP expression showing region of transfection. (**C**) Histogram of data shows that co-electroporating full-length N-cadherin and Robo2Δ-GFP markedly reduces the severe effects of Robo2Δ-GFP. Numbers below bar graphs represent the number of transfected ganglia analyzed.

Figure 9.

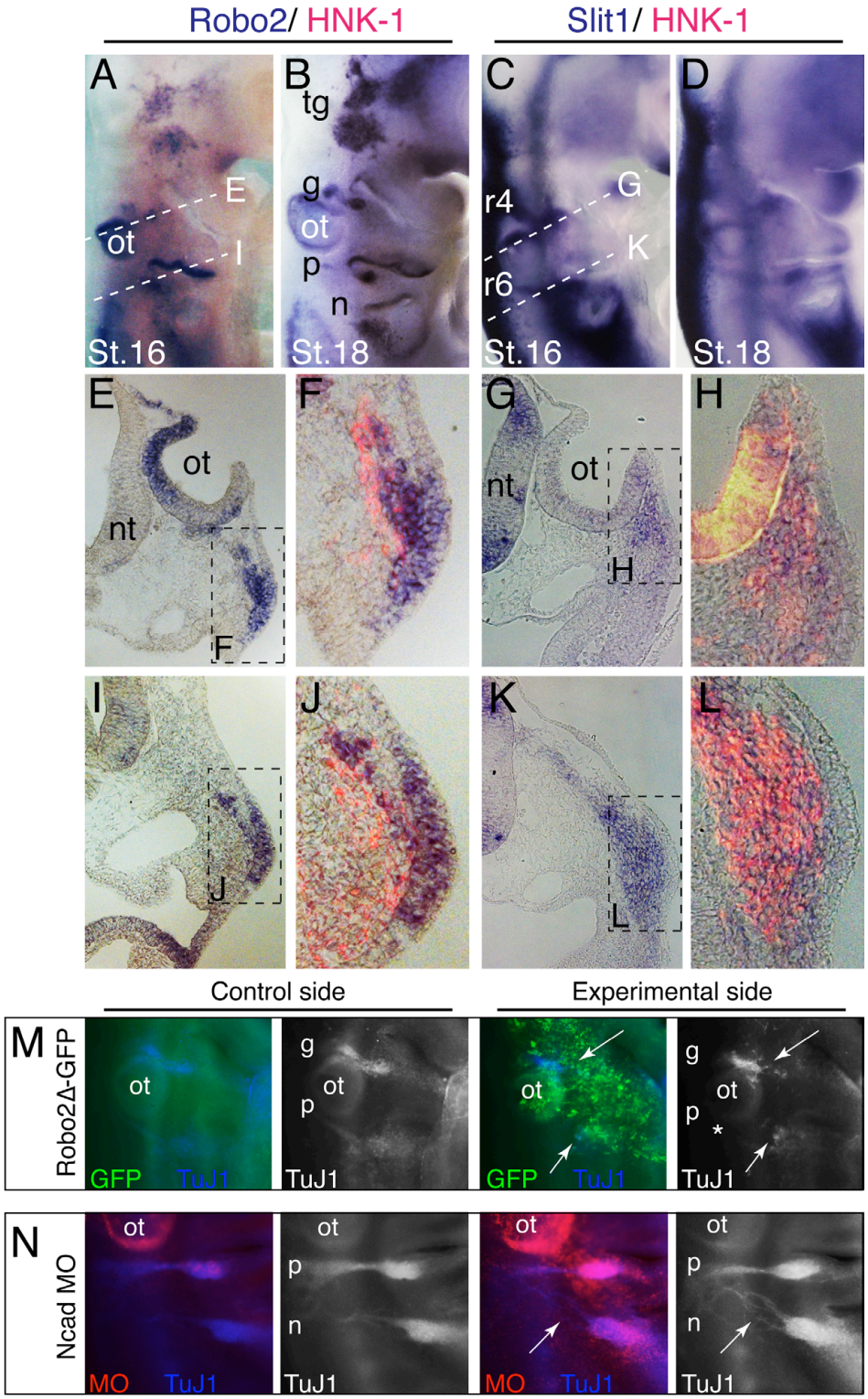
Robo2/ HNK-1
Slit1/ HNK-1
A
B
tg
g
ot
p
n
C
r4
G
K
r6
D
E
I
St.16
St.18
St.16
St.18
E
ot
nt
F
F
G
nt
ot
H
H
I
J
J
K
L
L
Control side
Experimental side
M
Robo2Δ-GFP
ot
GFP
TuJ1
g
ot
p
TuJ1
ot
GFP
TuJ1
g
ot
p
*
TuJ1
N
Ncad MO
ot
MO
TuJ1
ot
p
n
TuJ1
ot
MO
TuJ1
ot
p
n
TuJ1

Figure 9. Expression of Robo2 and Slit1, and the functions of Robo2 and N-cadherin in the forming epibranchial ganglia suggest a common mechanism underlying neural crest–placode interaction during cranial gangliogenesis. Robo2 mRNA is expressed in all the epibranchial placodes shown (**A**) at early ganglia assembly at stage 16 and (**B**) persists in the condensing ganglia at stage 18. Hindbrain neural crest streams at rhombomeres 4 and 6 that intermingle with epibranchial placodes concurrently express Slit1 mRNA (**C**) during ganglia assembly at stage 16 but (**D**) begin to downregulate Slit1 in the condensed ganglia by stage 18. (**E**) Cross section at stage16 at the level indicated in **A** shows Robo2 expression in the otic vesicle and in both ectodermal and ingressing geniculate placodes, which (**F**) is complementary to the HNK-1 expression by neural crest cells that (**G**,**H**) are expressing Slit1. Similarly, (**I**) petrosal placodes express Robo2 in the surface ectoderm and during ingression at stage 16 as shown in a cross section at the level indicated in **A** and (**J**) associate with HNK-1+ neural crest cells (**K**,**L**) that express Slit1. (**M**) Compared to the control side with no DNA transfection, the Robo2Δ-GFP electroporated epibranchial ectoderm of the same stage 15 embryo showed severely disorganized geniculate and petrosal placodal ganglia (arrows), and reduction or loss of axonal projections to the hindbrain by the forming petrosal ganglion (asterisk). (**N**) In contrast to the control side with no transfection in the nodose ganglion, knockdown of N-cadherin by Ncad MO caused disorganization of the nodose placodal neurons, namely their central axonal projections at stage 17 (arrow). ot, otic vesicle; tg, trigeminal; g, geniculate; p, petrosal; n, nodose; r4, rhombomere 4; r6, rhombomere 6; nt, neural tube.

Chapter 4

Role of Cadherin-7 in cranial neural crest development and its potential heterotypic interaction with N-cadherin in trigeminal ganglion formation

4.1 Abstract

Cadherins are transmembrane molecules best known for mediating intercellular adhesion through homophilic binding of identical cadherins. A widely held view is that expression of different cadherins drives selective intercellular adhesion that is crucial for tissue segregation and boundary formation. This is largely based on their dynamic spatiotemporal expression patterns during morphogenesis, as well as results from in vitro cell aggregation assays showing segregation of cells expressing different cadherins. However, cadherin interaction is likely more broad. Several recent studies have shown that cadherins of different subtypes can interact with each other in vitro indistinguishably from homophilic binding. This idea remains to be explored in vivo. Here, departing from the conventional model, we test the possibility that interactions between neural crest and ectodermal placodes during trigeminal ganglion formation in the chick may rely on both heterotypic and homotypic interactions of at least two different cadherins. We have shown in Chapter 3 that N-cadherin is expressed by placodal neurons during condensation of cranial ganglia and is critical for proper gangliogenesis. Because of their dual origin, coalescence of trigeminal ganglion may involve crest–crest, crest–placode, and/or placode–placode adhesion. However, the molecular mechanism mediating neural crest–placode condensation remains to be explored. To test the intriguing poassibility that interactions between Cadherin-7, which is expressed by migrating neural crest cells (Nakagawa and Takeichi, 1995), and N-cadherin on placodal neurons, may be involved in

ganglion formation, we first examined the protein expression and function of Cadherin-7 relative to N-cadherin. The results show that neural crest cells express the Cadherin-7 protein while they are intermixing with placodal neurons expressing N-cadherin in the forming ganglion. Moreover, perturbation of Cadherin-7 affects cell morphology and cell–cell interactions during migration and later leads to malformed cranial ganglia. In contrast, the overall migration stream pattern of cranial neural crest appeared unaffected. Misexpression of Cadherin-7 in the placodal ectoderm severely interrupts normal placodal morphogenesis and causes an increase in neuronal cells in the ectoderm. Our results suggest the possibility that both heterophilic and homophilic cadherin mediated adhesion drive coalescence of cranial sensory ganglia, and that there are distinct functions of Cadherin-7 contributing to neural crest cell migration versus cranial ganglia formation.

4.2 Introduction

The expression of classical (type I and type II) cadherins during vertebrate development is tightly regulated and coincides with crucial morphogenetic events, such as gastrulation, neurulation, nephrogenesis, neural crest emigration as well as in pathological cases such as cancer (Pla et al., 2001; Taneyhill, 2008; Wheelock et al., 2008). In these examples, the switching of expression of one cadherin subtype to another appears to match changes in tissue adhesive properties. For example, as neural crest cells undergo an epithelial-mesenchymal transition, acquire motility and exit the neural tube, they shift from expressing N-cadherin to Cadherin-6b in the chick dorsal neural tube and then to Cadherin 7 in migrating neural crest cells. Cadherins are thought to primarily mediate selective adhesion between cells expressing the same cadherin subtype. Evidence to this effect

comes from experiments showing that distinct cells expressing different cadherin segregate from one another and form distinct aggregates (Nose et al., 1988), suggesting that homophilic binding of cadherins drives tissue segregation and maintains tissue integrity (Takeichi, 1990). More recently, however, in vitro cell binding and aggregation assays have shown that heterophilic interaction can also occur. Cells expressing different classical cadherins either of type I or type II can heterotypically bind and intermix to form aggregates indistinguishable from homotypic interaction (Duguay et al., 2003; Shimoyama et al., 2000). Consistent with this, cadherin bond strengths by force measurements show similar adhesion between heterotypic and homotypic interactions (Prakasam et al., 2006). However, there is little information regarding whether classical type I and type II cadherins interact. A study on the protein structure of the ectodomain of type II suggests that type I and type II are overall very similar but have distinct adhesive interfaces at the EC1 domain— type I has one conserved tryptophan residue (W2) versus two conserved tryptophan residues (W2 and W4) and a larger hydrophobic pocket in type II— that are thought to preclude their binding (Patel et al., 2006). However, this remains unexplored in vivo.

We have previously shown that N-cadherin plays an important role during aggregation of placode-derived neurons into ganglia. However, the mechanism underlying coalescence of their partner cells, the neural crest, is not known. Here, we investigate Cadherin-7 as a possible candidate for mediating neural crest assembly, since it is expressed in the migrating cranial neural crest (Nakagawa and Takeichi, 1995). We find that neural crest cells express the Cadherin-7 protein in a complementary pattern to N-cadherin on placodal neurons, raising the intriguing possibility for interactions between two distinct classes of cadherins (N-cadherin, a type I, and Cadherin-7, a type II) during trigeminal gangliogenesis. Perturbation of Cadherin-7 affects crest–crest interactions and morphology, later resulting in disfigurement of the ganglion. The results provide a basis for

testing the possibility of a novel heterophilic interaction between classical type I and type II cadherins in vivo. The interaction between neural crest and placodes serves as an excellent new model to examine the dynamic role of cadherins in cell–cell interactions during cellular coalescence in vivo.

4.3 Materials and methods

Embryos

Fertilized chicken *(Gallus gallus domesticus)* eggs were obtained from local commercial sources and incubated at 37°C to the desired stages according to the criteria of Hamburger and Hamilton (Hamburger and Hamilton, 1992).

In situ hybridization

Whole mount chick in situ hybridization was performed as described (Shiau et al., 2008). cDNA plasmids obtained from BBSRC (ChickEST clones 445e6 and 854n16) were used to transcribe antisense riboprobes against chick Cadherin-7. The plasmids were sequenced and determined to contain the coding sequence of the chick Cadherin-7 gene (NCBI accession number: NM_204187.1) corresponding to nucleotides 1950-2433 (445e6 clone) and 1873-2963 (854n16 clone). Both riboprobes gave the same expression patterns. Embryos were imaged and subsequently sectioned at 12 μm.

Immunohistochemistry

Whole chick embryos were fixed in 4% paraformaldehyde overnight at 4ºC, washed in PBT (PBS + 0.2% tween) and either immunostained as whole embryos and/or processed for 10 μm cryostat sections. Primary antibodies used were anti-N-cadherin (DSHB, MNCD2 clone; 1:1), anti-GFP (Molecular Probes; 1:1000 to 1:2500), anti-HNK-1 (American Type Culture; 1:3 or 1:5), anti-Cadherin-7 (DSHB, clone CCD7-1; 1:1), and anti-TuJ1 (Covance; 1:250). Secondary antibodies: cyanine 2 or rhodamine red-x conjugated donkey anti-rat IgG (Jackson ImmunoResearch) used at 1:1000 and all others were obtained from Molecular Probes and used at 1:1000 or 1:2000 dilutions (except 1:250 dilution for Alexa Flour 350 conjugated antibodies). Images were taken using the AxioVision software from a Zeiss Axioskop2 plus fluorescence microscope, and processed using Adobe Photoshop CS3.

In ovo electroporation of cranial neural crest and the trigeminal ectoderm

For the presumptive cranial neural crest, DNA injection was targeted in the neural folds at stage 8 or presumptive neural crest region at gastrula stages 4–6 in ovo. Platinum electrodes were placed horizontally across the neural folds at stage 8 and electrical pulses of 2 × 25 V in 50 ms at 100 ms intervals were delivered. At stages 4–6, the electrodes were placed vertically across the epiblast and 5 × 4–7 V in 50 ms at 100 ms pulses were delivered. For stages 4–6 electroporation, two points of special care were used: first, eggs were taken out of the incubator individually, manipulated, and immediately placed back into the incubator to minimize the time they sat at room temperature, and second the amount of india ink used to visualize the embryo was minimized (just enough to faintly depict the embryo). For the trigeminal ectoderm, DNA was injected overlying the presumptive trigeminal placodal ectoderm at stages 8–10 by air pressure using a glass micropipette. Platinum electrodes were placed vertically across the chick embryo

delivering 5 × 8 V in 50 ms at 100 ms intervals current pulses. Electroporated eggs were resealed and re-incubated at 37˚C to reach the desired stages.

Plasmid constructs

FL-Cad7-cytopcig expression vector was cloned from excising the full-length coding sequence plus the FLAG epitope at BsiWI (later blunted) and NotI sites from pCMV-c7/FLAG-pA, a vector derived from (Nakagawa and Takeichi, 1998). This fragment was inserted into the pBS II KS cloning vector (Stratagene) at EcoRV and NotI sites. Full-length Cadherin-7 fragment was then cut out at NotI (later blunted) and also at ClaI; this was inserted into the cyto-pcig vector (Shiau et al., 2008) at ClaI/EcoRV (where the EcorRV site is disrupted). FL-cad7 (clone C1) was determined to be correct by sequencing. EC-Cad7-cytopcig encodes the extracellular Cadherin-7 protein up to the pre-transmembrane domain, corresponding to nucleotides 479–2080 of the chick Cadherin-7 mRNA (accession: NM_204187.2). This fragment was cloned by PCR from the original vector pCMV-c7/FLAG-pA into the PCRII-TOPO vector. Clones were sequenced and the correct clone (TC-4) was used for the subsequent steps. The 5' to 3' sequence of the PCR primers were: (cd7-F) ggaaaaaaaagatgaagttgggc and (dncd7-R) tcatcaattatggttatttgctgc. As an intermediate step, the fragment was cut at EcoRV/BamHI and ligated into the pBS II KS vector at the same sites. Lastly, the EC-Cad7 fragment was excised at BamHI (later blunted) and then at ClaI, and was then inserted into cyto-pcig at ClaI/EcoRV (where the EcorRV site is disrupted). EC-cad7 or tn-cad7 (clone n9) was determined to be correct by sequencing.

4.4 Results and discussions

4.4.1 Cadherin-7 mRNA is expressed in migrating cranial neural crest cells and later restricted to dorsal regions of cranial ganglia

We characterized the mRNA expression of Cadherin-7 in chick embryos from stages of early cranial neural crest migration to ganglion formation (stages 10–18). By whole mount in situ hybridization, we found that cranial neural crest cells begin to express Cadherin-7 only after they have left the neural tube at all axial levels in the head. By stage 16 when the ganglia have begun coalescing, the mRNA expression is mostly restricted to those neural crest cells occupying the dorsal portion of the ganglia (adjacent to the hindbrain) (Fig. 1, A-E). This dorsal expression of Cadherin-7 at exit points of cranial motor axons which correspond to the even-numbered rhombomeres (r2, r4, and r6) has been reported previously; these sites also represent the entry points where sensory axons from the cranial ganglia enter the hindbrain (Nakagawa and Takeichi, 1995; Niederlander and Lumsden, 1996; Osborne et al., 2005).

Neural crest cells migrate in well-characterized streams along almost the entire length of the body axis in a rostrocaudal progression. The first migrating neural crest cells emerging from the midbrain region express Cadherin-7 at stage 10, as shown in Fig. 1A. Interestingly, even at stage 10, the expression of Cadherin-7 mRNA appears to be downregulated in the most distally located cells that have migrated furthest. Cranial neural crest cells migrate in three streams along the rostrocaudal cranial neuraxis: first (midbrain and r1/r2), second (r4), and third (r6) (Fig. 1, F-M). Cadherin-7 expression appears to be increasingly fainter in migrating neural crest cells as migration progresses. For example, most cells in the first stream express Cadherin-7 at the beginning of migration at stage 10 with the exception of the most ventrally migrating cells (Fig. 1F,G). Toward the end of

their migration at stage 13, most neural crest cells have downregulated Cadherin-7 mRNA except for those in the dorsal region near the trigeminal motor exit point (Fig. 1, K-M). This expression pattern further refines and becomes smaller after migration and during ganglion coalescence at stages 16–18 (Fig. 1D,E). Cadherin-7 expression is also detected weakly in the ventrolateral neural tube and in some parts of the surface ectoderm, including the otic placode, but is not in surface ectoderm or placode-derived cells during ganglion formation (Fig. 1G, J).

The results suggest that the transcription of Cadherin-7 is dynamically regulated during neural crest migration, such that neural crest cells that have migrated more ventrally downregulate Cadherin-7, whereas late migrating cells that reside near cranial motor exit points retain expression. This contrasts with the idea initially proposed by Nakagawa and Takiechi (1995) that Cadherin-7 is expressed by a distinct subpopulation of neural crest cells that segregate and sequester near the exit points. Our interpretation is supported by in vivo time-lapse imaging that shows that cranial neural crest cells undergo progressive spatially-ordered cell migration. They first leave the dorsal neural tube and then move laterally beneath the surface ectoderm, and thus directionally away from the neural tube. There is no indication of early segregation or clustering of cells near the exit points (Kulesa and Fraser, 2000; Kulesa et al., 2008). Furthermore, previous studies have also shown that late- emigrating neural crest cells remain closer to the dorsal portion of the embryo, whereas early- emigrating cells occupy and give rise to more ventral structures (Baker et al., 1997; Niederlander and Lumsden, 1996).

4.4.2 Cadherin-7 protein is similar but broader than the mRNA and complementary to N-cadherin expression in the trigeminal ganglion

Since mRNA expression does not necessarily reflect that of protein which is more directly indicative of function, we examined the expression pattern of Cadherin-7 protein at times of cranial neural crest migration (stage 11) and ganglion condensation (stage 18) (Fig. 2). Surprisingly, Cadherin-7 protein was expressed more broadly than its mRNA in the first migratory neural crest stream (Fig. 2A) and during condensation into the trigeminal ganglion (Fig. 2D). During migration, the vast majority of neural crest cells express Cadherin-7 protein, but the cells that have migrated furthest distally appear to have lower expression compared to that of the proximally located cells. This difference may indicate that though the transcript is readily downregulated, Cadherin-7 protein has a slow turnover and is retained on the neural crest cell surface. Cadherin-7 protein expression was found in the most proximal region of the ganglion, which is neural crest derived (Fig. 2B,C) and throughout the forming trigeminal ganglion at stage 18 (Fig. 2D,E). Cadherin-7 protein expression is largely reciprocal to that of N-cadherin on placodal neurons, which can be recognized using the neuronal marker β-neurotubulin (TuJ1) (Fig. 2D,E) with the exception of a few neurons that had weak Cadherin-7 expression, just above background (see example in Fig. 2E, gray arrow). Because the Cadherin-7 protein expression persists longer than mRNA, fewer differences were seen in expression levels between dorsal and ventral portions of the trigeminal ganglion. The complementary protein expression of Cadherin-7 on neural crest and N-cadherin on placodal neurons raises an intriguing possibility for heterophilic cadherin interaction in mediating condensation of these highly intermixed cell populations.

Similar to the head, distinction between Cadherin-7 mRNA and protein also can be noted in the trunk neural crest where mRNA is restricted to the proximal dorsal and

ventral roots (Nakagawa and Takeichi, 1995), but protein is expressed by migratory cells forming the dorsal root ganglia (Nakagawa and Takeichi, 1998).

4.4.3 In vivo perturbation of Cadherin-7 function in the cranial neural crest affects cell–cell interactions and cellular protrusions

To investigate the possible role of Cadherin-7 in ganglion formation, we examined the effects of increasing Cadherin-7 levels or blocking its function in the cranial neural crest, which is known to have abundant and dynamic cell–cell contacts during migration (Kulesa and Fraser, 2000; Teddy and Kulesa, 2004). For this purpose, we cloned into a bicistronic vector encoding IRES-GFP with a chick β–actin promoter (cyto-pcig), a full-length Cadherin-7 (FL-Cad7-cytopcig) as well as a truncated Cadherin-7 (EC-Cad7-cytopcig), coding sequence. EC-Cad7 was designed to encode the first four cadherin repeats based on a natural splice Cadherin-7 variant previously shown to inhibit full-length Cadheirn-7 (Kawano et al., 2002). Empty vector (cytopcig) was used as a negative control. Constructs were electroporated in ovo into one side of the dorsal neural tube prior to neural crest emigration at stage 8 (3–5 somites stage). Embryos with high levels of GFP expression were analyzed after about 15–24 hours of incubation (stages 10–14). For controls, we compared the electroporated side of experimental embryos to control GFP embryos as well as to the contralateral side of the same embryos as an internal control. Many embryos that were highly transfected also received construct within the surface ectoderm on the contralateral side (due to leakage of injected DNA outside of the neural tube). Embryos were analyzed for the three characteristic cranial neural crest migration streams using several neural crest markers: HNK-1, *FoxD3*, and *Sox10*. No differences were noted in the overall migration pattern between control GFP (n=13), FL-Cad7 (n=7) and EC-Cad7 (n=13) embryos (Fig. 3, A-C and data not shown).

However, careful examination of the neural crest cells in transverse sections through these embryos revealed marked differences between experimental and control embryos. Transfection of both FL- and EC- Cad7 vectors into neural crest cells resulted in significant protein overexpression (Fig. 3D). Since endogenous Cadherin-7 levels were generally very weak by immunostaining, most of the antibody staining reflects exogenous expression of FL- or EC- Cad7 expression. The strong Cadherin-7 staining noted in GFP expressing transfected neural crest and neural tube cells on the electroporated compared with the control contralateral side confirms that the expression reflects exogenous proteins. Interestingly, neural crest cells overexpressing FL-Cad7 tend to cluster with each other in a manner that correlates with high expression of FL-Cad7 at the adherens junction (Fig. 3D). Even though these cells interact abnormally, they still manage to leave the neural tube and migrate in separate streams. In contrast, neural crest cells expressing high levels of EC-Cad7 appear to have normal organization, making cell contacts with one another and migrating similarly to control GFP embryos (Fig. 3D). In the future, dynamic analysis of these cells using live imaging will be used to more fully characterize their behaviors. Aberrant protrusion of EC-Cad7 and wild type neural crest cells was observed on the apical side of the dorsal neural tube adjacent to the second rhombomere (r2) level but not elsewhere (Fig. 3D). This suggests that perhaps the EC-Cad7 constructs can disrupt Cadherin-7 or other cadherins in the neural tube (i.e. Cadherin 6b) that are required for emigration in a cell-autonomous and non-autonomous manner. Both transfected and non-transfected (HNK-1+ but GFP-) neural crest cells were found in the protrusion. This is not surprising, since the construct is designed to produce a soluble extracellular form of Cadherin-7 which perhaps may bind to other cadherins at lower affinities and affect other cells. However, this effect may be marginal since most neural crest cells still migrate away from the neural tube normally.

Since neural tube electroporation is mosaic and often less than 50% of the neural crest population is transfected, we cannot completely assess effects of exogenous expressions without achieving higher transfection levels. To circumvent this potential limitation, we also introduced these constructs at gastrula stages (stages 4-6) where most if not all of the neural crest cells, as well as some ectodermal cells are transfected. In these embryos, the effect of overexpressing Cadherin-7 on neural crest cell morphology was more severe than that described above at stage 8. Analysis by HNK-1 staining showed that these cells were more clustered and appeared rounded with fewer cellular protrusions (n=4, Fig. 4D). Again the overall pattern of migration streams was normal (Fig. 4, A-B). Taken together, altering the levels of Cadherin-7 appears to have some effects on neural crest cell clustering and morphology but not the formation of the separate migratory streams.

4.4.4 Subcellular localization and expression pattern of exogeneous full-length Cadherin-7 on migrating neural crest cells suggest dynamic regulation of the Cadherin-7 protein

We observed interesting differences in the expressions of full-length (FL) versus extracellular (EC) Cad7 protein in the neural crest. First, the FL-Cad7 was detected mainly at cell boundaries or at junctions between cells that appear more tightly associated and can be either punctate or continuous along the cell membrane (Fig. 3D and Fig. 4C). This is different from the EC-Cad7 protein whose subcellular localization is more widespread, detected both in the cytoplasm and at the membrane but not restricted to the adherens junction (Fig. 3D). The expression of FL-Cad7 is consistent with the idea that FL-Cad7 is mediating cell adhesion and that the protein is dynamically regulated at the cell surface. Second, EC-Cad7 is expressed by most, if not all transfected neural crest cells whereas FL-Cad7 is expressed strongly in only some GFP expressing transfected cells. Other GFP cells express little or no detectable FL-Cad7, at stages 12–13 (Fig. 3D).

The expression of FL-Cad7 often correlates with GFP transfected cells that appear more adherent, usually in a cluster of a few cells but sometimes only two cells along the migration pathway. The regulation of the FL-Cad7 expression pattern may be dependent on the stage of migration and/or levels of the FL-Cad7, as suggested by the observation that GFP transfected cells electroporated at gastrula stages and examined at stages 10–11, appear to all express FL-Cad7 (Fig. 4C). It is intriguing to speculate that there may be some post-translational regulation of the Cadherin-7 protein during neural crest migration. This is unlikely to involve transcriptional control, since the levels of GFP, which is encoded on the same bicistronic mRNA with FL-Cad7, were unaffected.

One possibility is that Cadherin-7 may undergo similar post-translational modification as that observed for Cadherin-11 by ADAM metalloproteases during Xenopus neural crest migration (McCusker et al., 2009). Regulation of cadherins by ADAMs has also been shown in the trunk neural tube in chick, prior to neural crest emigration (Shoval et al., 2007), as well as in other systems (Maretzky et al., 2005; Reiss et al., 2005). The expression of Cadherin-7 in chick is similar to Cadherin-11 in Xenopus (Vallin et al., 1998), as both are specifically expressed in migrating neural crest cells, whereas in mouse neural crest, Cadherin-6 is expressed in both premigratory and migrating neural crest (Inoue et al., 1997); therefore studies on Xcadherin-11, also a classical type II cadherin, may be relevant to our understanding of Cadherin-7. McCusker et al. (2009) shows that endogenous Cadherin-11 undergoes cleavage during neural crest migration producing a putative extracellular product encompassing the first three cadherin repeats (EC1–3) and thus the remaining cleaved Cadherin-11 no longer has the first extracellular domain (EC1) sited for homophilic binding (Patel et al., 2006). Blocking this cleavage by reducing ADAMs or overexpressing Cadherin-11 inhibits neural crest migration, likely due to an increase in cadherin-mediated adhesion. Increasing ADAMs or the putative extracellular cleavage product can reverse the

blockage of migration by Cadherin-11 (McCusker et al., 2009). Thus, cleavage of Cadherin-11 by ADAMs may regulate the levels of full-length and cleaved cadherin proteins which modulates levels of cell–cell adhesion between migrating neural crest cells. Since we used an antibody that recognizes the extracellular portion of the Cadherin-7 to detect FL-Cad7, it is possible that the loss or reduced detection of the extracellular portion of FL-Cad7 on the transfected GFP neural crest cells results from the cleavage of the Cadherin-7 protein by ADAMs during migration. Alternatively, the regulation of catenins by phosphorylation may control the levels of Cadherin-7 protein. For example, the intracellular binding partner p120-catenin of cadherins has been shown to stabilize cadherins and regulate their turnover at the cell surface (Kowalczyk and Reynolds, 2004; Perez-Moreno and Fuchs, 2006).

4.4.5 Perturbation of Cadherin-7 in precursors causes malformed cranial ganglia

To test the function of Cadherin-7 during ganglion formation, we introduced FL-Cad7 or EC-Cad7 and control GFP into embryos in ovo at early stages 4–6 in order to achieve high transfection efficiency in the neural crest cells. Embryos were analyzed after 48 hours (~ stage 16). Either overexpressing or blocking Cadherin-7 caused defects in ganglia formation, with most dramatic phenotypes in FL-Cad7 embryos (Fig. 5). In FL-Cad7 embryos, trigeminal and epibranchial ganglia appeared reduced in size, were more condensed, and had aberrant placement of placodal neurons (regions of gaps within the ganglia and also aberrant connection between the glossopharyngeal and vagal ganglia at the third and fourth branchial arches) (Fig. 5B). High levels of Cadherin-7 caused dramatic ganglia malformation but normal development of the remaining head. EC-Cad7 overexpressing embryos had much less severe defects, generally with slightly misshapen ganglia that were not reduced in size (Fig. 5C). Control GFP embryos as well as the

contralateral unelectroporated side had no apparent effects. The data suggest that overexpression of Cadherin-7 has notable effects on ganglia formation. Whether or not Cadherin-7 is essential for gangliogenesis requires further investigation using a gene knockdown approach (i.e. RNAi or morpholino).

4.4.6 Misexpression of Cadherin-7 in the trigeminal ectoderm disrupts placodal morphogenesis and augments the neuronal population in the ectoderm

We further examined the phenotype of overexpressing FL-Cad7 on the organization and coalecence of placodal neurons by examining embryos in transverse sections. We observed that misexpression of Cadherin-7 in the placodal ectoderm causes dramatic disruptions (Fig. 6), with aberrant placode-derived neuronal nodules, delamination of sheets of differentiating placodal ectoderm, and widespread neuronal cells in the surface ectoderm, which coexpresses GFP and TuJ1 (Fig. 6, B-D). The most proximal part of the ganglion adjacent to the hindbrain, which is mostly neural crest-derived, appears to assemble properly in whole mount (Fig. 5B), probably due to low level transfection of the neural crest (Fig. 6A).

Since placodal neurons generally do not express Cadherin-7 but neural crest cells do, we predicted that introducing Cadherin-7 into the placodal cells would cause neural crest cells to be abnormally more adherent to placodal neurons. However, we found that intermixing and association between neural crest and placodal neurons throughout the region of ganglion formation are aberrant. In fact, there are several instances where placodal neurons are devoid of neural crest association (Fig. 6B-D). These are generally placodal cells that appear excessively adherent to each other as they form placodal nodules and delaminate as a sheet of neurogenic ectoderm instead of undergoing proper ingression. Other regions containing placodal neurons that are less adherent and normally associated

with each other appear to intermingle with neural crest cells, however there are still spots of segregated placodal cells in the mix (Fig. 6D-D'''). This may suggest that cell adhesion between placodes and neural crest may depend less on cadherin subtype identity and more on adhesive properties (i.e. cadherin expression levels) and/or that other factors play a larger role in mediating neural crest–placode coalescence than simply expressing the same cadherin (e.g. heterophilic interaction may be required, which perhaps is disrupted by Cadherin-7 overexpression). This is consistent with in vitro cell binding assays that show two cell populations expressing two distinct cadherin subtypes can sort out or intermix depending on their relative cadherin expression levels, independent of subtype specificity. Furthermore two cell lines expressing identical cadherin but at different concentrations also sort out (Duguay et al., 2003).

The abnormal, widespread expression of the neuronal marker TuJ1 in the placodal ectoderm may indicate that Cadherin-7 expression has blocked ingression of differentiating placodal neurons and thus has kept many of these cells at the surface and/or increased neuronal differentiation within the placodal ectoderm. The large number of placodal neurons in the surface ectoderm in the distal ganglion, particularly around the first branchial arch, together with the blocked ingression may explain the appearance of the reduced trigeminal ganglion in whole mount (Fig. 5). Taken together, misexpression of Cadherin-7 can severely disrupt normal placodal morphogenesis and perhaps differentiation, likely by causing excessive cell adhesion between placodes.

4.5 Conclusion and future work

Our data suggest that Cadherin-7 may regulate neural crest cell interactions and adhesion, and later, if overexpressed, can cause severe defects in cranial ganglia formation. However, Cadherin-7 does not appear to play a role in patterning cranial neural crest cell migration into stereotypic streams. This is consistent with results of Cadherin-11 perturbation in Xenopus cranial neural crest (Borchers et al., 2001). In contrast to results observed with Cadherin-11, however, overexpression of Cadherin-7 did not block neural crest migration (Borchers et al., 2001; McCusker et al., 2009). However, the penetrance of this phenotype may depend upon the amount of mRNA injected (Borchers et al., 2001). The difference may be due to the levels of transfection, since single blastomere injections (which are not possible in the chick) can achieve higher transfection than electroporation. Cadherin-7 overexpression in the trunk neural tube has previously been reported to block neural crest emigration along the dorsolateral pathway, but not the dorsoventral stream to the dorsal root ganglia (Nakagawa and Takeichi, 1998). However, no such inhibition was observed in the cranial regions, though overexpression of the truncated Cadherin-7 (EC-Cad7) that presumably acts as a dominant-negative can affect proper emigration. During cranial neural crest migration, both mRNA and protein expression pattern of Cadherin-7 suggest dynamic regulation not only at transcriptional but also post-translational levels.

The largely complementary expression of Cadherin-7 on neural crest and N-cadherin on placodal neurons suggests that coalescence of these precursor cell types may rely on both homophilic and heterophilic interactions between Cadherin-7 and N-cadherin. We propose two testable models for neural crest–placode coalescence: 1) that Cadherin-7–N-cadherin heterotypic binding mediates adhesion between neural crest and placodal cells and a smaller proportion of this interaction may be mediated through Cadherin-7 homotypically; or 2) neural crest–placode adhesion is mediated by homotypic Cadherin-7

interaction and N-cadherin acts only on placodal neurons, suggesting that at early stages of ganglion formation, there would be far fewer adherens junctions between neural crest–placode than between the same precursor type cells. Interestingly, Cadherin-7 misexpression did not increase but instead prevented neural crest–placode association. The data suggest that altering cadherin levels is sufficient to block proper placodal morphogenesis and intermixing of neural crest and placodal cells. It remains to be seen whether the difference in cadherin subtype is also crucial for proper neural crest–placode coalescence into ganglion.

Further investigation using Cadherin-7 gene knockdown approaches (i.e. RNAi or morpholino) will provide deeper insights into the endogenous Cadherin-7 role and its interaction with N-cadherin during gangliogenesis. Co-immunoprecipitation of N-cadherin and Cadherin-7 from cells in the trigeminal ganglion would directly test whether heterophilic interactions occur in vivo. Furthermore, if blocking or depleting N-cadherin whose expression is specific to placodal neurons affects placode–neural crest association, this would lend support for heterotypic cadherin interaction. Rescue experiments using one to test whether it can restore the loss of function of the other would establish whether or not these two cadherin members may be functionally equivalent or have distinct biological effects on neural crest and placodal cells. This could also address the significance of subtype specificity on the integration of neural crest and placodal cells. Another pertinent question is whether one cadherin can regulate the other, either cell-autonomously or non-cell-autonomously. For example, does misexpression of Cadherin-7 on the placodal ectoderm or reduction of Cadherin-7 on the neural crest, or both, alter N-cadherin expression on placodal cells? Taken together, the results provide exciting new avenues for exploration of cadherin-mediated neural crest–placode interactions during cranial gangliogenesis. Future investigation will explore the nature of the functional interactions between these two distinct cadherins and their biological significance.

4.6 Acknowledgements

I thank my undergraduate students, Emma Broom and Emma Hindley, who were supported by the SURF/Caltech-Cambridge exchange program, for their contribution on the preliminary studies of Cadherin-7 expression and its function during cranial neural crest development. This work was supported by US National Institutes of Health (NIH) National Research Service Award 5T32 GM07616 to C. E. S. and NIH grant DE16459 to M.B.-F.

Figure 1.

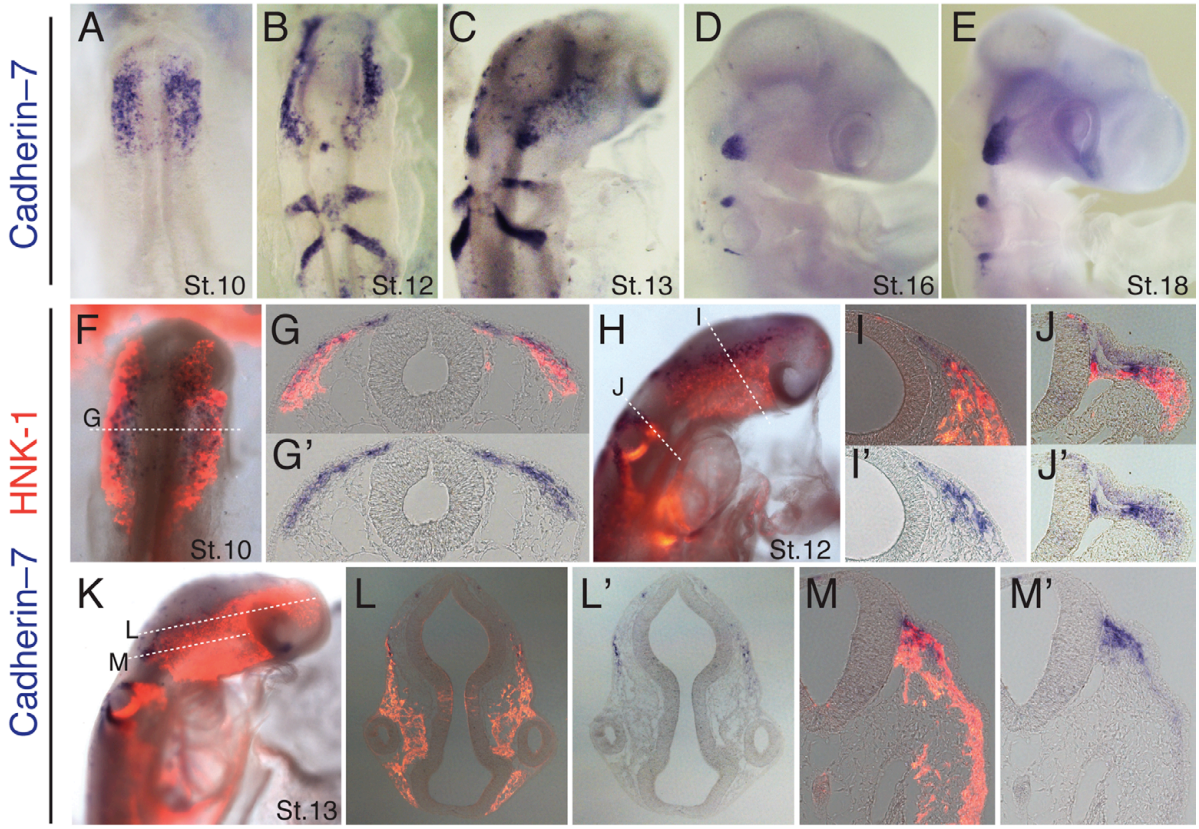

Figure 1. Cadherin-7 mRNA is transiently expressed by migrating cranial neural crest, and later retained in neural crest at the cranial entry/exit points and in the trigeminal ganglion. In situ hybridization with the Cadherin-7 riboprobe shows Cad-7 mRNA expression in the (**A**) first migration stream at stage 10 and subsequently in all three streams as migration progresses at (**B**) stage 12 and (**C**) stage 13. Later Cad-7 is expressed in discrete neural crest regions at the cranial motor exit points in the forming ganglia at (**D**) stage 16 and (**E**) stage 18 with the expression in the trigeminal ganglion appearing more broad. (**F**-**M**) Cad-7 expression overlaps with neural crest marker HNK-1 but is downregulated in the neural crest cells that have migrated the furthest. Downregulation of Cad-7 is apparent early at the beginning of migration (**F**-**G**) at stage 10 and (**H**-**M**) throughout the time of migration in all three streams. (**M**, **M'**) Section through the presumptive trigeminal exit point at the level indicated in **K** showing high expression in the neural crest cells adjacent to the neural tube at stage 13.

Figure 2.

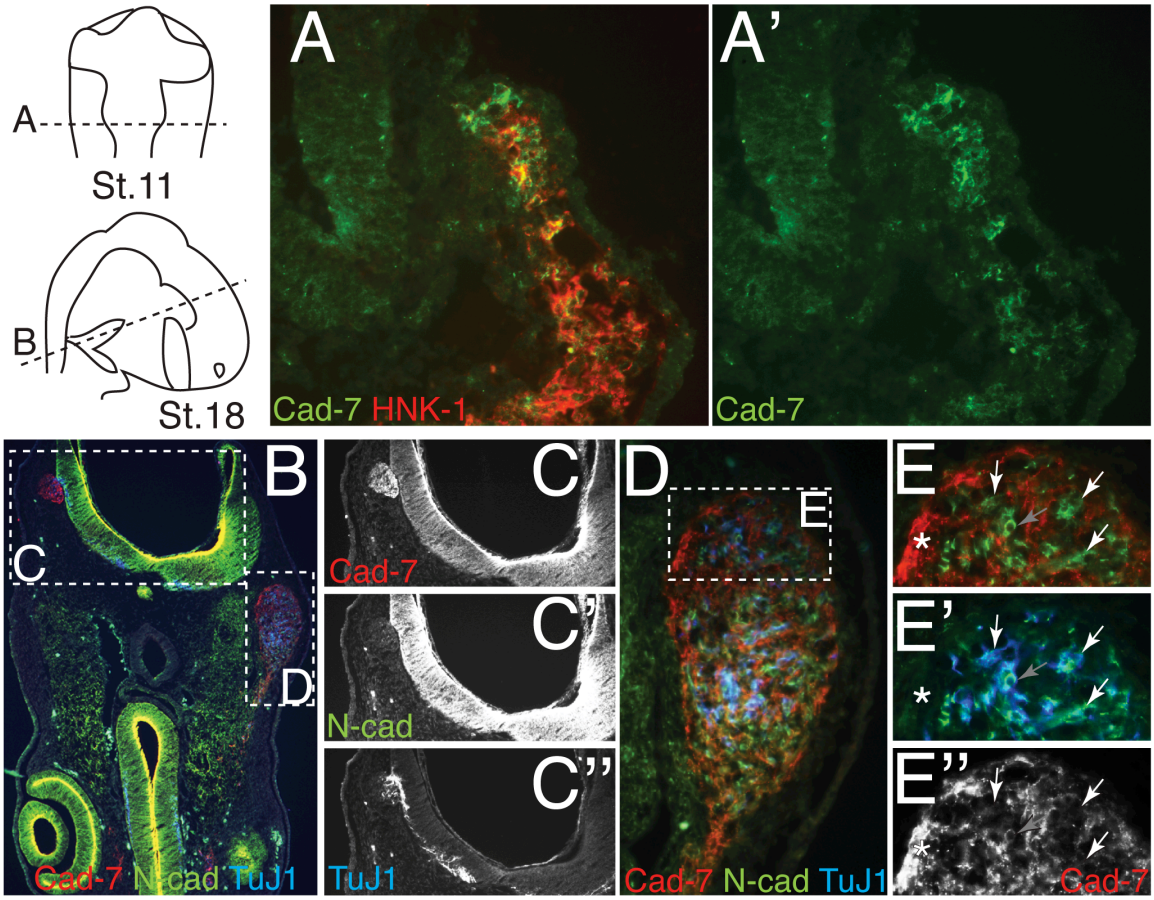

Figure 2. Cadherin-7 protein expression is broader than the mRNA. Schematics of the chick embryos at stage 11 and stage 18 indicate the levels of the sections. (**A**,**A'**) Cross section through stage 11 showing overlap of Cad-7 with neural crest marker HNK-1. Cad-7 protein expression is detected throughout the neural crest stream, albeit weaker in the ventrally migrating neural crest cells. (**B**) Cross section through the trigeminal ganglion at stage 18. (**C**,**C'**, **C''**) High magnification of the dotted box in **B** showing the most dorsal region of the ganglion which is neural crest-derived expressing Cad-7 and not N-cad. The neurotubulin TuJ1 staining outside of the neural tube is probably exiting motor axons rather than placodal neuronal processes. (**D**) High magnification of the dotted box in **B** showing a section through the OpV region of the trigeminal ganglion. (**E**,**E'**,**E''**) Magnification of the boxed region in **D** showing a predominantly complementary expression of Cad-7 and N-cad. Placodal neurons as labeled by TuJ1 mostly express N-cad but not Cad-7 (arrows), although some may express weak or background levels of Cad-7 (gray arrow). Cad-7 expression is present at the perimeter of the ganglion lobe as expected for expression in the neural crest which lacks N-cad expression (asterisk).

Figure 3.

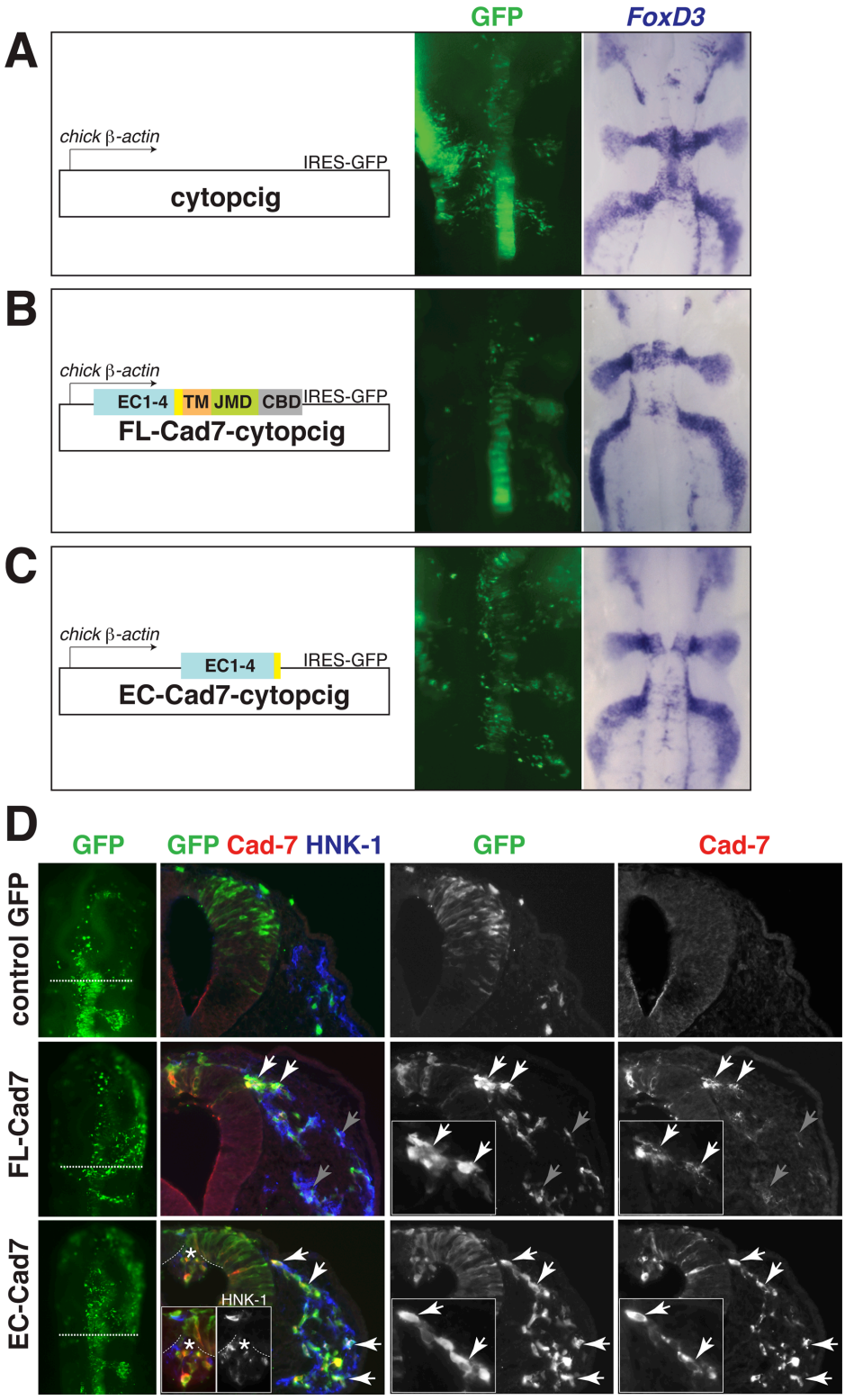
GFP
FoxD3
A
chick β-actin
IRES-GFP
cytopcig
B
chick β-actin
EC1-4
TM
JMD
CBD
IRES-GFP
FL-Cad7-cytopcig
C
chick β-actin
EC1-4
IRES-GFP
EC-Cad7-cytopcig
D
GFP
GFP Cad-7 HNK-1
GFP
Cad-7
control GFP
FL-Cad7
EC-Cad7
HNK-1

Figure 3. Perturbation of Cadherin-7 does not affect the pattern of cranial neural crest streams but alters cell–cell interactions. (**A**, **B**, **C**) Left subpanel showing a schematic of the vector used. Middle subpanel showing the level and region of DNA transfection as indicated by the GFP expression. Right, the same embryo as that shown in the middle subpanel was processed for the neural crest marker *FoxD3* in situ hybridization. (**A**) Control embryo at stage 12. (**B**) FL-Cad7 embryo and (**C**) EC-Cad7 embryo at stage 12 also show the typical pattern of the three migration streams. (**D**) First column from the left shows the neural crest region of transfection by GFP expression in whole mount embryos. Second column shows the color overlay image of GFP (green), Cad-7 protein (red), and HNK-1 (blue) of a cross section through the whole mount embryo at the level indicated by the dotted line. Single channel images of GFP and Cad-7 from the color overlay image are shown in the third and fourth columns. Neural crest cells transfected with FL-Cad7 appear to aberrantly associate with each other and tend to cluster (white arrows), in contrast to the control GFP and EC-Cad7 expressing neural crest cells. Exogenous FL-Cad7 protein is expressed mostly at adherens junctions between neural crest cells (white arrows) and is downregulated in many GFP expressing transfected cells (gray arrows), whereas the EC-Cad7 protein is localized less specifically to the cell membrane and is expressed at high levels in most, if not all, GFP expressing cells (white arrows). Expression of EC-Cad7 can cause disruption to neural crest emigration as shown by the aberrant protrusions of neural crest (HNK-1+) and neural tube cells in the lumen of the neural tube (asterisk).

Figure 4.

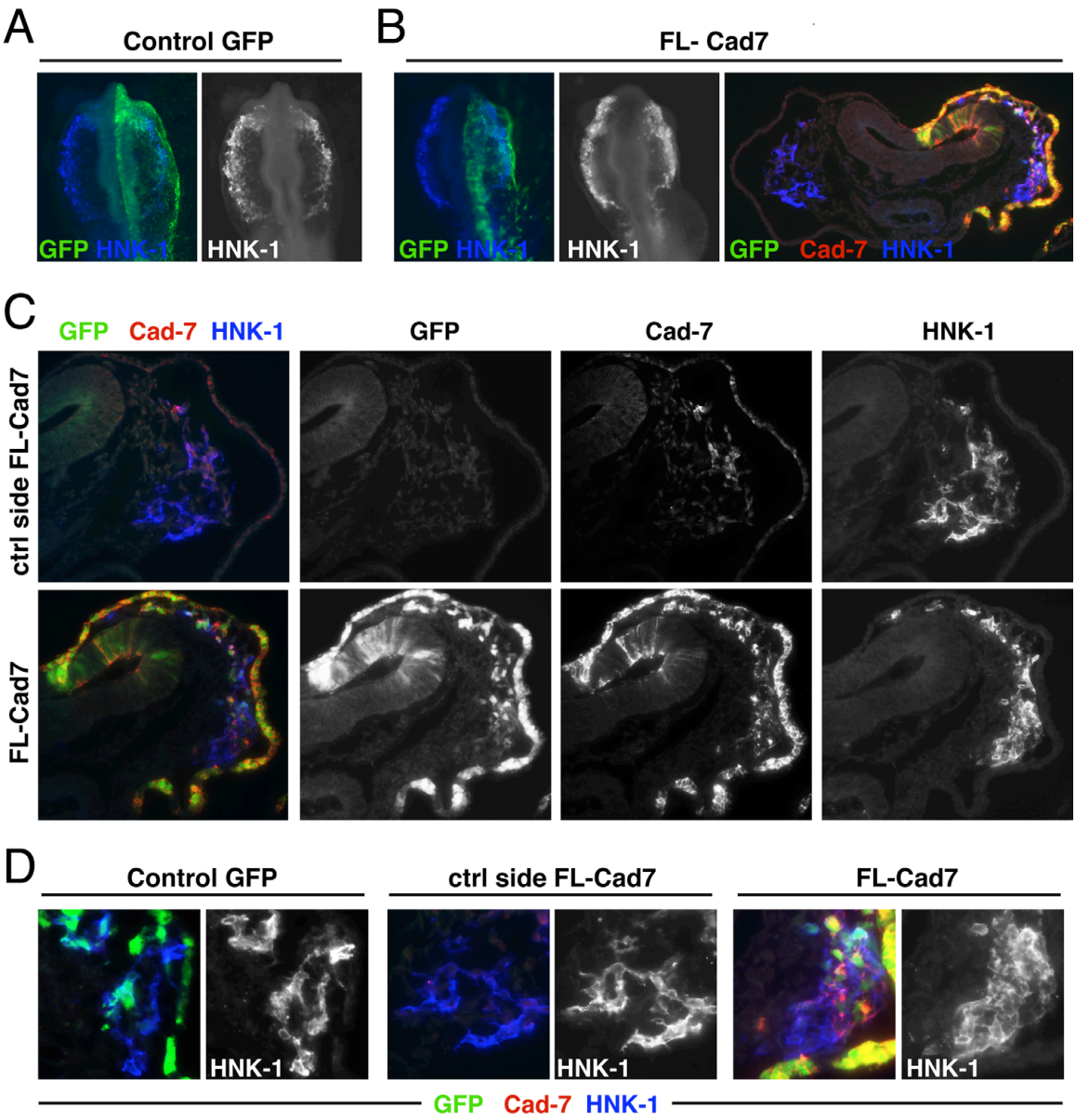
A
Control GFP
GFP HNK-1
HNK-1
B
FL- Cad7
GFP HNK-1
HNK-1
GFP Cad-7 HNK-1
C
GFP Cad-7 HNK-1
GFP
Cad-7
HNK-1
ctrl side FL-Cad7
FL-Cad7
D
Control GFP
ctrl side FL-Cad7
FL-Cad7
HNK-1
HNK-1
HNK-1
GFP Cad-7 HNK-1

Figure 4. Abundant full-length Cadherin-7 in the cranial neural crest causes abnormal neural crest cell morphology but does not inhibit migration. To increase the percentage of transfected neural crest cells, control GFP or FL-Cad7 expression vectors were introduced into the presumptive neural crest region (neural plate border) at gastrula stages 4–6 by electroporation. Control GFP (**A**) or FL-Cad7 (**B**) embryos were electroporated on one side as indicated by the GFP expression, and analyzed at stages 10–11. Cross section through the midbrain region of the FL-Cad7 embryo at stage 10+ showing the tightly clustered migration stream on the transfected side in contrast to the unelectroporated control side. (**C**) Higher magnfication of the same section showing the control and electroporated FL-Cad7 sides in the color overlay of GFP (green), Cad-7 protein (red), and HNK-1 (blue) expressions (also shown as individual images). (**D**) Close examination of the neural crest cell morphology in the control GFP, control side of FL-Cad7, and FL-Cad7 cases shows that the neural crest cells (HNK-1+) expressing high levels of Cad-7 are abnormally more adhered to one another and appear more rounded with fewer cellular protrusions. This contrasts the loosely connecting and mesenchymal appearance of the control neural crest cells.

Figure 5.

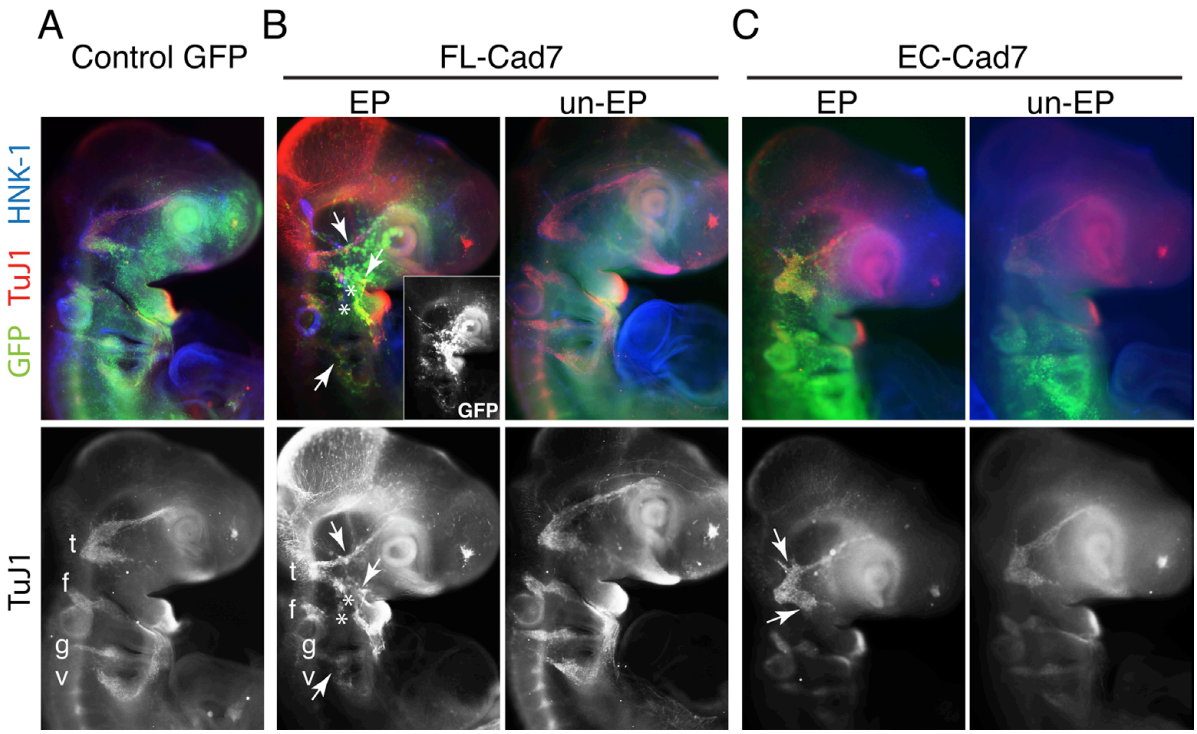

Figure 5. Perturbation of Cadherin-7 in the precursors severely disrupts cranial sensory ganglia formation. Top panels show color overlay of GFP expression (green) indicating area of transfection, neuronal marker TuJ1 (red) on placodal neurons, and HNK-1 (blue) on neural crest cells. To achieve high transfection levels, embryos were electroporated at stages 4–6 and analyzed at stage 16 in the forming ganglia. (**A**) Control GFP embryo displays typical ganglia formation. (**B**) By contrast, overexpression of Cadherin-7 resulted in severe ganglia defects, including reduced (or tightly coalesced) trigeminal and epibranchial ganglia (top arrows), with abnormal organization of placodal neurons (regions of gaps within the ganglia [asterisk] and abnormal link between the glossopharyngeal and vagal ganglia [bottom arrow]). These abnormalities correspond to regions of transfection as shown by GFP expression in color overlay image and inset. (**C**) Blocking Cadherin-7 by EC-Cad7 showed less severe effects, generally with misshapen ganglia (arrows) that were not reduced in size. Unelectroporated control sides of the FL-Cad7 and EC-Cad7 embryos showed no apparent defects. t, trigeminal; f, facial; g, glossopharyngeal; v,vagal; EP, electroporated.

Figure 6.

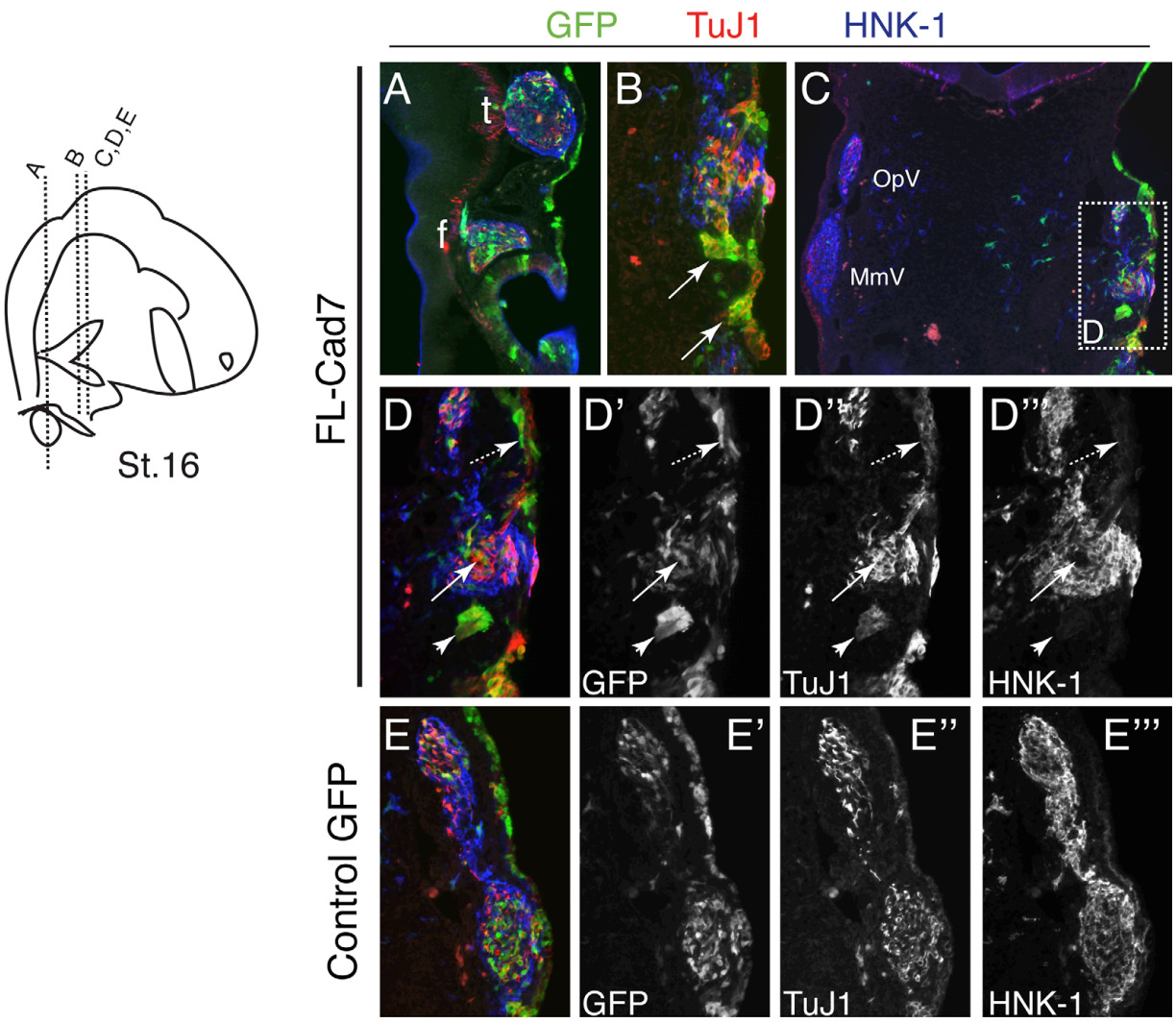
GFP
TuJ1
HNK-1
A
B
C,D,E
St.16
FL-Cad7
Control GFP
t
f
OpV
MmV
D
D'
D''
D'''
E
E'
E''
E'''
GFP
TuJ1
HNK-1

Figure 6. Misexpression of Cadherin-7 leads to aberrant placodal morphogenesis and increased neuronal cells in the ectoderm. Schematic of chick stage 16 embryo showing the levels of the frontal plane sections. FL-Cad7 embryo electroporated in the precursor cell populations (both neural crest and placodal ectoderm) at stages 4–6 showing transfection mostly in the placodal cells by the time of analysis at stage 16. (**A**) Most proximal part of the trigeminal and facial ganglia adjacent to the hindbrain, which is mostly neural crest-derived, appears to assemble properly. (**B**) Misexpression of Cadherin-7 in the trigeminal placodal ectoderm causes dramatic disruptions of the placodal ectoderm— delaminating sheets of differentiating placodal ectoderm (TuJ1+) that do not associate with neural crest cells (arrows). (**C**-**D’’’**) It also causes aberrant placode-derived neuronal nodules (arrowhead, GFP+/TuJ1+) and widespread neuronal cells in the surface ectoderm (dotted arrow, TuJ1+/GFP+). Placode–neural crest interaction appears abnormal. The aberrant nodules and some regions in the ganglion clusters (arrow) are devoid of neural crest (HNK-1+) association. The unelectroporated control side forms the typical OpV and MmV lobes as shown in **C**. (**E**-**E’’’**) Control embryo electroporated with a GFP expression vector also at stages 4–6 shows normal trigeminal ganglion formation and intermixing of neural crest (HNK-1+) and placodal neurons (TuJ1+). OpV, ophthalmic; MmV, maxillo-mandibular; t, trigeminal; f, facial.

Chapter 5

Conclusions

5.1 Summary

The experimental studies presented in this thesis provide the first molecular insights into the cellular processes of assembly, and aggregation of neural crest and placodal cells into discrete cranial sensory ganglia. The results show that throughout trigeminal gangliogenesis (starting from ingression of placodal neurons to forming a condensed ganglion), neural crest and placodal cells are highly intermingled in vivo and in vitro.

To test their interactions, we performed classical tissue ablation experiments with several key improvements. We were able to make clearer conclusions about their relationship during gangliogenesis since we performed ablation at the stages that minimize regeneration, analyzed the ablated embryos at the time of ganglion formation, and most importantly, carefully distinguished the two cell types by cell or molecular markers which provided information on both the extent of ablation and also the causal effects on the other cell population. Results show that after ablation of neural crest, placodal neurons failed to integrate, instead forming separated aggregates and aberrant central and peripheral axonal projections. On the other hand, ablation of the placodal ectoderm led to loss of ganglion, whereby neural crest cells failed to coalesce, showing that the presence of placodal neurons is essential. This provides the first insight into the role of the placodal tissue on neural crest, which had been difficult to obtain due to regeneration issues noted by previous investigators (Hamburger, 1961; Stark et al., 1997), as well as the lack of use of markers to distinguish the two cell types. The data demonstrate that interactions between neural crest

and placodal cells are necessary to drive ganglion formation and are highly interdependent. Bi-directional neural crest–placode signaling likely mediates this process.

The concurrent expression of Slit1 in the migratory neural crest and its cognate receptor Robo2 in the placodal cells during trigeminal ganglion assembly prompted us to ask whether this ligand–receptor pair may mediate neural crest–placode interaction. Loss-of-function of either Robo2 or Slit1 in vivo resulted in severely disorganized assembly of placodal neurons into dispersed or aberrantly condensed ganglion, consistent with the effects of neural crest ablation. Furthermore, the aberrant pattern of placodal neurons by blocking Robo2 function caused wild type neural crest cells to also coalesce abnormally. The results establish a critical role of Slit1–Robo2 signaling in organizing placodal neurons and underscores the reciprocal nature of neural crest–placode interaction. A striking defect in Slit1–Robo2 deficient embryos is the abnormal coalescence of ganglion, suggesting a role for cell adhesion in this process.

As a possible downstream mechanism, the function of the cell–cell adhesion molecule N-cadherin was tested during trigeminal gangliogenesis. Our results reveal a role for N-cadherin in mediating aggregation of placodal neurons into the ganglion downstream of Slit1–Robo2. We show that Slit1–Robo2 interaction can positively regulate N-cadherin mediated placodal adhesion by modulating N-cadherin expression. Since neural crest and placodal neurons are highly intermixed, condensation of ganglia may require adhesion of not only placode–placode, but also crest–crest and crest–placode cells. Our results also suggest that another adhesion molecule, Cadherin-7, may play a complementary role with N-cadherin in driving ganglion coalescence. Finally, the mechanisms of Slit1–Robo2 and N-cadherin may be general for all cranial ganglia of dual origin, as the expression and function of these molecules in the epibranchial regions closely resemble that in the trigeminal ganglion.

In summary, the results of this thesis have identified several key molecular players involved in neural crest–placode formation of the chick cranial sensory ganglia. We hypothesize that the process of cranial gangliogenesis can be divided into at least five distinct but overlapping steps—1) neural crest migration to the site of ganglion assembly, 2) cell fate specification and differentiation of placodal cells into neurons in the ectoderm, 3) ingression of placodal neurons into the ganglion anlage, 4) interactions between neural crest and placodal neurons at the border of ectoderm and mesenchyme, and within the mesenchyme, and 5) the condensation of the intermixed neural crest cells and placodal neurons into discrete ganglion structure. It is interesting to note that several of these steps are interactive. For example, the production and ingression of placodal neurons from the surface ectoderm continues throughout most of gangliogenesis while the ganglion is condensing, and interactions between neural crest and placode underlie this entire process.

We show that Robo2–Slit1 mediated neural crest– placode interaction has an important role in several of these steps at times of placodal ingression and coalescence (see Fig. 1 for a schematic summary). The downstream mechanisms of Robo2 dependent signaling in mediating ingression is not clear, but we elucidate a critical role for N-cadherin in placodal aggregation and suggest that ganglion coalescence may be driven by a novel interplay of two distinct cadherins, Cadherin-7 and N-cadherin, from which we propose two possible models (see Fig. 2). Finally, three points of difference between the early (during gangliogenesis) and late (in the nearly mature ganglion at embryonic day 12 (D'Amico-Martel and Noden, 1983)) stages of trigeminal ganglion development can be emphasized. First, the description of the segregation of placodal cells to the distal region as in the nearly mature ganglion does not apply during gangliogenesis since placodal cells are intermixed with neural crest cells throughout almost the entire ganglion region. Second, neural crest cells remain undifferentiated through gangliogenesis at least up to stage 18. Third, placodal neurons during gangliogenesis have generally short processes such that

disorganization of axonal projections was accompanied by displacement of neuronal cell bodies in the same pattern. This could have interesting implications on how similar signals may mediate both migration of early trigeminal neuronal cells and guidance of their growing axons.

The results provide the first molecular insights into the roles of a putative signaling by Slit–Robo and cadherin-mediated aggregation that underlie neural crest–placode formation of the cranial sensory ganglia. They demonstrate the importance of heterotypic cell interactions during cranial gangliogenesis for cellular condensation, casting light on the critical interplay of cell–cell communication and cell adhesion in formation of complex structures in the developing vertebrate embryo.

5.2 Future perspectives

The work presented in this thesis lays a foundation for many more questions about the fascinating process of cell–cell interactions and morphogenesis during cranial sensory ganglia formation. Many aspects of neural crest–placode interactions remain to be investigated to fully understand the intricate and complex process of cranial ganglia assembly. In this thesis, I have identified a critical role for Slit1–Robo2 in mediating one aspect of neural crest–placode interactions: the signaling from neural crest to placodal cells for proper placodal cell organization. However, other aspects of their interactions remain unknown at a molecular level. These include the mechanisms underlying the reciprocal or reverse signaling from placode to neural crest cells, whether multiple signaling pathways are involved in their communication, and finally if there are direct protein interactions bridging neural crest–placode cell–cell contacts. Because Robo2 is not expressed by neural

crest cells, the data suggest that the reciprocal signaling would involve a Robo2 independent pathway. Although we cannot rule out the possibility that reverse signaling is mediated by Slit–Robo interactions but through a different Robo receptor, this seems unlikely for several reasons. Robo1 does not appear to be a candidate receptor for neural crest–placode interaction during trigeminal gangliogenesis, since its expression was not detected strongly or specifically in either neural crest or placodal cells at times of ganglion assembly (st.12–18). The possible functions for Robo3 and Robo4 were not examined here, but based on their expressions in other systems, they appear to be restricted to the central nervous system (Sabatier et al., 2004) and endothelial cells (Park et al., 2003; Suchting et al., 2005) respectively. Therefore, it is more likely that the reciprocal signaling relies on other yet unknown signaling molecules.

The precise way in which Slit1–Robo2 signaling regulates trigeminal ganglion assembly over time remains to be determined. A range of defects was found after Slit1–Robo2 perturbation including defects in placodal ingression, organization, coalescence, and axonal guidance of cranial ganglia. This suggests that Slit1–Robo2 may have a range of different spatiotemporally regulated functions to participate in proper ganglion formation, or its actions at earlier events led consequentially to the later defects. Since the expression of Robo2 begins by about stages 11–12 in the trigeminal placodes and that perturbation of Robo2 just prior to ingression at mostly stages 9–10 did not appear to affect placodal cell differentiation or cell number, we suspect that its role in placodal ingression would represent its earliest action. We provide two possible models for Slit1–Robo2 actions that may explain the different defects. First, the delayed ingression caused by blocking Robo2 led subsequently to abnormal organization and coalescence of the placodal ganglia, or second, different actions of Robo2 may mediate placodal migration from the surface ectoderm versus organization and coalescence of cells into ganglion. We favor the latter model since we find that although ingression occurs at later stages of

ganglion assembly, the organization of the ganglion remains chaotic over time, or alternatively, we think that the combination of both models may explain the different defects. Further understanding of the downstream and intracellular events activated by Robo2 in the different placodal regions as well as testing the consequence of ganglion assembly when Robo2 is blocked only in the ingressed placodal cells would clarify this point.

The conventional model assumes that Robo–Slit signaling involves binding of the receptor and ligand that mediates its actions; however other form of interactions between the ligand and receptor and between the receptors themselves may exist. This is especially relevant to our finding that Robo2 signaling plays a critical role for coalescence of placodal neurons, suggesting a role in placodal cell–cell adhesion. We have so far demonstrated a role for N-cadherin in placodal cell adhesion as discussed in Chapter 3 and its implicated link with Slit1–Robo2. However, there are at least two other possible models for Robo2 interactions that may also mediate placode–placode adhesion.

First, we cannot rule out the possibility that binding of Robo2 to itself also is involved in placode–placode adhesion. This is consistent with findings that Robos can bind homophilically in vitro and that Slit independent functions of Robos have been implicated in other systems (Hivert et al., 2002; Parsons et al., 2003). Second, an interesting model called the 'Slit sandwich' by Kraut and Zinn (2004), proposes that a Robo–Slit–Robo interaction mediates signaling between the visceral mesoderm and chordotonal neurons that blocks migration of the latter in the fruit fly (Kraut and Zinn, 2004). A similar scenario may apply to placode interactions in our system. Accordingly, the interaction between placodal cells may be mediated by binding of Robo2 from one cell to its cognate ligand, Slit1, extracellularly, which in turn binds to Robo2 on the neighboring cell. This mechanism may explain the role of the Robo2 in cell adhesion, but not its function in promoting placodal ingression. However, it is not clear if a single Slit can bind

to two Robo receptors. Alternatively, the 'Slit sandwich' may involve dimerization of Slit to bind Robos on neighboring cells. These additional scenarios provide alternative models for Slit1 and Robo2 interactions during trigeminal gangliogenesis that depart from conventional view of a ligand–receptor binding. Uncovering the molecular interactions of Slit1 and Robo2 at different times and in different regions of the forming ganglion (e.g. surface placodal ectoderm versus ingressed placodal cells) is important for understanding how this signaling mechanism drives proper ganglion assembly.

Here, I present six possible future directions that stem from this study for addressing some of these open questions. The study of neural crest–placode interactions would not only elucidate a critical process during development of the peripheral nervous system, but also serves as an excellent new model to study and unravel cell–cell signaling and subsequent cellular changes in vivo that have been traditionally studied in vitro.

First, uncovering the cadherin-based mechanism of ganglion coalescence would provide important insights into the process of cellular condensation (thus organ formation) and potentially novel cadherin interactions in vivo. As discussed in Chapter 4, the aggregation of neural crest and placodal neurons may rely on either a homotypic or a mix of homotypic and heterotypic cadherin interactions. This study may also elucidate whether cadherin binding may mediate direct neural crest–placode cell–cell contacts. Exploration of other classical and non-classical cadherins during ganglion formation may also elucidate additional molecular players.

Second, examining Slit1–Robo2 interaction at the protein level during gangliogenesis is a necessary step for understanding the function of this signaling pair more deeply. Previous Slit–Robo studies in *Drosophila* have shown interesting differences between mRNA and protein expressions during midline commissural axon crossing as well as specific localization of Slit and Robo proteins at the cell surfaces in the forming heart tube that provided important information about their functions that might otherwise be

obscured by only mRNA expression. Protein expression of Slit1 and Robo2 at the different stages of ganglion formation would provide information on the spatiotemporal pattern of when and where signaling might be occurring. This may be different from the uniform expression of Slit1 on the migratory neural crest stream and Robo2 on all the placodal cells that the mRNA expressions suggest. Along with immunoblot studies, this would also address whether proteolytic processing of Slit1 occurs in the neural crest, as has been shown for Slit2 in other systems, which may modulate its signaling activity. Furthermore, the role of heparan sulfate proteoglycans in regulating distribution and activity of Slit1 signaling could also be elucidated.

Third, exploring the downstream transduction of Slit–Robo signaling in the placodal neurons would elucidate the precise intracellular mechanisms dictating the placodal cellular changes during gangliogenesis. The interaction of Slit–Robo could elicit different outcomes at different steps of placodal development (e.g. placodal ingression versus placodal condensation). Our results showing a range of effects upon Robo2 inhibition are consistent with this possiblity. Screening for changes in gene transcription downstream of Robo2 activation and inhibition and for presence and activities of candidate intracellular proteins (e.g. Rho GTPases, Abl tyrosine kinase, and other actin regulators, among others) would provide further information about the downstream events. This information in addition to functional experiments involving removal of the Slit source may also clarify whether Slit1 independent functions may also be present during gangliogenesis.

Fourth, little is known about the later development of the trigeminal ganglion and the role of Robo2 therein. An area ripe for exploration is the molecular and cellular mechanisms underlying the differential differentiation of neural crest cells into neurons in the proximal ganglion and glia along the entire region. It would be interesting to ask if interactions with placodal neurons have a role in this process. Furthermore, does the embryonic origin of the sensory neurons in the ganglion correlate with different neuronal

cell types of different functions (e.g. nociceptors, thermoreceptors, mechanoreceptors)? Does Robo2 signaling have a role in any of these events?

Fifth, it would be fruitful to dynamically analyze neural crest–placode interactions through the process of ganglion formation by time-lapse imaging in real time. This would uncover indispensable information about the dynamics and cellular processes underlying this developmental event. Imaging placodal neurons as they ingress, interact, and coalesce with neural crest cells in the living embryo in real time will be an exciting future objective that will provide direct insights into the sequence of events and cellular changes leading to ganglion formation.

Finally, exploring whether neural crest–placode interactions and the roles of Slit–Robo signaling and Cadherin dependent cell adhesion are conserved in mediating cranial sensory gangliogenesis in other vertebrate species (e.g. mouse, zebrafish, and Xenopus) promises to reveal the evolutionary significance of these mechanisms. In line with the possibility that Slit–Robo may have a conserved role in cranial gangliogenesis, Robo2 is expressed by the trigeminal ganglion in zebrafish (Lee et al., 2001) and mouse embryos (Ma and Tessier-Lavigne, 2007), but its role in ganglion formation is elusive. Taken together, the findings presented in this thesis motivate many exciting future investigations and research directions.

Figure 1. Multiple possible roles for Robo2 dependent signaling during cranial gangliogenesis. Three major defects are found in Robo2 deficient embryos as compared to wild type (WT) or control cases. First, ingression appears to be delayed in Robo2 inhibited placodal neurons at early stages of migration. At times of coalescence, Robo2 deficient placodal neurons do not assemble in their normal positions and are more disorganized while their axonal projections are affected in the same way. The aberrant organization of placodal neurons also caused non-cell-autonomous effects on the assembly of neural crest cells which mirrored the same abnormal placodal patterning. This is likely mediated by other, as yet unknown, molecules involved in the reciprocal signaling from placode to neural crest cells. Perturbation of Robo2 dependent signaling in placodal neurons causes a range of defects, which may suggest a role for Robo2 at different steps of ganglion formation in particular to cell migration and coalescence.

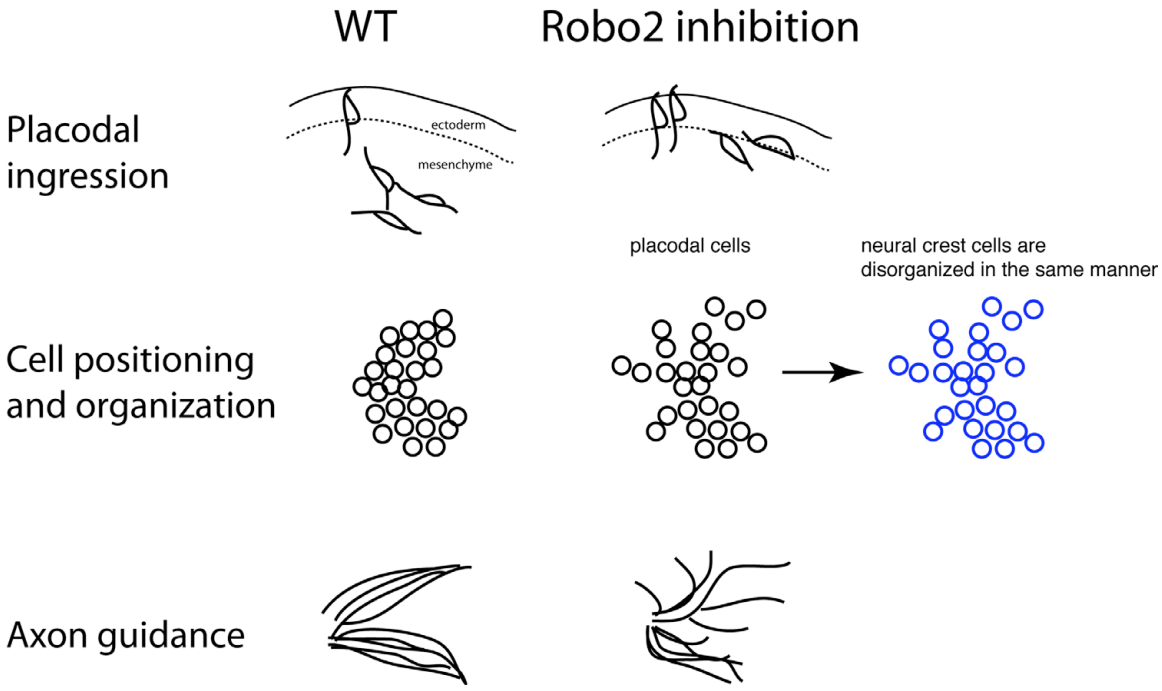

Figure 2. Two possible models for cadherin-based cellular condensation during trigeminal ganglion formation. Model 1 proposes that heterophilic binding between Cadherin-7 (Cad-7) and N-cadherin (N-cad) does not occur and therefore any neural crest–placode cell–cell adhesion would rely on a few number of Cad7–Cad7 interaction between the few placodal neurons that express the Cad-7 protein and the Cad-7 positive neural crest cells. Departing from the conventional view of the homophilic binding of cadherin molecules, Model 2 presents the alternative hypothesis, by which heterophilic interaction is present between Cad-7 and N-cad to mediate crest–placode adhesion.

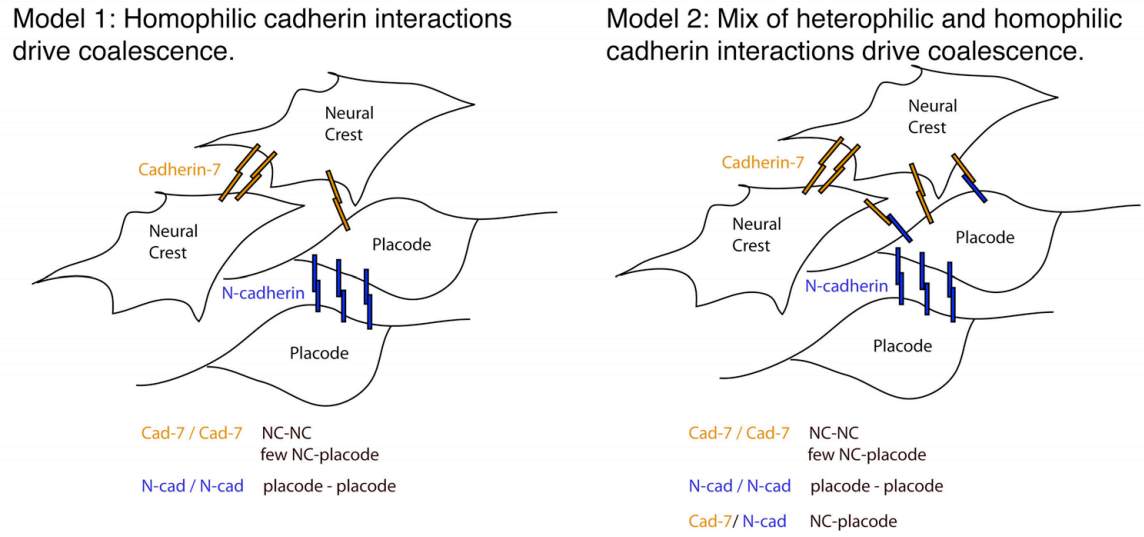

Appendix A

Cell surface heparan sulfate proteoglycan Glypican-1 and placodal ganglion formation

A.1 Abstract

Biochemical studies have implicated a specific interaction between a cell surface heparan sulfate proteoglycan (HSPG), Glypican-1 (GPC1), and Slits in rat brain lysate (Liang et al., 1999; Ronca et al., 2001). However, the link between glypicans and Slit-Robo signaling in vivo during development remains elusive. More specifically, the mechanism of the Slit1 distribution and its reception by Robo2 on trigeminal placodal neurons may rely on a co-receptor, such as GPC1, but this process is unknown. To more deeply investigate the nature of Slit1–Robo2 signaling, we sought to characterize the potential role of GPC1 during cranial sensory ganglia formation. In this chapter, we show that GPC1 mRNA is expressed in the placodal cells at the right time and place for a role during cranial gangliogenesis, and additionally the expression of GPC1 on early migrating hindbrain neural crest cells also indicate a possibility for its role in the neural crest. GPC1 gain-of-function caused both reduced and disorganized placodal neurons at early assembly and later severely reduced trigeminal ganglion at times of condensation. In extreme cases, this caused elimination of nearly the entire ophthalmic lobe of the ganglion. The data so far suggest that proper regulation of GPC1 expression is essential for placodal ganglion formation and that GPC1 function is sufficient to affect placodal cell survival and/or proliferation, and possibly morphogenesis. In summary, the results show a previously unknown expression and potential role for a glypican family member in both neural crest and placodal development. These provide an exciting outlook for further exploration on the

function of GPC1 and the general role of HSPGs in neural crest and cranial sensory ganglia development.

A.2 Introduction

Glypicans (GPCs) constitute one of two major families of cell surface heparan sulfate proteoglycans (HSPGs). The other family is the syndecans which are transmembrane proteins as compared to the glypicans which are anchored to the membrane through a glycosyl-phosphatidylinositol (GPI) link. There are six members of glypicans (GPC1-6) in mammals, two in *Drosophila melanogaster* (*Dally* and *Dally-like*), two in *Caenohabiditis elegans* (*gpn-1* and *lon-2*), and one in zebrafish (*knypek*) (Fico et al., 2007) which have so far been identified. The core protein of the glypican molecules are well conserved which consist of a large globular cysteine-rich domain, a smaller domain encompassing the heparan sulfate (HS) attachment sites, and a sequence signal for the GPI attachment (Filmus and Song, 2000). On the glypican core protein, HS side chains are attached near the membrane anchor and are thought to facilitate binding of heparin-binding growth factors and ligands. Therefore, glypicans are considered co-receptors for various signals and possibly act to regulate the distribution and activity of these factors. Additionally, however, there is also a possibility for glypican functions independent of its HS side chain. Overexpression of GPC3 can induce apoptosis in a cell line specific manner but this does not require its HS chains (Gonzalez et al., 1998). Furthermore, multiple types of post-translational processing can take place on glypicans, such as complex modifications

of the HS chains and proteolytic cleavage at the GPI anchor or at the N-terminal cysteine-rich domain, which can yield tissue-specific as well as non-cell-autonomous effects as reviewed in (Fico et al., 2007).

During vertebrate development, glypicans are known to be expressed in a spatiotemporally regulated manner in the nervous system as well as in various other tissues (Litwack et al., 1998; Luxardi et al., 2007; Niu et al., 1996; Saunders et al., 1997). Their expression also changes in pathological cases, such as cancer. GPC3 and/or GPC1 have been found to be either downregulated in some ovarian cancer and mesothelioma cell lines (Lin et al., 1999; Murthy et al., 2000) or upregulated in others (e.g. pancreatic tumors) (Filmus, 2001; Kleeff et al., 1998; Matsuda et al., 2001; Su et al., 2006).

The functions of proteoglycans during embryonic development are profound. Functional perturbation of glypicans in mice, *Xenopus laevis*, *Drosophila*, and zebrafish has been shown to affect Wingless/Wnt, Dpp/BMP, Fgf and/or Hh signaling in affecting cell fates, body size, cell movements (e.g. during gastrulation), cell survival and proliferation (Fico et al., 2007; Filmus and Song, 2000). Loss of function mutations in OCI-5/GPC3 in humans cause the Simpson-Golabi-Behmel syndrome (SGBS), which is characterized by pre- and post- natal overgrowth and visceral and skeletal defects and an increased risk for tumors (Pilia et al, 1996). *GPC3* knockout mouse model also exhibit similar phenotypes (Cano-Gauci et al., 1999). The first *Drosophila* homolog for glypican, *division abnormally delayed* (*dally*) gene, was found in a screen for defects in cell division patterning in the forming CNS (Nakato et al., 1995). *dally* mutants have delayed G2–M transition in dividing cells in the eye disc and lamina as well as defects in morphogenesis of adult tissues (i.e. the eye, antenna, wing, and genitalia) and viability. Dally-like, the second glypican member in *Drosophila*, has been shown to facilitate long range Wingless signaling by transporting the signal to neighboring cells in the wing imaginal disc, while Dally acts as classical co-receptor (Franch-Marro et al., 2005). In terms of regulation of cell

proliferation, the effects of glypican in vertebrates appear to be the opposite of that in the fly, such that glypican-3 is a negative regulator whereas dally promotes cell division. Taken together, genetic evidence from glypican mutants implicate functions for glypican in regulating cell survival, proliferation, and/or morphogenesis, likely reflecting its association with a wide range of major signaling pathways. How specificity is conferred in a spatiotemporal manner that link the function of a proteoglycan to a particular signaling pathway on a cell remains to be uncovered.

Recent evidence have implicated direct interaction of heparan sulfate proteoglycans (HSPGs) with Slit for its function (reviewed in (Hohenester, 2008)). Structural studies have suggested a Slit–Robo–HS complex based on the result that the second leucine rich repeat of Slit binds to heparin and both can bind to Robo (Fukuhara et al., 2008; Hussain et al., 2006). Disruption of heparan sulfate (HS) chains by heparinase decreases affinity of Slit–Robo binding and also blocks Slit repulsive activity in vitro (Hu, 2001; Piper et al., 2006). Consistent with this, when excess HS is applied to compete with endogenous HS, Slit activity is also compromised in a growth cone collapse assay (Piper et al., 2006). Genetic evidence from *Drosophila*, also indicate the interaction of syndecan, a HSPG, with Slit–Robo in regulating distribution and efficiency of Slit signaling (Johnson et al., 2004; Steigemann et al., 2004). In vertebrates, the role of syndecan with Slit–Robo has not been characterized, but recombinant vertebrate Glypican-1 has been found to bind specifically to Slit1 and Slit2 from rat brain extracts in a heparan sulfate dependent manner (Liang et al., 1999; Ronca et al., 2001). The functional relationship of HSPG and Slit–Robo in vivo is unknown.

We have previously identified the critical role of Slit1–Robo2 in mediating neural crest-placode assembly of the trigeminal ganglion as presented in Chapter 2. The nature of the slit ligand reception and distribution required for proper gangliogenesis remains unexplored. The biochemical interaction reported for Glypican-1 and Slit1 prompted us to

wonder if there may be a possible connection between GPC1 and Slit1–Robo2 signaling during trigeminal gangliogenesis. The expression and function of glypicans during cranial gangliogenesis have not been investigated previously. As a first step, we sought to explore whether Glypican-1 may be involved in neural crest and/or placode development. We characterized the gene expression pattern of Glypican-1 during cranial gangliogenesis and we found that trigeminal and epibranchial placodal cells and early hindbrain neural crest cells express Glypican-1 at the time of ganglion assembly and crest migration, respectively. The results show a previously unknown expression of a glypican family member which is potentially involved in both neural crest and placodal development. Furthermore the proper expression level of Glypican-1 in the placodal tissue appears to be crucial for formation of the trigeminal ganglion. Overexpression of GPC1 causes both reduced and disorganized placodal neurons at early assembly and severely reduced trigeminal ganglion later at times of coalescence. In extreme cases, this caused elimination of nearly the entire ophthalmic lobe of the ganglion. The data so far suggest that proper regulation of GPC1 expression is essential for placodal ganglion formation and provide a basis for further exploration on its function in neural crest and cranial sensory ganglia development.

A. 3 Materials and Methods

Embryos

Fertilized chicken *(Gallus gallus domesticus)* eggs were obtained from local commercial sources and incubated at 37°C to the desired stages according to the criteria of Hamburger and Hamilton (Hamburger and Hamilton, 1992).

In situ hybridization

Whole mount chick in situ hybridization was performed as described (Shiau et al., 2008). cDNA plasmids obtained from BBSRC (ChickEST clone 418p2) was used to transcribe the antisense riboprobe against chick Glypican-1. The plasmid was sequenced and determined to contain the coding sequence of the chick Glypican-1 gene (NCBI accession number: XM_422590.1) corresponding to nucleotides 1233-2107. Embryos were imaged and subsequently sectioned at 12 μm.

Immunohistochemistry

Whole chick embryos were fixed in 4% paraformaldehyde overnight at 4ºC, washed in PBT (PBS + 0.2% tween) and either immunostained as whole embryos and/or processed for 10 μm cryostat sections. Primary antibodies used were anti-HNK-1 (American Type Culture; 1:3 or 1:5), anti-Islet1 (DSHB, clone 40.2D6; 1:250), and anti-TuJ1 (Covance; 1:250). Secondary antibodies were obtained from Molecular Probes and used at 1:1000 or 1:2000 dilutions, except 1:250 dilution for Alexa Flour 350 conjugated antibodies. Images were taken using the AxioVision software from a Zeiss Axioskop2 plus fluorescence microscope, and processed using Adobe Photoshop CS3.

In ovo electroporation of the trigeminal ectoderm

DNA was injected overlying the presumptive trigeminal placodal ectoderm at stages 8–10 by air pressure using a glass micropipette. Platinum electrodes were placed vertically across the chick embryo delivering 5 × 8 V in 50 ms at 100 ms intervals current pulses. Electroporated eggs were re-sealed and re-incubated at 37˚C to reach the desired stages (i.e. 30–36 hours to stages 15–16 and 36–48 hours to stages 17–19).

Plasmid constructs

Full length chick Glypican-1 cDNA (clone CS5) was isolated from a 4– to 12– somites stage chick macroarray library as previously described (Gammill and Bronner-Fraser, 2002). The coding sequence (1.65 kb) was amplified from the library clone by PCR using a 5' primer with a flanking a XhoI site and a 3' primer with a flanking ClaI site. This fragment was inserted into PCRII-Topo vector using the TOPO TA cloning kit (Invitrogen) and clone G1 (PCRII-Topo + GPC1, size = 5.65 kb) was determined to be correct by sequencing. The fragment was then digested at the XhoI/ClaI sites and directionally cloned into the XhoI/ClaI sites in the cyto-pcig vector, yielding clones CG2 and CG3 (cytopcig + GCP1, size = 7.8 kb) which were determined to be correct by sequencing.

A.4 Results and discussions

A.4.1 Expression of Glypican-1 mRNA in the precursors of cranial sensory ganglia suggests its potential role in ganglion formation

To investigate whether Glypican-1 (GPC1) may have a role during cranial gangliogenesis, I have characterized the mRNA expression of GPC1 in the chick embryo at stages 9–18 by whole mount in situ hybridization (Fig. 1). This represents the time window prior to or at the beginning of neural crest migration up to ganglion condensation. In the presumptive trigeminal region, the neural crest cells migrating at the midbrain and anterior hindbrain (R1/R2) level starting at stage 9 through stages 13–14 do not appear to express

GPC1 (Fig. 1, A-C, E). At stages 12–13, low levels of GPC1 were sometimes detected in the ectoderm bilateral to the midbrain region in a salt-and-pepper pattern indicative that it may be in trigeminal placodes (data not shown) but this remains to be confirmed. Later, at stages 14–16 during trigeminal ganglion assembly, GPC1 is expressed by both the ophthalmic (OpV) and maxillo-mandibular (MmV) placodes that form the trigeminal ganglion (Fig. 1, E-F). To confirm that these GPC1 expressing cells are in fact placode-derived, I have labeled the placodal ectoderm with GFP by ectoderm electroporation prior to its ingression and collected these embryos at later stages to process for GPC1 in situ hybridization. Results show that all GFP expressing placode-derived cells and discrete regions of the placodal ectoderm express GPC1 (Fig. 1, G-K), while they interact with the trigeminal neural crest cells which do not. The matching expression pattern of GPC1 and Robo2 as previously described (Shiau et al., 2008) in the trigeminal placodal cells lends a possibility for GPC1 to act as a co-receptor in regulating Slit1–Robo2. Alternatively, GPC1 may have an independent function during trigeminal gangliogenesis. This expression pattern may be conserved with the mammalian GPC1 as it is also expressed in the peripheral cranial and trunk sensory ganglia (i.e. trigeminal and dorsal root) in mouse and rat embryos (Litwack et al., 1998), though the distinction between the neural crest and placode cell types was not made.

The expression pattern is somewhat different in the hindbrain region corresponding to the presumptive epibranchial ganglia region, which is at around the second to the fourth branchial arches. Unlike the trigeminal neural crest, GPC1 is detected in the hindbrain neural crest cells during migration (Fig. 1, C-D), albeit expression is transient, since by stage 14, it is downregulated (Fig. 1, L-M). In addition, GPC1 is expressed in the epibranchial placodal ectoderm at later stages 14–16 (Fig. 1, E-F and L-M). The expression pattern of GPC1 in the hindbrain region suggests that it may potentially have an early role in hindbrain neural crest migration and later in epibranchial placodal gangliogenesis.

A.4.2 Expression of Glypican-1 mRNA in other tissues, including the neural tube, otic vesicle, limb, and somite

Expression of GPC1 mRNA was found in several other tissues besides the neural crest and placodal cells at stages 9–18. GPC1 was weakly expressed in the forming neural tube and notochord throughout these stages at the cranial levels (Fig. 1, A-L). By stage 12, the otic placode is found to express GPC1 albeit weakly but later through stage 18, its expression is strong in the invaginating and forming otic vesicle (Fig. 1, C, E-F, L, P). The forming limb bud also expresses GPC1 (Fig. 1P). Among these, the tissue expressing GPC1 in the most dynamic manner is probably the somitic tissue. Through the stages examined (st. 9–18), the GPC1 mRNA appears to be expressed in a gradient fashion in the presomitic mesoderm (PSM) highest at the newly forming somites and decreases both rostrally (towards the more anterior somites) and caudally towards the tail of the embryo. The expression found for GPC1 may suggest potentially interesting functions both early in specifying segmentation of the anterior PSM and later in epithelialization or boundary formation of the newly forming somite. The different expression of GPC1 from that of Robo2 and Slit1 in the trunk region, such that Robo2 is expressed in the neural folds and restricted portions of the somites similar to Slit1 (data not shown) (De Bellard et al., 2003), suggests that GPC1 may interact with signaling pathways other than Slit–Robo in the somites (Fig. 1, N-P). These expression patterns of GPC1 were consistent with that found previously in the forming neural tube, somite, and limb (Niu et al., 1996). It is also important to note that since Niu et al. examined mostly different stages (st.7–12 and 20–25), we have identified several previously unknown expression patterns of GPC1, including its expression in the cranial ganglia. They also characterized expressions of GPC1 that were not studied here at later stages 20–25, including expression of GPC1 in the

mantle zone of the telencephalon, apical epidermal ridge, the proximal limb, atrioventricular canal, and in the heart outflow tract which they suggest is endothelial- and not neural crest- derived mesenchyme.

A.4.3 Overexpression of Glypican-1 causes early disorganization of trigeminal placodal neurons and later severely reduced ganglion

The expression of Glypican-1 in the placodal ectoderm and derived cells as the trigeminal ganglion assembles suggests a possibility for its function in placodal gangliogenesis. To begin to test the function of GPC1, I have designed a full-length chick Glypican-1 expression construct (cytopcig + GPC1) and introduced it in the trigeminal placodal ectoderm prior to ingression at stages 8–10 to study the effects of GPC1 gain-of-function on ganglion formation. Strikingly, overexpression of GPC1 in the trigeminal placodal cells caused severe reduction in placodal cell number, giving rise to diminished ganglia, as well as effects on placodal assembly at early stages. At times of early ganglion assembly (stages 15–16), a significant number of transfected ganglia showed aberrant defects (77%, n=7/9). These defects were classified into two general groups: either both disorganized (aberrant positioning) and reduced in cell number (33%, n= 3/9) (Fig. 2D-F) or only appeared reduced in cell number (44%, n=4/9) (Fig. 2G-I). Later after the ganglion is well condensed at stages 17–19, the transfected ganglia with GPC1 overexpression were severely reduced in cell number and/or disorganized (69%, n=11/16). Out of the total number of ganglia exhibiting a phenotype, 82% (n=9/11) of the cases were diminished ganglia (Fig. 2M-O) of which 44% (n=4/9) had nearly complete loss of the ophthalmic (OpV) lobe (Fig. 2P-R). The loss of OpV phenotype thus constituted a significant 25% (n=4/16) of the total GPC1 transfected ganglia analyzed at stages 17–19. Control untransfected sides of the GPC1 electroporated embryos and control GFP electroporated

embryos did not show apparent ganglion abnormalities at all stages analyzed (Fig. 2, A-C and J-L and data not shown).

The results suggest an intriguing possibility that GPC1 may have a role in regulating placodal cell survival and/or proliferation and possibly also cell organization. The potential effect on cell proliferation may reflect a role for GPC1 on neuronal differentiation of the placodal cells, which takes place in the placodal ectoderm prior to ingression. This is based on the fact that most, if not all, placodal cells express neuronal markers by the time they ingress. Furthermore, it is intriguing to examine whether ingression may be affected such that a blocked migration may cause a reduced number of placodal neurons; however, this may be a secondary effect to loss of neuronal differentiation. Alternatively if undifferentiated placodal cells are aberrantly found to migrate to the ganglion anlage by GPC1 overexpression, this would demonstrate that migration and differentiation can be uncoupled, but this is unknown. Taken together, the data suggest that GPC1 function is sufficient to affect several aspects of the development of the placodal neurons during trigeminal ganglion formation, which likely involves various signaling pathways.

A.5 Conclusion and future work

The gene expression pattern and gain-of-function of GPC1 suggest its potential role in development of the trigeminal placodal ganglion. GPC1 was also expressed in the early migrating hindbrain neural crest cells and the epibranchial placodes but its role in these cells has not yet been examined. There are several lines of future research that would be

important to fully uncover the role of GPC1 in neural crest and placode development in the future.

First, understanding the cellular and molecular mechanisms mediated by GPC1 gain-of-function in causing the severe phenotype of trigeminal ganglion loss would provide important insights into the function of GPC1. It would be necessary to clarify the cellular effects as to whether this effect is on placodal cell survival, proliferation, and/or differentiation and also whether it alters placodal cell assembly. To identify the molecular mechanism responsible for mediating this function, it would be important to first identify the protein domain of GPC1 required for this phenotype, whether this requires the HS chain or not. Function of the core glypican protein has been suggested previously (i.e. transient expression of GPC-3 can induce apoptosis and this requires membrane anchorage but not the heparan sulfate chains (Gonzalez et al., 1998)). This suggests a potential role for GPC1 independent of its HS based co-receptor function. Overexpression of GPC1 may have an effect on Slit1 signaling or on other pathways (e.g. Wnt (Lassiter et al., 2007) and Fgf signaling (Stark et al., 2000)) implicated in trigeminal placodal development. Thus, the examination of whether this alters distribution of the protein expression patterns of these ligands and whether this may activate pathway specific downstream mediators would be revealing on the potential association of GPC1 to the different signaling pathways.

To further reveal its function, it would also be important to identify the subcellular localization and the potential proteolytic processing of the GPC1 proteins in these cells. Since an antibody against chick GPC1 that works for immunohistochemistry may not be available, the characterization of the exogenous GPC1 tagged with a reporter may yield useful information as to its localization on the cell membrane and/or possibly in the nucleus (which has been suggested but remains to be verified (Filmus and Song, 2000; Liang et al., 1997)) as well as its potential post-translational modifications (i.e. proteolytic cleavage at the GPI anchor or at a different site).

Gene knockdown of GPC1 in the trigeminal and epibranchial placodal cells as well as in the hindbrain neural crest would be necessary to uncover its endogenous role during development of the peripheral nervous system. Finally, the interaction between GPC1 and Slit1–Robo2 signaling can be tested by exploring whether altering GPC1 expression changes Slit1 expression and also if they are functionally interdependent (i.e. does gain or loss of function of Slit1 or Robo2 rescue the GPC1 mutant phenotype and vice versa). Further work on any of these future directions would undoubtedly provide new insights into the role of HSPG and its potential link with signaling pathways involved in placode and neural crest development.

Figure 1.

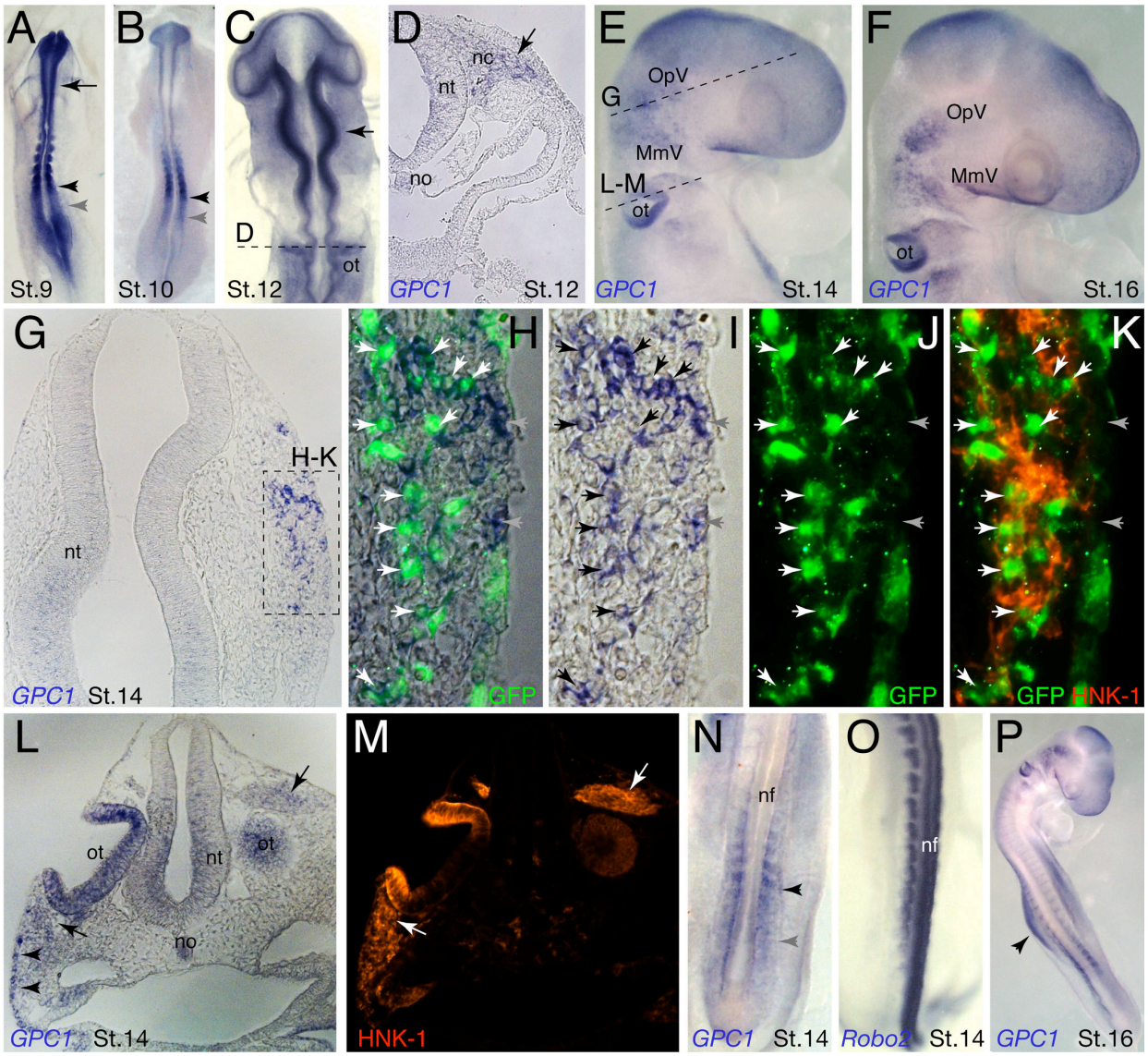
A
St.9
B
St.10
C
D
ot
St.12
D
nc
nt
no
GPC1
St.12
E
OpV
G
MmV
L-M
ot
GPC1
St.14
F
OpV
MmV
ot
GPC1
St.16
G
H-K
nt
GPC1
St.14
H
GFP
I
J
GFP
K
GFP
HNK-1
L
ot
nt
ot
no
GPC1
St.14
M
HNK-1
N
nf
GPC1
St.14
O
nf
Robo2
St.14
P
GPC1
St.16

Figure 1. Glypican-1 mRNA expression in trigeminal and epibranchial placodes, hindbrain neural crest, and various other tissues. GPC1 mRNA expression is revealed by whole mount in situ hybridization using an antisense chick GPC1 riboprobe. (**A**) Stage 9 chick embryo revealing a dynamic rostrocaudal gradient of GPC1 expression in the presomitic mesoderm (PSM) (black and gray arrowheads) and a strong expression in the neural tube (arrow). (**B**) Stage 10 embryo revealing the same gradient expression in the PSM (black and gray arrowheads). (**C**) Stage 12 embryo showing expression in the neural tube (arrow) and in the hindbrain neural crest at rhombomere 4 (dotted line). (**D**) Cross section at the level indicated by the dotted line in C. (**E**) Stage 14 and (**F**) stage 16 embryos showing expression in the OpV and MmV trigeminal and epibranchial placodes and otic vesicle. (**G**) Cross section at the level indicated in E showing the expression of GPC1 in the OpV placodes (dotted box) and weakly in the neural tube. (**H**) Overlay image showing overlap of GFP expression in the ectoderm and ectoderm-derived cells and GPC1 in situ expression (white arrowheads), and expression of GPC1 in an area of the placodal ectoderm not electroporated by GFP vector (gray arrowheads). Images of the same section as in H showing (**I**) GPC1 expression alone, (**J**) GFP expression alone and (**I**) overlay of GFP and neural crest marker HNK-1 expression. (**L**) Cross section at the level indicated in E showing GPC1 expression in the epibranchial placode (arrowheads), weakly in the hindbrain neural crest (arrows), otic vesicle, neural tube, and notochord. (**M**) Same section as in L showing HNK-1 expression on the hindbrain neural crest cells that also express GPC1 (arrows). (**N**) Expression of GPC1 and (**O**) Robo2 mRNA in the trunk regions of stage 14 embryos showing a mostly non-overlapping pattern. (**P**) Whole mount stage 16 embryo showing GPC1 expression in the limb bud as well as all other tissues aforementioned. OpV, ophthalmic; MmV, maxillo-mandibular; ot, otic vesicle; nt, neural tube; no, notochord; nc, neural crest; nf, neural folds.

Figure 2.

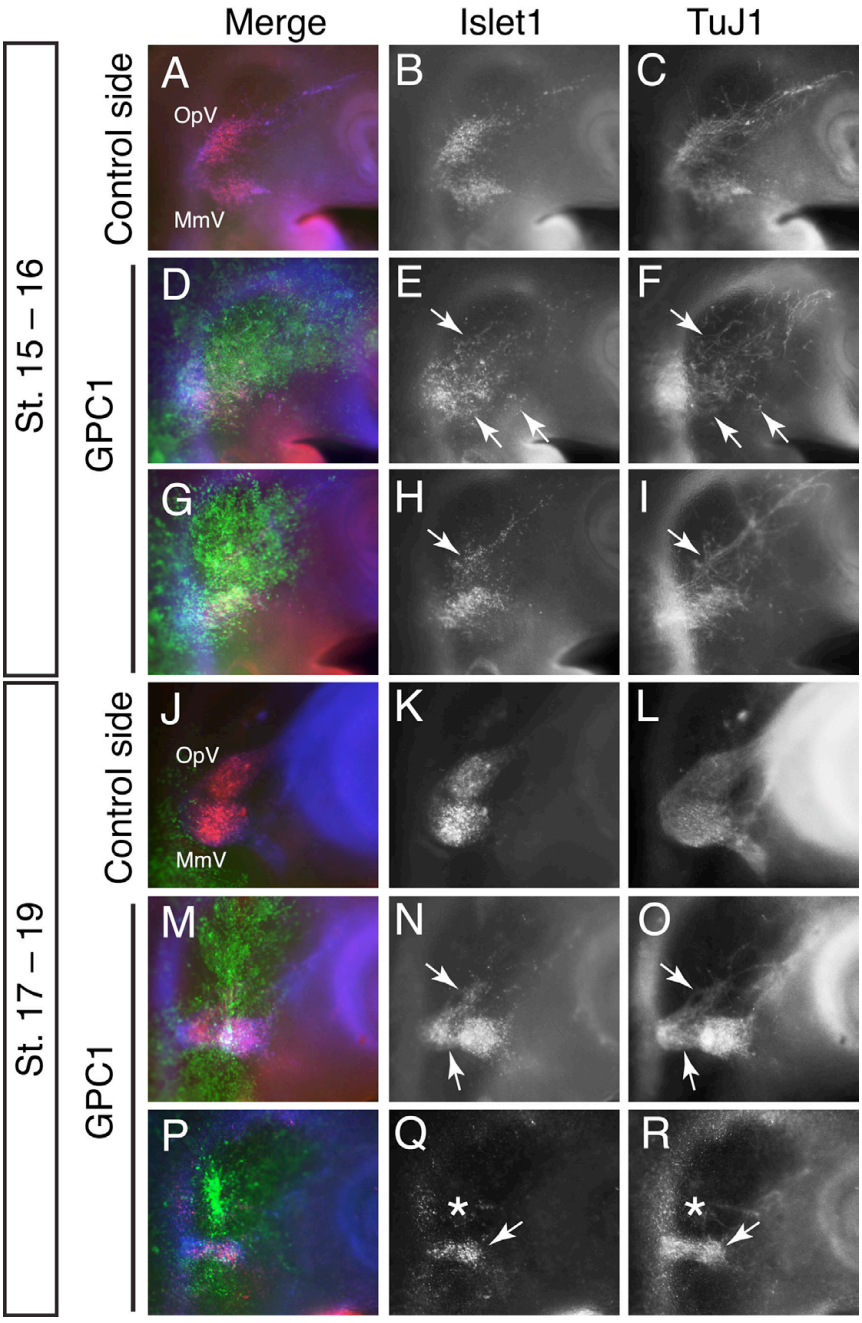
Merge
Islet1
TuJ1
St. 15 – 16
St. 17 – 19
Control side
GPC1
Control side
GPC1
A
OpV
MmV
B
C
D
E
F
G
H
I
J
OpV
MmV
K
L
M
N
O
P
Q
R
*
*

Figure 2. GPC1 overexpression in the trigeminal placodal ectoderm causes early disorganization of the placodal neurons and later severely reduced ganglion. Color overlay panel showing GFP (green) expression in area of transfection and double immunostaining for broad neuronal markers Islet1 (red) and TuJ1 (blue) to reveal placodal neuronal cell bodies and processes, respectively. Representative images of GPC1 electroporated embryos analyzed at stages 15-16 showing (**A**-**C**) a typical trigeminal ganglion on the control untransfected side, and aberrant GPC1 transfected ganglia which displayed two general categories of phenotypes: (**D**-**F**) severely disorganized and reduced population of placodal neurons (arrows) or (**G**-**I**) only markedly reduced population of the placodal neurons (arrow showing the OpV region). Later at stages 17-19, (**J**-**L**) control untransfected side (which had a small region of GFP expression but predominantly not in the ganglion region) showing normal ganglion formation, whereas the GPC1 transfected ganglia showed (**M**-**O**) dramatically reduced ganglion with some disorganization (arrows) and in extreme cases (**P**-**R**) near complete loss of the OpV lobe (asterisk) and a reduced MmV (arrow) ganglion. OpV, ophthalmic; MmV, maxillo-mandibular.

Appendix B

Supplementary materials and methods

Immunohistochemistry

All primary and secondary antibodies were diluted in blocking solution (PBS containing 5% sheep serum and 0.1% or 0.2% Triton X-100 or Tween-20). Primary antibodies used were anti-GFP (Molecular Probes; 1:1000 or 1:2000), anti-HNK-1 (American Type Culture; 1:3, 1:5, 1:20 or 1:50), anti-QCPN (Developmental Studies Hybridoma Bank; 1:1), anti-Islet1 (clone 40.2D6, Developmental Studies Hybridoma Bank; 1:250 or 1:500), and anti-TuJ1 (Covance; 1:250 or 1:500). The following secondary antibodies were obtained from Molecular Probes and used at 1:1000 or 1:2000 dilutions: Alexa Fluor 488 goat anti-rabbit IgG, Alexa Fluor 350 goat anti-mouse IgM, Alexa Fluor 568 goat anti-mouse IgM, Alexa Fluor 568 goat anti-mouse IgG1, Alexa Fluor 488 goat anti-mouse IgG2A, and Alexa Fluor 568 goat anti-mouse IgG2A. Staining was performed on whole chick embryos or 12 μm sections.

In ovo electroporation of trigeminal ectoderm or presumptive neural crest

DNA injection by air pressure using a glass micropipette was targeted on the trigeminal ectoderm for ectoderm electroporation and in the neural folds at stages 7–9 or presumptive neural crest region at stages 4–6 for neural crest electroporation. Platinum electrodes were placed vertically across the chick embryo for ectoderm electroporation (delivering 5 × 8 V in 50 ms at 100 ms intervals) and for neural crest electroporation at stages 4–6 (5 × 4–7 V in 50 ms at 100 ms intervals), or placed horizontally across the forming neural tube of the chick embryo for neural crest electroporation at stages 7–9 (5 × 12 V in 50 ms at 100 ms

intervals). Electroporated eggs were re-sealed and re-incubated at 37˚C to reach the desired stages. For stages 4–6 electroporation in ovo, two points of special care were applied: first, eggs were taken out of the incubator individually, manipulated, and immediately placed back into an incubator to minimize the time they sit at room temperature, and second the amount of india ink used to visualize the embryo was minimized (just enough to faintly depict the embryo). For short term analysis of RNAi constructs in neural crest at stages 8–10, electroporations were conducted on whole chick embryo explants at stages 4–6 placed ventral side up on filter paper rings. DNA was injected on the left side of the embryo between the vitelline membrane and the epiblast. Platinum electrodes were placed vertically across the embryo and a current of 5 × 7 V in 50 ms duration at 100 ms intervals were delivered. Embryos were cultured in 1 ml of albumen in tissue culture dishes (35 × 10 mm, NUNC) for 6–16 hours. cyto-pCIG is a modified version of pCIG (Megason and McMahon, 2002) that drives cytoplasmic GFP expression where 3×NLS is digested out at the NcoI site and re-ligated at the blunted NcoI sites.

Neural fold and ectoderm tissue ablations

For neural crest ablation, neural folds were bilaterally removed from stage 8 (3–4 somites) chick embryos (to eliminate any cross-over of neural crest migration from one side to the other) at the axial level corresponding to the region between caudal diencephalon and the first pair of somites. Eggs were re-sealed and collected after 40 hours of further incubation at 37ºC to reach approximately stage 18. Neural crest ablated embryos did not have neural tubes that healed completely in the region of ablation, however, at these stages normal development seemed to occur in the rest of the head. For placode ablation, the dorsolateral ectoderm adjacent to the neural tube in the region between the optic and the otic vesicles was removed from one side of the chick embryo at stages 11/12, with the unoperated side

as control. Eggs were re-sealed and re-incubated at 37ºC for about 24 hours to reach stage 18. Placode ablated embryos appeared to develop normally.

GFP labeling of the ectoderm combined with quail-chick grafts

In ovo electroporation of the trigeminal ectoderm with cyto-pCIG was performed on stage 9 (6–7 somites) chick embryos followed by a quail-chick neural fold graft. Dorsal neural tube from the region of caudal diencephalon to rhombomere 2 of a quail embryo was isotopically grafted into a stage-matched electroporated chick host from which this region had been ablated. Embryos were re-incubated at 37ºC for 36–40 hours, collected at stages 17/18, and then processed further for immunohistochemistry as described previously.

Analysis of Islet1+ placode cells during ingression

Chick embryos at stages 9–10 (6–10 somites) were electroporated with control GFP (cyto-pCIG or pCAβ-IRES-mGFP) or Robo2Δ-GFP expression vectors in the trigeminal ectoderm. Electroporated eggs were incubated for 20–24 hours at 37ºC to obtain stage 14 embryos. Embryos with broad and high GFP expression in the trigeminal region of the head ectoderm in at least one side of the head were collected for analysis and cryosectioned at 12 μm along the frontal plane through the head encompassing the entire presumptive trigeminal area. Each side of the embryo head that was well transfected was individually analyzed. Sections were immunostained using antibodies against GFP, HNK-1, and Islet1 as aforementioned. All sections were imaged and all Islet1 positive cells in the surface ectoderm, associated with the basal margin of the ectoderm, and in the mesenchyme of the head anterior to the otic placode were counted. In the region of analysis, uniformly ubiquitous, and sometimes weak, Islet1 signals were observed in the ventral and/or pharyngeal ectoderm, as previously described (Begbie et al., 2002). These signals were not counted, as they appeared to be non-specific to trigeminal placode cells. Average and

standard deviation of the percentages of Islet1+ placode cells associated with the ectoderm and in the mesenchyme were obtained.

RNAi

The RNAi vector backbone was pRFPRNAiC in which the *Afl*II site was replaced with an *Mlu*I site and the outer 3' oligoneucleotide sequence for amplifying the miRNA hairpins also incorporated the *Mlu*I restriction site sequence for cloning.

Appendix C

LITERATURE CITED

Akitaya, T. and Bronner-Fraser, M. (1992). Expression of cell adhesion molecules during initiation and cessation of neural crest cell migration. ***Dev Dyn*** **194, 12-20.**

Anselmo, M. A., Dalvin, S., Prodhan, P., Komatsuzaki, K., Aidlen, J. T., Schnitzer, J. J., Wu, J. Y. and Kinane, T. B. (2003). Slit and robo: expression patterns in lung development. ***Gene Expr Patterns*** **3, 13-9.**

Ayer-Le Lievre, C. S. and Le Douarin, N. M. (1982). The early development of cranial sensory ganglia and the potentialities of their component cells studied in quail-chick chimeras. ***Dev Biol*** **94, 291-310.**

Bagri, A., Marin, O., Plump, A. S., Mak, J., Pleasure, S. J., Rubenstein, J. L. and Tessier-Lavigne, M. (2002). Slit proteins prevent midline crossing and determine the dorsoventral position of major axonal pathways in the mammalian forebrain. ***Neuron*** **33, 233-48.**

Bailey, A. P. and Streit, A. (2006). Sensory organs: making and breaking the pre-placodal region. ***Curr Top Dev Biol*** **72, 167-204.**

Baker, C. V. (2005). Neural Crest and Cranial Ectodermal Placodes. In ***Developmental Neurobiology*****, (ed. M. S. R. a. M. Jacobson), pp. 67-127. New York: Kluwer Academic/ Plenum Publishers.**

Baker, C. V. and Bronner-Fraser, M. (2001). Vertebrate cranial placodes I. Embryonic induction. ***Dev Biol*** **232, 1-61.**

Baker, C. V., Bronner-Fraser, M., Le Douarin, N. M. and Teillet, M. A. (1997). Early- and late-migrating cranial neural crest cell populations have equivalent developmental potential in vivo. ***Development*** **124, 3077-87.**

Bashaw, G. J., Kidd, T., Murray, D., Pawson, T. and Goodman, C. S. (2000). Repulsive axon guidance: Abelson and Enabled play opposing roles downstream of the roundabout receptor. ***Cell*** **101, 703-15.**

Batten, E. H. (1957). The activity of the trigeminal placode in the sheep embryo. ***J Anat*** **91, 174-87.**

Battisti, A. C. and Fekete, D. M. (2008). Slits and Robos in the developing chicken inner ear. ***Dev Dyn*** **237, 476-84.**

Bedell, V. M., Yeo, S. Y., Park, K. W., Chung, J., Seth, P., Shivalingappa, V., Zhao, J., Obara, T., Sukhatme, V. P., Drummond, I. A. et al. (2005). roundabout4 is essential for angiogenesis in vivo. ***Proc Natl Acad Sci U S A*** **102, 6373-8.**

Begbie, J., Ballivet, M. and Graham, A. (2002). Early steps in the production of sensory neurons by the neurogenic placodes. ***Mol Cell Neurosci*** **21, 502-11.**

Begbie, J., Brunet, J. F., Rubenstein, J. L. and Graham, A. (1999). Induction of the epibranchial placodes. ***Development*** **126, 895-902.**

Begbie, J. and Graham, A. (2001a). Integration between the epibranchial placodes and the hindbrain. ***Science*** **294, 595-8.**

Begbie, J. and Graham, A. (2001b). The ectodermal placodes: a dysfunctional family. ***Philos Trans R Soc Lond B Biol Sci*** **356, 1655-60.**

Borchers, A., David, R. and Wedlich, D. (2001). Xenopus cadherin-11 restrains cranial neural crest migration and influences neural crest specification. ***Development*** **128, 3049-60.**

Braga, V. M. (1999). Small GTPases and regulation of cadherin dependent cell-cell adhesion. ***Mol Pathol*** **52, 197-202.**

Braga, V. M., Del Maschio, A., Machesky, L. and Dejana, E. (1999). Regulation of cadherin function by Rho and Rac: modulation by junction maturation and cellular context. ***Mol Biol Cell*** **10, 9-22.**

Bronner-Fraser, M. (1986). Analysis of the early stages of trunk neural crest migration in avian embryos using monoclonal antibody HNK-1. ***Dev Biol*** **115, 44-55.**

Brose, K., Bland, K. S., Wang, K. H., Arnott, D., Henzel, W., Goodman, C. S., Tessier-Lavigne, M. and Kidd, T. (1999). Slit proteins bind Robo receptors and have an evolutionarily conserved role in repulsive axon guidance. ***Cell*** **96, 795-806.**

Brose, K. and Tessier-Lavigne, M. (2000). Slit proteins: key regulators of axon guidance, axonal branching, and cell migration. ***Curr Opin Neurobiol*** **10, 95-102.**

Cano-Gauci, D. F., Song, H. H., Yang, H., McKerlie, C., Choo, B., Shi, W., Pullano, R., Piscione, T. D., Grisaru, S., Soon, S. et al. (1999). Glypican-3-deficient mice exhibit developmental overgrowth and some of the abnormalities typical of Simpson-Golabi-Behmel syndrome. ***J Cell Biol*** **146, 255-64.**

Charrasse, S., Meriane, M., Comunale, F., Blangy, A. and Gauthier-Rouviere, C. (2002). N-cadherin-dependent cell-cell contact regulates Rho GTPases and beta-catenin localization in mouse C2C12 myoblasts. ***J Cell Biol*** **158, 953-65.**

Chedotal, A. (2007). Slits and Their Receptors. In ***Axon Growth and Guidance*****, vol. 621 (ed. D. Bagnard), pp. 65–80. New York: Landes Bioscience, Springer.**

Chen, J. H., Wen, L., Dupuis, S., Wu, J. Y. and Rao, Y. (2001). The N-terminal leucine-rich regions in Slit are sufficient to repel olfactory bulb axons and subventricular zone neurons. ***J Neurosci*** **21, 1548-56.**

Cheng, Y., Cheung, M., Abu-Elmagd, M. M., Orme, A. and Scotting, P. J. (2000). Chick sox10, a transcription factor expressed in both early neural crest cells and central nervous system. ***Brain Res Dev Brain Res*** **121, 233-41.**

Coles, E. G., Gammill, L. S., Miner, J. H. and Bronner-Fraser, M. (2006). Abnormalities in neural crest cell migration in laminin alpha5 mutant mice. ***Dev Biol*** **289, 218-28.**

D'Amico-Martel, A. (1982). Temporal patterns of neurogenesis in avian cranial sensory and autonomic ganglia. ***Am J Anat*** **163, 351-72.**

D'Amico-Martel, A. and Noden, D. M. (1980). An autoradiographic analysis of the development of the chick trigeminal ganglion. ***J Embryol Exp Morphol*** **55, 167-82.**

D'Amico-Martel, A. and Noden, D. M. (1983). Contributions of placodal and neural crest cells to avian cranial peripheral ganglia. ***Am J Anat*** **166, 445-68.**

Das, R. M., Van Hateren, N. J., Howell, G. R., Farrell, E. R., Bangs, F. K., Porteous, V. C., Manning, E. M., McGrew, M. J., Ohyama, K., Sacco, M. A. et al. (2006). A robust system for RNA interference in the chicken using a modified microRNA operon. ***Dev Biol*** **294, 554-63.**

De Bellard, M. E., Rao, Y. and Bronner-Fraser, M. (2003). Dual function of Slit2 in repulsion and enhanced migration of trunk, but not vagal, neural crest cells. ***J Cell Biol*** **162, 269-79.**

Dickson, B. J. and Gilestro, G. F. (2006). Regulation of commissural axon pathfinding by slit and its Robo receptors. ***Annu Rev Cell Dev Biol*** **22, 651-75.**

Duband, J. L., Dufour, S., Hatta, K., Takeichi, M., Edelman, G. M. and Thiery, J. P. (1987). Adhesion molecules during somitogenesis in the avian embryo. ***J Cell Biol*** **104, 1361-74.**

Duguay, D., Foty, R. A. and Steinberg, M. S. (2003). Cadherin-mediated cell adhesion and tissue segregation: qualitative and quantitative determinants. ***Dev Biol*** **253, 309-23.**

El Sayegh, T. Y., Kapus, A. and McCulloch, C. A. (2007). Beyond the epithelium: cadherin function in fibrous connective tissues. ***FEBS Lett*** **581, 167-74.**

Fan, X., Labrador, J. P., Hing, H. and Bashaw, G. J. (2003). Slit stimulation recruits Dock and Pak to the roundabout receptor and increases Rac activity to regulate axon repulsion at the CNS midline. ***Neuron*** **40, 113-27.**

Fico, A., Maina, F. and Dono, R. (2007). Fine-tuning of cell signalling by glypicans. ***Cell Mol Life Sci*****.**

Filmus, J. (2001). Glypicans in growth control and cancer. ***Glycobiology*** **11, 19R-23R.**

Filmus, J. and Song, H. H. (2000). Glypicans. In *Proteoglycans: Structure, Biology, and Molecular Interactions*, (ed. R. V. Iozzo), pp. 161-176: CRC Press.

Fouquet, C., Di Meglio, T., Ma, L., Kawasaki, T., Long, H., Hirata, T., Tessier-Lavigne, M., Chedotal, A. and Nguyen-Ba-Charvet, K. T. (2007). Robo1 and robo2 control the development of the lateral olfactory tract. *J Neurosci* 27, 3037-45.

Franch-Marro, X., Marchand, O., Piddini, E., Ricardo, S., Alexandre, C. and Vincent, J. P. (2005). Glypicans shunt the Wingless signal between local signalling and further transport. *Development* 132, 659-66.

Fujiwara, M., Ghazizadeh, M. and Kawanami, O. (2006). Potential role of the Slit–Robo signal pathway in angiogenesis. *Vasc Med* 11, 115-21.

Fukata, M. and Kaibuchi, K. (2001). Rho-family GTPases in cadherin-mediated cell-cell adhesion. *Nat Rev Mol Cell Biol* 2, 887-97.

Fukuhara, N., Howitt, J. A., Hussain, S. A. and Hohenester, E. (2008). Structural and functional analysis of slit and heparin binding to immunoglobulin-like domains 1 and 2 of Drosophila Robo. *J Biol Chem* 283, 16226-34.

Gammill, L. S. and Bronner-Fraser, M. (2002). Genomic analysis of neural crest induction. *Development* 129, 5731-41.

Gammill, L. S., Gonzalez, C. and Bronner-Fraser, M. (2006). Neuropilin 2/semaphorin 3F signaling is essential for cranial neural crest migration and trigeminal ganglion condensation. *J Neurobiol* 67, 47-56.

Ghose, A. and Van Vactor, D. (2002). GAPs in Slit-Robo signaling. *Bioessays* 24, 401-4.

Gonzalez, A. D., Kaya, M., Shi, W., Song, H., Testa, J. R., Penn, L. Z. and Filmus, J. (1998). OCI-5/GPC3, a glypican encoded by a gene that is mutated in the Simpson-Golabi-Behmel overgrowth syndrome, induces apoptosis in a cell line-specific manner. *J Cell Biol* 141, 1407-14.

Guan, K. L. and Rao, Y. (2003). Signalling mechanisms mediating neuronal responses to guidance cues. *Nat Rev Neurosci* 4, 941-56.

Gumbiner, B. M. (2005). Regulation of cadherin-mediated adhesion in morphogenesis. *Nat Rev Mol Cell Biol* 6, 622-34.

Hall, B. K. (1999). The Neural Crest in Development and Evolution. New York: Springer-Verlag New York, Inc.

Hamburger, V. (1961). Experimental analysis of the dual origin of the trigeminal ganglion in the chick embryo. *J Exp Zool* 148, 91-123.

Hamburger, V. and Hamilton, H. L. (1992). A series of normal stages in the development of the chick embryo. 1951. ***Dev Dyn*** **195, 231-72.**

Hammond, R., Vivancos, V., Naeem, A., Chilton, J., Mambetisaeva, E., Andrews, W., Sundaresan, V. and Guthrie, S. (2005). Slit-mediated repulsion is a key regulator of motor axon pathfinding in the hindbrain. ***Development*** **132, 4483-95.**

Hatta, K., Takagi, S., Fujisawa, H. and Takeichi, M. (1987). Spatial and temporal expression pattern of N-cadherin cell adhesion molecules correlated with morphogenetic processes of chicken embryos. ***Dev Biol*** **120, 215-27.**

Hatta, K. and Takeichi, M. (1986). Expression of N-cadherin adhesion molecules associated with early morphogenetic events in chick development. ***Nature*** **320, 447-9.**

Hinck, L. (2004). The versatile roles of "axon guidance" cues in tissue morphogenesis. ***Dev Cell*** **7, 783-93.**

His, W. (1868). Untersuchungen über die erste Anlage des Wirbeltierliebes. ***Die erste Entwicklung des Hühnchens im Ei, F.C.W. Vogel, Leipzig.***

Hivert, B., Liu, Z., Chuang, C. Y., Doherty, P. and Sundaresan, V. (2002). Robo1 and Robo2 are homophilic binding molecules that promote axonal growth. ***Mol Cell Neurosci*** **21, 534-45.**

Hohenester, E. (2008). Structural insight into Slit-Robo signalling. ***Biochem Soc Trans*** **36, 251-6.**

Hohenester, E., Hussain, S. and Howitt, J. A. (2006). Interaction of the guidance molecule Slit with cellular receptors. ***Biochem Soc Trans*** **34, 418-21.**

Howitt, J. A., Clout, N. J. and Hohenester, E. (2004). Binding site for Robo receptors revealed by dissection of the leucine-rich repeat region of Slit. ***EMBO J*** **23, 4406-12.**

Hu, H. (1999). Chemorepulsion of neuronal migration by Slit2 in the developing mammalian forebrain. ***Neuron*** **23, 703-11.**

Hu, H. (2001). Cell-surface heparan sulfate is involved in the repulsive guidance activities of Slit2 protein. ***Nat Neurosci*** **4, 695-701.**

Hu, H., Li, M., Labrador, J. P., McEwen, J., Lai, E. C., Goodman, C. S. and Bashaw, G. J. (2005). Cross GTPase-activating protein (CrossGAP)/Vilse links the Roundabout receptor to Rac to regulate midline repulsion. ***Proc Natl Acad Sci U S A*** **102, 4613-8.**

Huminiecki, L., Gorn, M., Suchting, S., Poulsom, R. and Bicknell, R. (2002). Magic roundabout is a new member of the roundabout receptor family that is endothelial specific and expressed at sites of active angiogenesis. ***Genomics*** **79, 547-52.**

Hummel, T., Schimmelpfeng, K. and Klambt, C. (1999). Commissure formation in the embryonic CNS of Drosophila. ***Dev Biol*** **209, 381-98.**

Hussain, S. A., Piper, M., Fukuhara, N., Strochlic, L., Cho, G., Howitt, J. A., Ahmed, Y., Powell, A. K., Turnbull, J. E., Holt, C. E. et al. (2006). A molecular mechanism for the heparan sulfate dependence of slit-robo signaling. ***J Biol Chem*** **281, 39693-8.**

Inoue, T., Chisaka, O., Matsunami, H. and Takeichi, M. (1997). Cadherin-6 expression transiently delineates specific rhombomeres, other neural tube subdivisions, and neural crest subpopulations in mouse embryos. ***Dev Biol*** **183, 183-94.**

Inuzuka, H., Redies, C. and Takeichi, M. (1991). Differential expression of R- and N-cadherin in neural and mesodermal tissues during early chicken development. ***Development*** **113, 959-67.**

Ishii, M., Han, J., Yen, H. Y., Sucov, H. M., Chai, Y. and Maxson, R. E., Jr. (2005). Combined deficiencies of Msx1 and Msx2 cause impaired patterning and survival of the cranial neural crest. ***Development*** **132, 4937-50.**

Jeanes, A., Gottardi, C. J. and Yap, A. S. (2008). Cadherins and cancer: how does cadherin dysfunction promote tumor progression? ***Oncogene*** **27, 6920-9.**

Jia, L., Cheng, L. and Raper, J. (2005). Slit–Robo signaling is necessary to confine early neural crest cells to the ventral migratory pathway in the trunk. ***Dev Biol*** **282, 411-21.**

Jin, Z., Zhang, J., Klar, A., Chedotal, A., Rao, Y., Cepko, C. L. and Bao, Z. Z. (2003). Irx4-mediated regulation of Slit1 expression contributes to the definition of early axonal paths inside the retina. ***Development*** **130, 1037-48.**

Johnson, K. G., Ghose, A., Epstein, E., Lincecum, J., O'Connor, M. B. and Van Vactor, D. (2004). Axonal heparan sulfate proteoglycans regulate the distribution and efficiency of the repellent slit during midline axon guidance. ***Curr Biol*** **14, 499-504.**

Johnston, M. C. (1966). A radioautographic study of the migration and fate of cranial neural crest cells in the chick embryo. ***Anat Rec*** **156, 143-55.**

Kasemeier-Kulesa, J. C., Bradley, R., Pasquale, E. B., Lefcort, F. and Kulesa, P. M. (2006). Eph/ephrins and N-cadherin coordinate to control the pattern of sympathetic ganglia. ***Development*** **133, 4839-47.**

Kasemeier-Kulesa, J. C., Kulesa, P. M. and Lefcort, F. (2005). Imaging neural crest cell dynamics during formation of dorsal root ganglia and sympathetic ganglia. ***Development*** **132, 235-45.**

Kawano, R., Matsuo, N., Tanaka, H., Nasu, M., Yoshioka, H. and Shirabe, K. (2002). Identification and characterization of a soluble Cadherin-7 isoform produced by alternative splicing. ***J Biol Chem*** **277, 47679-85.**

Kee, Y. and Bronner-Fraser, M. (2001). Temporally and spatially restricted expression of the helix-loop-helix transcriptional regulator Id1 during avian embryogenesis. ***Mech Dev*** **109, 331-5.**

Kerstetter, A. E., Azodi, E., Marrs, J. A. and Liu, Q. (2004). Cadherin-2 function in the cranial ganglia and lateral line system of developing zebrafish. ***Dev Dyn*** **230, 137-43.**

Keynes, R. J. and Stern, C. D. (1988). Mechanisms of vertebrate segmentation. ***Development*** **103, 413-29.**

Kidd, T., Bland, K. S. and Goodman, C. S. (1999). Slit is the midline repellent for the robo receptor in Drosophila. ***Cell*** **96, 785-94.**

Kidd, T., Brose, K., Mitchell, K. J., Fetter, R. D., Tessier-Lavigne, M., Goodman, C. S. and Tear, G. (1998). Roundabout controls axon crossing of the CNS midline and defines a novel subfamily of evolutionarily conserved guidance receptors. ***Cell*** **92, 205-15.**

Kil, S. H., Krull, C. E., Cann, G., Clegg, D. and Bronner-Fraser, M. (1998). The alpha4 subunit of integrin is important for neural crest cell migration. ***Dev Biol*** **202, 29-42.**

Kleeff, J., Ishiwata, T., Kumbasar, A., Friess, H., Buchler, M. W., Lander, A. D. and Korc, M. (1998). The cell-surface heparan sulfate proteoglycan Glypican-1 regulates growth factor action in pancreatic carcinoma cells and is overexpressed in human pancreatic cancer. ***J Clin Invest*** **102, 1662-73.**

Knaut, H., Blader, P., Strahle, U. and Schier, A. F. (2005). Assembly of trigeminal sensory ganglia by chemokine signaling. ***Neuron*** **47, 653-66.**

Knecht, A. K. and Bronner-Fraser, M. (2002). Induction of the neural crest: a multigene process. ***Nat Rev Genet*** **3, 453-61.**

Knudsen, K. A. and Wheelock, M. J. (2005). Cadherins and the mammary gland. ***J Cell Biochem*** **95, 488-96.**

Kovacs, E. M., Ali, R. G., McCormack, A. J. and Yap, A. S. (2002). E-cadherin homophilic ligation directly signals through Rac and phosphatidylinositol 3-kinase to regulate adhesive contacts. ***J Biol Chem*** **277, 6708-18.**

Kowalczyk, A. P. and Reynolds, A. B. (2004). Protecting your tail: regulation of cadherin degradation by p120-catenin. ***Curr Opin Cell Biol*** **16, 522-7.**

Kramer, S. G., Kidd, T., Simpson, J. H. and Goodman, C. S. (2001). Switching repulsion to attraction: changing responses to slit during transition in mesoderm migration. ***Science*** **292, 737-40.**

Kraut, R. and Zinn, K. (2004). Roundabout 2 regulates migration of sensory neurons by signaling in trans. ***Curr Biol*** **14, 1319-29.**

Krull, C. E., Lansford, R., Gale, N. W., Collazo, A., Marcelle, C., Yancopoulos, G. D., Fraser, S. E. and Bronner-Fraser, M. (1997). Interactions of Eph-related receptors and ligands confer rostrocaudal pattern to trunk neural crest migration. ***Curr Biol*** **7, 571-80.**

Kulesa, P. M. and Fraser, S. E. (2000). In ovo time-lapse analysis of chick hindbrain neural crest cell migration shows cell interactions during migration to the branchial arches. ***Development*** **127, 1161-72.**

Kulesa, P. M., Lu, C. C. and Fraser, S. E. (2005). Time-lapse analysis reveals a series of events by which cranial neural crest cells reroute around physical barriers. ***Brain Behav Evol*** **66, 255-65.**

Kulesa, P. M., Teddy, J. M., Stark, D. A., Smith, S. E. and McLennan, R. (2008). Neural crest invasion is a spatially-ordered progression into the head with higher cell proliferation at the migratory front as revealed by the photoactivatable protein, KikGR. ***Dev Biol*** **316, 275-87.**

Lallier, T. E. and Bronner-Fraser, M. (1988). A spatial and temporal analysis of dorsal root and sympathetic ganglion formation in the avian embryo. ***Dev Biol*** **127, 99-112.**

Lassiter, R. N., Dude, C. M., Reynolds, S. B., Winters, N. I., Baker, C. V. and Stark, M. R. (2007). Canonical Wnt signaling is required for ophthalmic trigeminal placode cell fate determination and maintenance. ***Dev Biol*** **308, 392-406.**

Le Douarin, N. M. (1973). A biological cell labeling technique and its use in experimental embryology. ***Dev Biol*** **30, 217-22.**

Le Douarin, N. M. and Kalcheim, C. (1999). The Neural Crest. U.K.: Cambridge University Press.

Lee, J. S., Ray, R. and Chien, C. B. (2001). Cloning and expression of three zebrafish roundabout homologs suggest roles in axon guidance and cell migration. ***Dev Dyn*** **221, 216-30.**

Legg, J. A., Herbert, J. M., Clissold, P. and Bicknell, R. (2008). Slits and Roundabouts in cancer, tumour angiogenesis and endothelial cell migration. ***Angiogenesis*** **11, 13-21.**

Li, H. S., Chen, J. H., Wu, W., Fagaly, T., Zhou, L., Yuan, W., Dupuis, S., Jiang, Z. H., Nash, W., Gick, C. et al. (1999). Vertebrate slit, a secreted ligand for the transmembrane protein roundabout, is a repellent for olfactory bulb axons. ***Cell*** **96, 807-18.**

Li, X., Chen, Y., Liu, Y., Gao, J., Gao, F., Bartlam, M., Wu, J. Y. and Rao, Z. (2006). Structural basis of Robo proline-rich motif recognition by the srGAP1 Src homology 3 domain in the Slit-Robo signaling pathway. ***J Biol Chem*** **281, 28430-7.**

Liang, Y., Annan, R. S., Carr, S. A., Popp, S., Mevissen, M., Margolis, R. K. and Margolis, R. U. (1999). Mammalian homologues of the Drosophila slit protein are

ligands of the heparan sulfate proteoglycan Glypican-1 in brain. *J Biol Chem* 274, 17885-92.

Liang, Y., Haring, M., Roughley, P. J., Margolis, R. K. and Margolis, R. U. (1997). Glypican and biglycan in the nuclei of neurons and glioma cells: presence of functional nuclear localization signals and dynamic changes in glypican during the cell cycle. *J Cell Biol* 139, 851-64.

Lin, H., Huber, R., Schlessinger, D. and Morin, P. J. (1999). Frequent silencing of the GPC3 gene in ovarian cancer cell lines. *Cancer Res* 59, 807-10.

Linask, K. K., Ludwig, C., Han, M. D., Liu, X., Radice, G. L. and Knudsen, K. A. (1998). N-cadherin/catenin-mediated morphoregulation of somite formation. *Dev Biol* 202, 85-102.

Litwack, E. D., Ivins, J. K., Kumbasar, A., Paine-Saunders, S., Stipp, C. S. and Lander, A. D. (1998). Expression of the heparan sulfate proteoglycan Glypican-1 in the developing rodent. *Dev Dyn* 211, 72-87.

Liu, Q., Ensign, R. D. and Azodi, E. (2003). Cadherin-1, -2 and -4 expression in the cranial ganglia and lateral line system of developing zebrafish. *Gene Expr Patterns* 3, 653-8.

Liu, Z., Patel, K., Schmidt, H., Andrews, W., Pini, A. and Sundaresan, V. (2004). Extracellular Ig domains 1 and 2 of Robo are important for ligand (Slit) binding. *Mol Cell Neurosci* 26, 232-40.

Loes, S., Luukko, K., Kvinnsland, I. H. and Kettunen, P. (2001). Slit1 is specifically expressed in the primary and secondary enamel knots during molar tooth cusp formation. *Mech Dev* 107, 155-7.

Long, H., Sabatier, C., Ma, L., Plump, A., Yuan, W., Ornitz, D. M., Tamada, A., Murakami, F., Goodman, C. S. and Tessier-Lavigne, M. (2004). Conserved roles for Slit and Robo proteins in midline commissural axon guidance. *Neuron* 42, 213-23.

Lundstrom, A., Gallio, M., Englund, C., Steneberg, P., Hemphala, J., Aspenstrom, P., Keleman, K., Falileeva, L., Dickson, B. J. and Samakovlis, C. (2004). Vilse, a conserved Rac/Cdc42 GAP mediating Robo repulsion in tracheal cells and axons. *Genes Dev* 18, 2161-71.

Luxardi, G., Galli, A., Forlani, S., Lawson, K., Maina, F. and Dono, R. (2007). Glypicans are differentially expressed during patterning and neurogenesis of early mouse brain. *Biochem Biophys Res Commun* 352, 55-60.

Lwigale, P. Y. (2001). Embryonic origin of avian corneal sensory nerves. *Dev Biol* 239, 323-37.

Ma, L. and Tessier-Lavigne, M. (2007). Dual branch-promoting and branch-repelling actions of Slit–Robo signaling on peripheral and central branches of developing sensory axons. *J Neurosci* 27, 6843-51.

MacMullin, A. and Jacobs, J. R. (2006). Slit coordinates cardiac morphogenesis in Drosophila. ***Dev Biol*** **293, 154-64.**

Maretzky, T., Reiss, K., Ludwig, A., Buchholz, J., Scholz, F., Proksch, E., de Strooper, B., Hartmann, D. and Saftig, P. (2005). ADAM10 mediates E-cadherin shedding and regulates epithelial cell-cell adhesion, migration, and beta-catenin translocation. ***Proc Natl Acad Sci U S A*** **102, 9182-7.**

Matsuda, K., Maruyama, H., Guo, F., Kleeff, J., Itakura, J., Matsumoto, Y., Lander, A. D. and Korc, M. (2001). Glypican-1 is overexpressed in human breast cancer and modulates the mitogenic effects of multiple heparin-binding growth factors in breast cancer cells. ***Cancer Res*** **61, 5562-9.**

McCabe, K. L. and Bronner-Fraser, M. (2008). Essential role for PDGF signaling in ophthalmic trigeminal placode induction. ***Development*** **135, 1863-74.**

McCabe, K. L., Shiau, C. E. and Bronner-Fraser, M. (2007). Identification of candidate secreted factors involved in trigeminal placode induction. ***Dev Dyn*** **236, 2925-35.**

McCusker, C., Cousin, H., Neuner, R. and Alfandari, D. (2009). Extracellular cleavage of cadherin-11 by ADAM metalloproteases is essential for Xenopus cranial neural crest cell migration. ***Mol Biol Cell*** **20, 78-89.**

McLarren, K. W., Litsiou, A. and Streit, A. (2003). DLX5 positions the neural crest and preplacode region at the border of the neural plate. ***Dev Biol*** **259, 34-47.**

Megason, S. G. and McMahon, A. P. (2002). A mitogen gradient of dorsal midline Wnts organizes growth in the CNS. ***Development*** **129, 2087-98.**

Moody, S. A., Quigg, M. S. and Frankfurter, A. (1989). Development of the peripheral trigeminal system in the chick revealed by an isotype-specific anti-beta-tubulin monoclonal antibody. ***J Comp Neurol*** **279, 567-80.**

Morlot, C., Thielens, N. M., Ravelli, R. B., Hemrika, W., Romijn, R. A., Gros, P., Cusack, S. and McCarthy, A. A. (2007). Structural insights into the Slit-Robo complex. ***Proc Natl Acad Sci U S A*** **104, 14923-8.**

Murthy, S. S., Shen, T., De Rienzo, A., Lee, W. C., Ferriola, P. C., Jhanwar, S. C., Mossman, B. T., Filmus, J. and Testa, J. R. (2000). Expression of GPC3, an X-linked recessive overgrowth gene, is silenced in malignant mesothelioma. ***Oncogene*** **19, 410-6.**

Nakagawa, S. and Takeichi, M. (1995). Neural crest cell-cell adhesion controlled by sequential and subpopulation-specific expression of novel cadherins. ***Development*** **121, 1321-32.**

Nakagawa, S. and Takeichi, M. (1998). Neural crest emigration from the neural tube depends on regulated cadherin expression. ***Development*** **125, 2963-71.**

Nakato, H., Futch, T. A. and Selleck, S. B. (1995). The division abnormally delayed (dally) gene: a putative integral membrane proteoglycan required for cell division patterning during postembryonic development of the nervous system in Drosophila. *Development* 121, 3687-702.

Nechiporuk, A., Linbo, T., Poss, K. D. and Raible, D. W. (2007). Specification of epibranchial placodes in zebrafish. *Development* 134, 611-23.

Nguyen Ba-Charvet, K. T., Brose, K., Marillat, V., Kidd, T., Goodman, C. S., Tessier-Lavigne, M., Sotelo, C. and Chedotal, A. (1999). Slit2-Mediated chemorepulsion and collapse of developing forebrain axons. *Neuron* 22, 463-73.

Nguyen-Ba-Charvet, K. T., Brose, K., Marillat, V., Sotelo, C., Tessier-Lavigne, M. and Chedotal, A. (2001). Sensory axon response to substrate-bound Slit2 is modulated by laminin and cyclic GMP. *Mol Cell Neurosci* 17, 1048-58.

Nguyen-Ba-Charvet, K. T., Picard-Riera, N., Tessier-Lavigne, M., Baron-Van Evercooren, A., Sotelo, C. and Chedotal, A. (2004). Multiple roles for slits in the control of cell migration in the rostral migratory stream. *J Neurosci* 24, 1497-506.

Nguyen-Ba-Charvet, K. T., Plump, A. S., Tessier-Lavigne, M. and Chedotal, A. (2002). Slit1 and slit2 proteins control the development of the lateral olfactory tract. *J Neurosci* 22, 5473-80.

Niclou, S. P., Jia, L. and Raper, J. A. (2000). Slit2 is a repellent for retinal ganglion cell axons. *J Neurosci* 20, 4962-74.

Niederlander, C. and Lumsden, A. (1996). Late emigrating neural crest cells migrate specifically to the exit points of cranial branchiomotor nerves. *Development* 122, 2367-74.

Nikaido, M., Doi, K., Shimizu, T., Hibi, M., Kikuchi, Y. and Yamasu, K. (2007). Initial specification of the epibranchial placode in zebrafish embryos depends on the fibroblast growth factor signal. *Dev Dyn* 236, 564-71.

Niu, S., Antin, P. B., Akimoto, K. and Morkin, E. (1996). Expression of avian glypican is developmentally regulated. *Dev Dyn* 207, 25-34.

Noden, D. M. (1975). An analysis of migratory behavior of avian cephalic neural crest cells. *Dev Biol* 42, 106-30.

Noden, D. M. (1978). The control of avian cephalic neural crest cytodifferentiation. II. Neural tissues. *Dev Biol* 67, 313-29.

Noren, N. K., Niessen, C. M., Gumbiner, B. M. and Burridge, K. (2001). Cadherin engagement regulates Rho family GTPases. *J Biol Chem* 276, 33305-8.

Northcutt, R. G. and Brandle, K. (1995). Development of branchiomeric and lateral line nerves in the axolotl. *J Comp Neurol* 355, 427-54.

Nose, A., Nagafuchi, A. and Takeichi, M. (1988). Expressed recombinant cadherins mediate cell sorting in model systems. ***Cell*** **54, 993-1001.**

Nusslein-Volhard, C., Wieschaus, E. and Kluding, H. (1984). Mutations affecting the pattern of the larval cuticle in Drosophila melanogaster. I. Zygotic loci on the second chromosome. ***Roux's Arch Dev Biol.*** **193, 267-282.**

O'Neill, P., McCole, R. B. and Baker, C. V. (2007). A molecular analysis of neurogenic placode and cranial sensory ganglion development in the shark, Scyliorhinus canicula. ***Dev Biol*** **304, 156-81.**

O'Rahilly, R. and Muller, F. (2007). The development of the neural crest in the human. ***J Anat*** **211, 335-51.**

Oberlender, S. A. and Tuan, R. S. (1994). Expression and functional involvement of N-cadherin in embryonic limb chondrogenesis. ***Development*** **120, 177-87.**

Osborne, N. J., Begbie, J., Chilton, J. K., Schmidt, H. and Eickholt, B. J. (2005). Semaphorin/neuropilin signaling influences the positioning of migratory neural crest cells within the hindbrain region of the chick. ***Dev Dyn*** **232, 939-49.**

Packer, A. I., Elwell, V. A., Parnass, J. D., Knudsen, K. A. and Wolgemuth, D. J. (1997). N-cadherin protein distribution in normal embryos and in embryos carrying mutations in the homeobox gene Hoxa-4. ***Int J Dev Biol*** **41, 459-68.**

Park, K. W., Morrison, C. M., Sorensen, L. K., Jones, C. A., Rao, Y., Chien, C. B., Wu, J. Y., Urness, L. D. and Li, D. Y. (2003). Robo4 is a vascular-specific receptor that inhibits endothelial migration. ***Dev Biol*** **261, 251-67.**

Parsons, L., Harris, K. L., Turner, K. and Whitington, P. M. (2003). Roundabout gene family functions during sensory axon guidance in the drosophila embryo are mediated by both Slit-dependent and Slit-independent mechanisms. ***Dev Biol*** **264, 363-75.**

Patel, K., Nash, J. A., Itoh, A., Liu, Z., Sundaresan, V. and Pini, A. (2001). Slit proteins are not dominant chemorepellents for olfactory tract and spinal motor axons. ***Development*** **128, 5031-7.**

Patel, S. D., Ciatto, C., Chen, C. P., Bahna, F., Rajebhosale, M., Arkus, N., Schieren, I., Jessell, T. M., Honig, B., Price, S. R. et al. (2006). Type II cadherin ectodomain structures: implications for classical cadherin specificity. ***Cell*** **124, 1255-68.**

Perez-Moreno, M. and Fuchs, E. (2006). Catenins: keeping cells from getting their signals crossed. ***Dev Cell*** **11, 601-12.**

Piotrowski, T. and Northcutt, R. G. (1996). The cranial nerves of the Senegal bichir, Polypterus senegalus [osteichthyes: actinopterygii: cladistia]. ***Brain Behav Evol*** **47, 55-102.**

Piper, M., Anderson, R., Dwivedy, A., Weinl, C., van Horck, F., Leung, K. M., Cogill, E. and Holt, C. (2006). Signaling mechanisms underlying Slit2-induced collapse of Xenopus retinal growth cones. ***Neuron*** **49, 215-28.**

Piper, M., Georgas, K., Yamada, T. and Little, M. (2000). Expression of the vertebrate Slit gene family and their putative receptors, the Robo genes, in the developing murine kidney. ***Mech Dev*** **94, 213-7.**

Piper, M. and Little, M. (2003). Movement through Slits: cellular migration via the Slit family. ***Bioessays*** **25, 32-8.**

Pla, P., Moore, R., Morali, O. G., Grille, S., Martinozzi, S., Delmas, V. and Larue, L. (2001). Cadherins in neural crest cell development and transformation. ***J Cell Physiol*** **189, 121-32.**

Prakasam, A. K., Maruthamuthu, V. and Leckband, D. E. (2006). Similarities between heterophilic and homophilic cadherin adhesion. ***Proc Natl Acad Sci U S A*** **103, 15434-9.**

Qian, L., Liu, J. and Bodmer, R. (2005). Slit and Robo control cardiac cell polarity and morphogenesis. ***Curr Biol*** **15, 2271-8.**

Radice, G. L., Rayburn, H., Matsunami, H., Knudsen, K. A., Takeichi, M. and Hynes, R. O. (1997). Developmental defects in mouse embryos lacking N-cadherin. ***Dev Biol*** **181, 64-78.**

Radice, G. L. and Takeichi, M. (2001). Cadherins. In ***Frontiers in Molecular Biology: Cell Adhesion*****, (ed. M. C. Beckerle), pp. 62-99. New York: Oxford University Press Inc.**

Redies, C., Inuzuka, H. and Takeichi, M. (1992). Restricted expression of N- and R-cadherin on neurites of the developing chicken CNS. ***J Neurosci*** **12, 3525-34.**

Reiss, K., Maretzky, T., Ludwig, A., Tousseyn, T., de Strooper, B., Hartmann, D. and Saftig, P. (2005). ADAM10 cleavage of N-cadherin and regulation of cell-cell adhesion and beta-catenin nuclear signalling. ***EMBO J*** **24, 742-52.**

Reynolds, A. B. and Roczniak-Ferguson, A. (2004). Emerging roles for p120-catenin in cell adhesion and cancer. ***Oncogene*** **23, 7947-56.**

Rhee, J., Buchan, T., Zukerberg, L., Lilien, J. and Balsamo, J. (2007). Cables links Robo-bound Abl kinase to N-cadherin-bound beta-catenin to mediate Slit-induced modulation of adhesion and transcription. ***Nat Cell Biol*** **9, 883-92.**

Rhee, J., Mahfooz, N. S., Arregui, C., Lilien, J., Balsamo, J. and VanBerkum, M. F. (2002). Activation of the repulsive receptor Roundabout inhibits N-cadherin-mediated cell adhesion. ***Nat Cell Biol*** **4, 798-805.**

Rickmann, M., Fawcett, J. W. and Keynes, R. J. (1985). The migration of neural crest cells and the growth of motor axons through the rostral half of the chick somite. *J Embryol Exp Morphol* 90, 437-55.

Ronca, F., Andersen, J. S., Paech, V. and Margolis, R. U. (2001). Characterization of Slit protein interactions with Glypican-1. *J Biol Chem* 276, 29141-7.

Sabatier, C., Plump, A. S., Le, M., Brose, K., Tamada, A., Murakami, F., Lee, E. Y. and Tessier-Lavigne, M. (2004). The divergent Robo family protein rig-1/Robo3 is a negative regulator of slit responsiveness required for midline crossing by commissural axons. *Cell* 117, 157-69.

Saldivar, J. R., Sechrist, J. W., Krull, C. E., Ruffins, S. and Bronner-Fraser, M. (1997). Dorsal hindbrain ablation results in rerouting of neural crest migration and changes in gene expression, but normal hyoid development. *Development* 124, 2729-39.

Santiago-Martinez, E., Soplop, N. H. and Kramer, S. G. (2006). Lateral positioning at the dorsal midline: Slit and Roundabout receptors guide Drosophila heart cell migration. *Proc Natl Acad Sci U S A* 103, 12441-6.

Santiago-Martinez, E., Soplop, N. H., Patel, R. and Kramer, S. G. (2008). Repulsion by Slit and Roundabout prevents Shotgun/E-cadherin-mediated cell adhesion during Drosophila heart tube lumen formation. *J Cell Biol* 182, 241-8.

Saunders, S., Paine-Saunders, S. and Lander, A. D. (1997). Expression of the cell surface proteoglycan glypican-5 is developmentally regulated in kidney, limb, and brain. *Dev Biol* 190, 78-93.

Schlosser, G. (2005). Evolutionary origins of vertebrate placodes: insights from developmental studies and from comparisons with other deuterostomes. *J Exp Zoolog B Mol Dev Evol* 304, 347-99.

Schlosser, G. (2006). Induction and specification of cranial placodes. *Dev Biol* 294, 303-51.

Schlosser, G. and Roth, G. (1997). Evolution of nerve development in frogs. I. The development of the peripheral nervous system in Discoglossus pictus (Discoglossidae). *Brain Behav Evol* 50, 61-93.

Schwarz, Q., Vieira, J. M., Howard, B., Eickholt, B. J. and Ruhrberg, C. (2008). Neuropilin 1 and 2 control cranial gangliogenesis and axon guidance through neural crest cells. *Development* 135, 1605-13.

Sechrist, J., Nieto, M. A., Zamanian, R. T. and Bronner-Fraser, M. (1995). Regulative response of the cranial neural tube after neural fold ablation: spatiotemporal nature of neural crest regeneration and up-regulation of Slug. *Development* 121, 4103-15.

Seeger, M., Tear, G., Ferres-Marco, D. and Goodman, C. S. (1993). Mutations affecting growth cone guidance in Drosophila: genes necessary for guidance toward or away from the midline. ***Neuron*** **10, 409-26.**

Shiau, C. E., Lwigale, P. Y., Das, R. M., Wilson, S. A. and Bronner-Fraser, M. (2008). Robo2-Slit1 dependent cell-cell interactions mediate assembly of the trigeminal ganglion. ***Nat Neurosci*** **11, 269-76.**

Shimoyama, Y., Tsujimoto, G., Kitajima, M. and Natori, M. (2000). Identification of three human type-II classic cadherins and frequent heterophilic interactions between different subclasses of type-II classic cadherins. ***Biochem J*** **349, 159-67.**

Shoval, I., Ludwig, A. and Kalcheim, C. (2007). Antagonistic roles of full-length N-cadherin and its soluble BMP cleavage product in neural crest delamination. ***Development*** **134, 491-501.**

Stark, M. R., Biggs, J. J., Schoenwolf, G. C. and Rao, M. S. (2000). Characterization of avian frizzled genes in cranial placode development. ***Mech Dev*** **93, 195-200.**

Stark, M. R., Sechrist, J., Bronner-Fraser, M. and Marcelle, C. (1997). Neural tube-ectoderm interactions are required for trigeminal placode formation. ***Development*** **124, 4287-95.**

Steigemann, P., Molitor, A., Fellert, S., Jackle, H. and Vorbruggen, G. (2004). Heparan sulfate proteoglycan syndecan promotes axonal and myotube guidance by Slit–Robo signaling. ***Curr Biol*** **14, 225-30.**

Stemmler, M. P. (2008). Cadherins in development and cancer. ***Mol Biosyst*** **4, 835-50.**

Streit, A. (2007). The preplacodal region: an ectodermal domain with multipotential progenitors that contribute to sense organs and cranial sensory ganglia. ***Int J Dev Biol*** **51, 447-61.**

Strickland, P., Shin, G. C., Plump, A., Tessier-Lavigne, M. and Hinck, L. (2006). Slit2 and netrin 1 act synergistically as adhesive cues to generate tubular bi-layers during ductal morphogenesis. ***Development*** **133, 823-32.**

Su, G., Meyer, K., Nandini, C. D., Qiao, D., Salamat, S. and Friedl, A. (2006). Glypican-1 is frequently overexpressed in human gliomas and enhances FGF-2 signaling in glioma cells. ***Am J Pathol*** **168, 2014-26.**

Suchting, S., Heal, P., Tahtis, K., Stewart, L. M. and Bicknell, R. (2005). Soluble Robo4 receptor inhibits in vivo angiogenesis and endothelial cell migration. ***Faseb J*** **19, 121-3.**

Takeichi, M. (1990). Cadherins: a molecular family important in selective cell-cell adhesion. ***Annu Rev Biochem*** **59, 237-52.**

Taneyhill, L. A. (2008). To adhere, or not to adhere: The role of Cadherins in neural crest development. ***Cell Adh Migr*** **2, 1-8.**

Taneyhill, L. A., Coles, E. G. and Bronner-Fraser, M. (2007). Snail2 directly represses cadherin6B during epithelial-to-mesenchymal transitions of the neural crest. *Development* 134, 1481-90.

Teddy, J. M. and Kulesa, P. M. (2004). In vivo evidence for short- and long-range cell communication in cranial neural crest cells. *Development* 131, 6141-51.

Vallin, J., Girault, J. M., Thiery, J. P. and Broders, F. (1998). Xenopus cadherin-11 is expressed in different populations of migrating neural crest cells. *Mech Dev* 75, 171-4.

van Wijhe, J. W. (1883). Über die Mesodermsegmente und die Entwicklung der Nerven des Selachierkopfes. *Verhandelingen der Koninklijke Akademie van Wetenschappen (Amsterdam)* 22(E), 1-50.

Vargesson, N., Luria, V., Messina, I., Erskine, L. and Laufer, E. (2001). Expression patterns of Slit and Robo family members during vertebrate limb development. *Mech Dev* 106, 175-80.

von Kupffer. (1894). Ueber Monorhinie und Amphirhinie. *Sitzungsberichte. der mathematisch-physikalischen Classe der k. Bayerischen Akademie der Wissenschaften zu München* 24, 51-60.

Wang, K. H., Brose, K., Arnott, D., Kidd, T., Goodman, C. S., Henzel, W. and Tessier-Lavigne, M. (1999). Biochemical purification of a mammalian slit protein as a positive regulator of sensory axon elongation and branching. *Cell* 96, 771-84.

Wang, L. J., Zhao, Y., Han, B., Ma, Y. G., Zhang, J., Yang, D. M., Mao, J. W., Tang, F. T., Li, W. D., Yang, Y. et al. (2008). Targeting Slit-Roundabout signaling inhibits tumor angiogenesis in chemical-induced squamous cell carcinogenesis. *Cancer Sci* 99, 510-7.

Wheelock, M. J., Shintani, Y., Maeda, M., Fukumoto, Y. and Johnson, K. R. (2008). Cadherin switching. *J Cell Sci* 121, 727-35.

Wong, K., Ren, X. R., Huang, Y. Z., Xie, Y., Liu, G., Saito, H., Tang, H., Wen, L., Brady-Kalnay, S. M., Mei, L. et al. (2001). Signal transduction in neuronal migration: roles of GTPase activating proteins and the small GTPase Cdc42 in the Slit-Robo pathway. *Cell* 107, 209-21.

Woods, A., Wang, G., Dupuis, H., Shao, Z. and Beier, F. (2007). Rac1 signaling stimulates N-cadherin expression, mesenchymal condensation, and chondrogenesis. *J Biol Chem* 282, 23500-8.

Yap, A. S. and Kovacs, E. M. (2003). Direct cadherin-activated cell signaling: a view from the plasma membrane. *J Cell Biol* 160, 11-6.

Yntema, C. L. (1937). An experimental study of the origin of the cells which constitute the VIIth and VIIIth ganglia and nerves in the embryo of Ablystoma punctatum. *J. Exp. Zool.*, 75-101.

Yntema, C. L. (1944). Experiments on the origin of the sensory ganglia of the facial nerve in the chick. ***The Journal of Comparative Neurology*** **81, 147-167.**

Yuan, W., Zhou, L., Chen, J. H., Wu, J. Y., Rao, Y. and Ornitz, D. M. (1999). The mouse SLIT family: secreted ligands for ROBO expressed in patterns that suggest a role in morphogenesis and axon guidance. ***Dev Biol*** **212, 290-306.**

Zinn, K. and Sun, Q. (1999). Slit branches out: a secreted protein mediates both attractive and repulsive axon guidance. ***Cell*** **97, 1-4.**